Channels of energy loss and relaxation in CsI : A (A=Tl, In) scintillation crystals

Sergii Gridin

N^o d'ordre 349 - 2014 Année 2014

Université Claude Bernard Lyon 1

Institut Lumière Matière

Thèse

Channels of Energy Loss and Relaxation in CsI:A (A=Tl, In) Scintillation Crystals

présentée pour obtenir le grade de Docteur
par

Sergii GRIDIN

Thèse soutenue le 15 Décembre 2014 devant le jury composé de:

M Andrei BELSKY	Directeur de thèse
M Christophe DUJARDIN	Examinateur
M Aleksandr GEKTIN	Directeur de thèse
Mme Marie-France JOUBERT	Président du jury
M Paul LECOQ	Rapporteur
M Patrick MARTIN	Rapporteur
M Andrey VASILYEV	Examinateur

UNIVERSITE CLAUDE BERNARD - LYON 1

Président de l'Université:

M. François-Noël GILLY

Vice-président du Conseil d'Administration:

M. le Professeur Hamda BEN HADID

Vice-président du Conseil des Etudes et de la Vie Universitaire:

M. le Professeur Philippe LALLE

Vice-président du Conseil Scientifique:

M. le Professeur Germain GILLET

Directeur Général des Services:

M. Alain HELLEU

COMPOSANTES SANTE

Faculté de Médecine Lyon Est – Claude Bernard

Directeur : M. le Professeur J. ETIENNE

Faculté de Médecine et de Maïeutique Lyon Sud – Charles Mérieux

Directeur : Mme la Professeure C. BURILLON

Faculté d'Odontologie

Directeur : M. le Professeur D. BOURGEOIS

Institut des Sciences Pharmaceutiques et Biologiques

Directeur : Mme la Professeure C. VINCIGUERRA

Institut des Sciences et Techniques de la Réadaptation

Directeur : M. le Professeur Y. MATILLON

Département de formation et Centre de Recherche en Biologie Humaine

Directeur : Mme. la Professeure A-M. SCHOTT

COMPOSANTES ET DEPARTEMENTS DE SCIENCES ET TECHNOLOGIE

Faculté des Sciences et Technologies

Directeur : M. F. DE MARCHI

Département Biologie

Directeur : M. le Professeur F. FLEURY

Département Chimie Biochimie

Directeur : Mme Caroline FELIX

Département GEP

Directeur : M. Hassan HAMMOURI

Département Informatique

Directeur : M. le Professeur S. AKKOUCHE

Département Mathématiques

Directeur : M. le Professeur Georges TOMANOV

Département Mécanique

Directeur : M. le Professeur H. BEN HADID

Département Physique

Directeur : M. Jean-Claude PLENET

UFR Sciences et Techniques des Activités Physiques et Sportives

Directeur : M. Y.VANPOULLE

Observatoire des Sciences de l'Univers de Lyon

Directeur : M. B. GUIDERDONI

Polytech Lyon

Directeur : M. P. FOURNIER

Ecole Supérieure de Chimie Physique Electronique

Directeur : M. G. PIGNAULT

Institut Universitaire de Technologie de Lyon 1

Directeur : M. le Professeur C. VITON

Ecole Supérieure du Professorat et de l'Education

Directeur : M. le Professeur A. MOUGNIOTTE

Institut de Science Financière et d'Assurances
Directeur : M. N. LEBOISNE

«*Canaux de pertes d'énergie et de relaxation dans les scintillateurs monocristallins CsI:A (A=Tl, In)*»

Ce travail est consacré à l'étude des processus de relaxation de l'énergie et des canaux de perte d'énergie dans les cristaux scintillateurs CsI:A (A = Tl, In).

Dans le chapitre 1 les principaux processus d'interaction des rayonnements ionisants avec les solides luminescents sont discutés. Les problèmes existant dans le domaine d'application des scintillateurs solides sont analysés et les objectifs de l'étude sont formulés.

L'histoire des matériaux scintillateurs et l'étude des processus de scintillation date de plus de 60 ans. La première percée historique a été la découverte et le développement du scintillateur Nal:TI par Hofstadter dans les années 40 (Hofstadter, 1948, 1949). Ensuite de nombreux composés inorganiques ont été testés, et de nombreux matériaux scintillateurs efficaces ont été découverts (Weber, 2002). Beaucoup de ces matériaux jouent un rôle dominant dans différentes applications. Parallèlement à cela, la recherche de nouveaux matériaux scintillateurs plus efficaces est toujours active. Durant la dernière décennie, une classe de nouveaux cristaux scintillateurs encore plus efficaces à base d'halogénures alcalins a été proposée. Ces matériaux donnent généralement un rendement de scintillation très élevé et une meilleure résolution en énergie par rapport aux scintillateurs classiques d'halogénure alcalin. Il sont cependant fortement hygroscopiques ce qui limite leur utilisation.

Toutefois, le rendement élevé de ces «nouveaux» scintillateurs halogénures pose la question des limites fondamentales du rendement dans scintillateurs classiques. Les limites fondamentales de rendement de scintillation dans les scintillateurs à base de CsI et NaI a-t-elle été atteinte? Y a-t-il un moyen d'améliorer encore leurs propriétés de scintillation et de quelle manière?

Pour répondre à ces questions, l'étude détaillée, étape par étape, a été effectuée sur les deux séries de cristaux CsI, la première contenant du thallium et la seconde de l'indium avec des concentrations variant entre 0.001m% et 0.1m%. Ces cristaux ne sont pas hygroscopiques et sont relativement faciles à élaborer. Cela permet d'utiliser toute la gamme des techniques expérimentales existant actuellement.

Les méthodes expérimentales et techniques utilisées dans cette étude ainsi que les méthodes de synthèse, de caractérisation cristal, de pureté, etc sont présentées dans la chapitre 2. La deuxième section traite de la description des méthodes spectroscopiques d'analyse utilisées. Il comprend des techniques spécifiques d'investigation,

telles que la spectroscopie en temps résolue, la méthode de thermoluminescence, la spectroscopie de photoluminescence excitée dans l'ultraviolet lointain, obtenues à l'aide des synchrotrons.

L'efficacité de scintillation peut être considérée comme le produit de trois paramètres correspondants aux trois processus consécutifs de l'interaction lumière -matière:

$$\eta = \beta SQ,$$

où β est l'efficacité de création de paires électron-trou (le rendement de conversion), S est l'efficacité de transfert entre la paire électron-trou et le centre luminescent et Q est le rendement quantique de luminescence du centre considéré.

Le rendement de conversion β de l'énergie du photon γ en plusieurs paires électron-trou est contrôlé par la structure électronique du cristal. Ce paramètre peut être relativement bien évalué. L'estimation des deux autres paramètres est plus complexe. Elle demande la poursuite des études théoriques et expérimentales, objets des chapitres suivants.

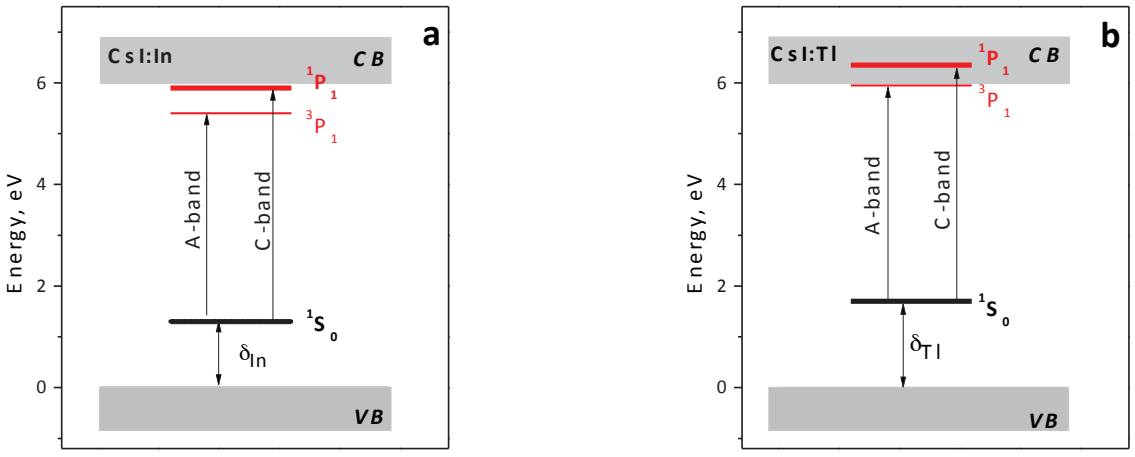

(a) (b)

Figure R1: *Diagramme des niveaux énergétiques des ions In^+ (a) et Tl^+ (b) ions relative la bande interdite de CsI*

L'étude des propriétés de luminescence des centres luminescents dans CsI:Tl et CsI:In est présentée dans le Chapitre 3 et permet de caractériser le paramètre Q. La spectroscopie d'excitation et d'émission de la luminescence (surface 3D) le type, la structure électronique et le rendement des centres luminescents liés aux ions dopants sont déterminés. Le résultat le plus marquant obtenu durant cette étape du travail

est le positionnement des niveaux d'énergie de l'activateur dans la bande interdite de CsI (Figure R1), en utilisant le modèle des courbes de configurations.

Dans le chapitre 4, les propriétés de scintillation de CsI:Tl et CsI:In sont présentés. Le rendement de scintillation et la résolution énergétique sont meilleurs dans les cristaux CsI:Tl (Figure R2). La principale différence entre ces deux séries de scintillateur est la présence d'une importante composante lente de déclin dans CsI:In. Cette lumière retardée limite le rendement de scintillation au temps courts, correspondant à la lumière « utile » dans les applications. Nous suggérons dans cette thèse que la composante de décroissance lente dans CsI:In est liée à un piège électronique associé à l'activateur.

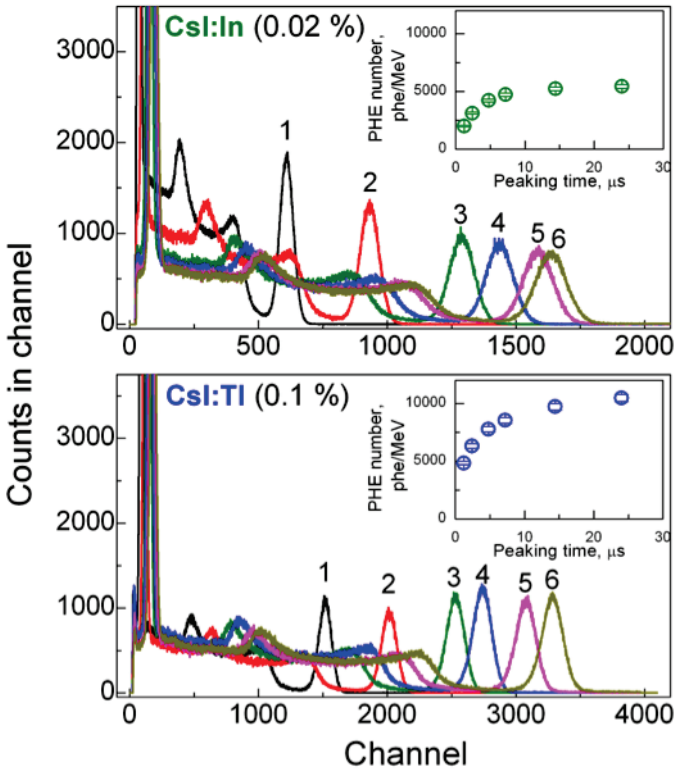

Figure R2: *Les spectres des amplitudes des scintillation de CsI:In (a) et de CsI:Tl (b) mesurés sous excitation de ^{137}Cs γ de 661.6 keV et pour les temps intégration variés*

L'étude des chaines de transfert d'énergie vers les centres luminescents et des pertes d'énergie sont décrits dans le chapitre 5. Un système d'équations cinétiques développé pour cette étude permet de simuler plusieurs propriétés de scintillation. En particulier la simulation de la variation du rendement de scintillation en fonction de la concentration d'activateur et de la température est effectuée pour les deux ions

Tl^+ et In^+. Les résultats de simulations sont en bonne concordance avec les mesures expérimentales (Figure R3). Pour assurer la qualité de la simulation, les paramètres des différents pièges des électrons et des trous ne sont pas laissés libres mais sont déterminés à partir des mesures de la luminescence thermostimulé.

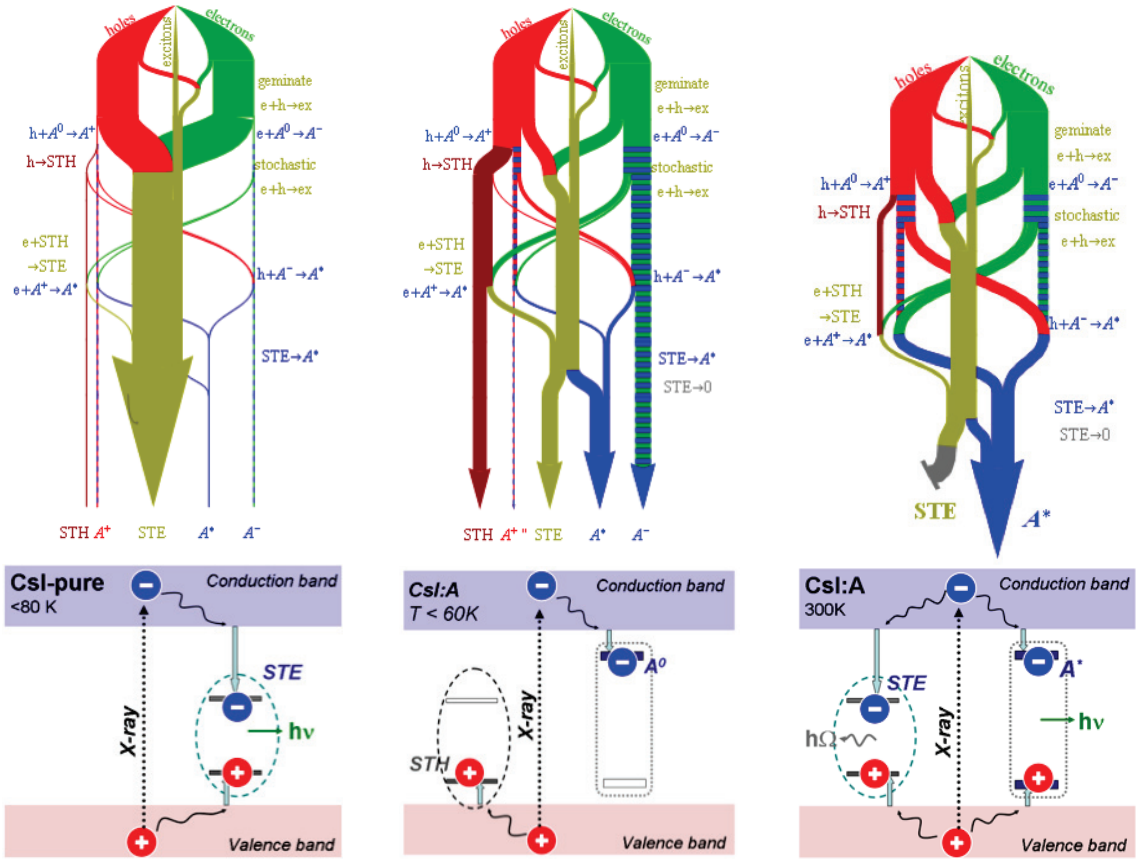

(a) (b) (c)

Figure R3: *Présentation graphique des chaines de la relaxation d'énergie (en haut) et des chaines de transferst vers le centre luminescent pour a - pure CsI, b - CsI:Tl à $T < 60K$ et c - CsI:Tl à 300 K*

Cette approche de modélisation appliquée comprend une solution numérique des équations de population. Elle est suffisamment générale pour être utilisée dans le cas d'une grande variété de matériaux scintillateurs.

Contents

Introduction **xiii**

1 General aspects of relaxation of electron excitations in inorganic scintillators **1**

1.1 Creation and relaxation of primary electron excitations in solids . . . 3

1.1.1 Interaction of ionizing radiation with crystal 3

1.1.2 Relaxation of hot electrons and holes 4

1.2 Electron-phonon interaction 7

1.2.1 Electron energy loss due to interaction with phonons 7

1.2.2 Thermalization in CsI 8

1.3 Energy migration and transfer 8

1.3.1 Structure of the excited region 9

1.3.2 Energy transfer to luminescent centers 11

1.4 Luminescence in CsI 13

1.4.1 Intrinsic luminescence in CsI 13

1.4.2 Luminescence of activator centers in CsI 14

1.5 Summary 18

2 Materials and experimental methods **21**

2.1 Investigated scintillation materials 22

2.1.1 Synthesis of CsI: Tl and CsI: In single crystals 22

2.1.2 Physico-chemical properties of CsI:Tl and CsI:In 25

2.2 Experimental techniques and equipment 27

2.2.1 Fluorescence spectroscopy of the activator centers 27

2.2.2 Synchrotron irradiation and VUV spectroscopy 28

2.2.3 Scintillation yield. Temperature dependence 29

2.2.4 Thermally stimulated luminescence 31

2.2.5 Experimental data treatment and mathematical modeling . . . 32
2.3 Conclusions . . . 32

3 Luminescent properties of In- and Tl- activated CsI crystals 35
3.1 Optical properties of Tl-like activator ions . . . 36
3.1.1 Tl-like activator energy levels . . . 36
3.1.2 Absorption spectra of Tl^+ and In^+ in CsI . . . 37
3.2 Activator luminescence of CsI:In and CsI:Tl crystals . . . 39
3.2.1 Excitation spectra from 200nm to 350nm at 15K . . . 39
3.2.2 Time resolved spectroscopy . . . 42
3.2.3 Temperature dependence of activator emission intensity . . . 43
3.3 Electron structure of the activator luminescence centers in CsI:In and CsI:Tl . . . 46
3.3.1 Activator levels positioning in the forbidden band . . . 46
3.3.2 Configuration diagrams of luminescent centers . . . 48
3.4 Activator ionization in CsI:A . . . 52
3.5 Conclusions . . . 56

4 Scintillation properties of CsI:In and CsI:Tl crystals 59
4.1 Light yield and energy resolution . . . 60
4.1.1 Pulse height spectra of scintillation response . . . 60
4.1.2 Non-proportionality of the light yield and the energy resolution 64
4.2 Time response of scintillation . . . 65
4.2.1 Microsecond decay and integraion time . . . 65
4.2.2 Afterglow in millisecond scale . . . 66
4.3 Temperature stability of the activator luminescence . . . 68
4.3.1 Low temperature range – competition with self-trapping . . . 68
4.3.2 High temperature range – influence of deep traps . . . 69
4.3.3 TSL diagrams of CsI:Tl and CsI:In . . . 71
4.4 Persistent luminescence in CsI:A . . . 72
4.4.1 Emission rise and afterglow under X-ray irradiation . . . 73
4.4.2 Role of the activator electron traps . . . 76
4.5 Conclusions . . . 78

5 Relaxation of electron excitations in CsI:In and CsI:Tl crystals 81

5.1 Electron excitations in CsI pure and CsI:A and their interaction . . . 82

5.1.1 Excitation of STE luminescence in CsI 83

5.1.2 Activator excitation channels in CsI:A 84

5.2 Kinetic model of energy relaxation in CsI:A 89

5.2.1 General scheme of electron excitations 90

5.2.2 Mathematical modeling of energy relaxation 91

5.2.3 System parameters determination and numerical solution . . . 94

5.2.4 Comparison of simulation and experiment 98

5.3 Model of the luminescence rise and the afterglow with account of the activator traps 108

5.4 Conclusions 113

General conclusions and perspectives 115

Bibliography 119

Acknowledgements 129

Introduction

History of scintillation materials and study of physical principles of scintillation process takes its origin over 60 years back. The historical breakthrough was discovery and development of NaI:Tl scintillation crystal by Hofstadter in the 1940th [Hofstadter, 1948, Hofstadter, 1949]. After that numerous inorganic compounds and activator have been tested, and many efficient scintillation materials were discovered [Weber, 2002]. Many of these materials still play dominating role in different applications. NaI:Tl, CsI:Tl, CsI:Na are used in scintillation spectrometry, PWO and CsI – in high energy physics, NaI:Tl is used in well logging, CsI:Tl, NaI:Tl, LSO, LYSO also find their application in medical imaging. Along with that, search for new more efficient scintillation material is all the time ongoing. During the last decade a class of new more efficient scintillation crystals based on alkali earth halides has been announced. The light yield measurements testify remarkably high scintillation efficiency. In particular many Eu^{2+} doped alkaline earth halides were found to emit up to 100 000 photons/MeV. The typical examples are Eu-doped SrI_2, $BaBrI$, $CsBa_2I_5$, $BaCl_2$ [Bizarri et al., 2011, Cherepy et al., 2008, Yan et al., 2013]. These materials usually give a higher scintillation yield and better energy resolution in comparison with the traditional alkali halide scintillators.

High scintillation efficiency of the "new" alkali earth halides arises some questions as to the physical views on the scintillation processes. More detailed analysis of the limits of scintillation efficiency is required. The common approach is to treat the scintillation efficiency with the classical Lempicki – Wojtowicz equation:

$$\eta = \beta S Q \tag{1}$$

where, β is the efficiency of electron-hole creation (the conversion efficiency), S is the transfer efficiency, and Q is the luminescence quantum efficiency. All these three processes, although somewhat separated in the time scale, are dependent on each other.

If the crystal contains single luminescence centers, which do not undergo any temperature or concentration quenching, their quantum efficiency Q should be close to unity. Then the efficiency of the scintillator is determined by the parameters S and β. Reconsideration of β involves account of the electron band structure, spatial distribution of electron excitation along the track and their interaction. Experimental means to directly measure the value of β are still an open question.

Efficiency of electron-hole pairs production β is limited by the crystal band gap E_g, as well as energy losses due to thermalization of electron excitations. Estimates of the average energy of an electron-hole pair creation in crystals are usually made on the basis of the light yield experimental measurements. Various scintillators give values about $2.5E_g$ and higher [Dorenbos, 2012, Robbins, 1980].

On the other hand, the intrinsic STE emission of pure CsI was found to be extremely efficient also [Moszynski et al., 2003, Moszynski et al., 2005]. This result drops out from the common pattern, as presented in Fig. I1.

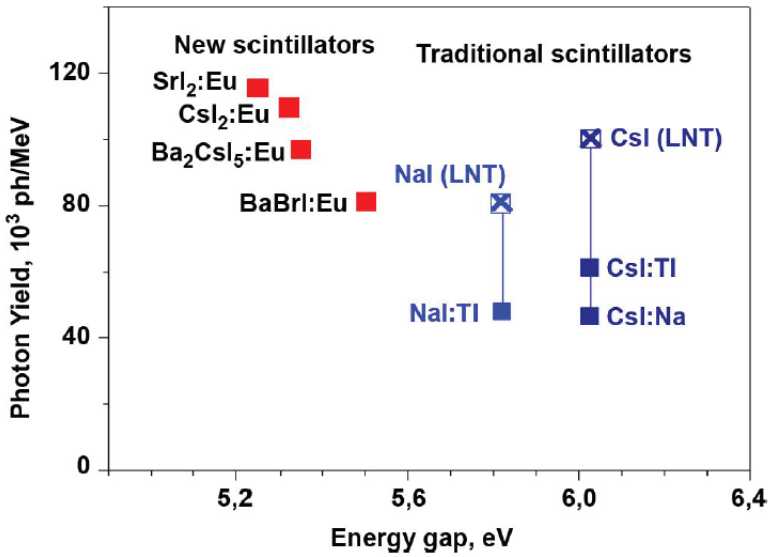

Figure I1: *Estimation of scintillation efficiency of halide scintillators*

High efficiency of "new" halide scintillation crystals arises the question of the fundamental limits of yield in classical scintillators. If the fundamental limits of scintillation yield in CsI and NaI based scintillators has been reached? Is there a possibility to still improve their scintillation properties and in what way?

Answer to that question requires detailed study of energy relaxation mechanisms and energy losses during each stage of the scintillation process. Traditional CsI based scintillators have been chosen for the experimental system. It allows using several

activator impurities (such as Na^+, Tl^+, and In^+ ions) to verify the role of the Q factor – the luminescence quantum efficiency. The crystals are not hygroscopic and relatively easy to grow. This allows using the whole range of available experimental techniques.

This work is devoted to study of energy relaxation processes and energy loss channels in CsI:A (A=Tl, In) scintillation crystals . This goal conditions the choice of the object of research (CsI:A scintillators), experimental techniques, and methods of analysis. Sequential study was planned to deal with the problem, providing the structure of this dissertation.

• In Chapter 1 the present view on the problem is reviewed, the local problems and goals which require solution are stated.

• Chapter 2 covers the experimental methods and techniques used in the study. First section of it contains mostly the description of the synthesis methods, crystal characterization, purity etc. The second section deals with description of spectroscopic methods of analysis used. It includes specific techniques of investigation, such as time resolves spectroscopy, method of thermally stimulated luminescence, spectroscopy in VUV using synchrotron irradiation.

• Chapter 3 deals with study of luminescent properties of activator center in CsI:Tl and CsI:In. UV fluorescent spectroscopy methods are used to investigate the properties of the activator emission centers. The most important results obtained here are positions of the activator levels relative to the energy bands of CsI, configuration diagram model of luminescent centers in CsI:Tl and CsI:In, and evidence of the activator ionization under photo excitation.

• In Chapter 4 we present features of CsI:In scintillation properties in comparison with CsI:Tl. The key difference is the slow component in CsI:In scintillation decay. This delayed light limits the scintillation yield if short integration times are used in measurements. It is suggested that the slow decay component in CsI:In is related to the activator electron trap.

• In Chapter 5 a general model of energy relaxation in CsI:A is suggested. It includes the activator-induced and the intrinsic (STE) energy relaxation channels, and three possible charge states of the activators. A system of kinetic rate equations (compiled based on the energy relaxation model) allows simulating many scintillation properties of CsI:A system as a function of temperature and the activator concentration.

Chapter 1

General aspects of relaxation of electron excitations in inorganic scintillators

Contents

1.1 Creation and relaxation of primary electron excitations in solids 3
1.1.1 Interaction of ionizing radiation with crystal 3
1.1.2 Relaxation of hot electrons and holes 4
1.2 Electron-phonon interaction 7
1.2.1 Electron energy loss due to interaction with phonons . . . 7
1.2.2 Thermalization in CsI 8
1.3 Energy migration and transfer 8
1.3.1 Structure of the excited region 9
1.3.2 Energy transfer to luminescent centers 11
1.4 Luminescence in CsI 13
1.4.1 Intrinsic luminescence in CsI 13
1.4.2 Luminescence of activator centers in CsI 14
1.5 Summary 18

This Chapter presents the basics of electron relaxation if inorganic scintillation crystals in general and in CsI crystals in particular. The chapter is divided into sections, representing the three stages of the scintillation process: generation of electron excitations in inorganic crystals, their spatial distribution in the track and migration, and finally creation of excited luminescence centers and emission. Influence of each stage on the scintillation efficiency is discussed.

Generally, the process of the incident particle energy conversion into visible light contains multiple processes. They include creation of primary electron excitations, electron-electron scattering, thermalization of the secondary electrons, interaction of the excitations, migration of thermalized free charge carriers and trapping, excitation of the luminescence centers, and finally photon emission (see Fig. 1.1). Role of individual aspects and mechanisms of each of the elementary steps remain unclear, since direct measurement of the effect of each separate step is usually not possible. Measured light yield value of a scintillator includes the superposition of all the processes of electron-hole creation and recombination. So the balance between the energy loss channels in scintillators remains unclear. This is why a comprehensive approach to study of energy relaxation process is required.

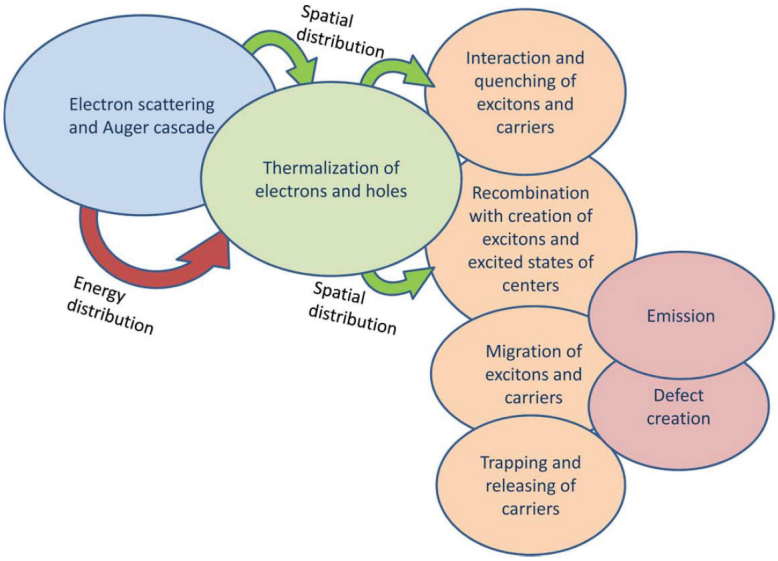

Figure 1.1: *Interconnected processes in scintillators from [Vasil'ev and Gektin, 2014]*

It was noted in the introduction that the main directions of revising and refining the classical concepts of the scintillation process are related to the three stages (β, S, Q). First of all, these are the new advances in computational analysis of the primary stages of the scintillation process and ionizing particle track structure formation. The second point is related to the development of ideas about the role of electron-phonon interaction in track development/relaxation of the secondary excitations. And finally, energy transfer efficiency to the emission centers, as well as the luminescence quantum efficiency of the recombination centers itself should be discussed in terms of possibility of the scintillation efficiency increase. The latter

one can be shown through the choice of different types of the activator impurities.

Recent theoretical studies attempting to describe some stages of the hot relaxation process give a reasonable image of the spatial distribution of excitations in the track. But characterization of the energy relaxation efficiency is still insufficient. In accordance with these considerations, a review of known data and physical concepts of the scintillation process is divided into corresponding subsections in Chapter 1.

1.1 Creation and relaxation of primary electron excitations in solids

Development of modern modeling methods of the track structure formation is primarily due to the advent of new computational capabilities. They have been implemented in the studies [Kerisit et al., 2008, Kerisit et al., 2009, Kerisit et al., 2014] and [Wang et al., 2011, Wang et al., 2012, Wang et al., 2013]. They are the basis for re-consideration of some basic concepts about the spatial distribution of the primary electron-hole pairs in the track. These calculations are carried out primarily for alkali halide crystals, for which there are initial parameters for the simulation.

1.1.1 Interaction of ionizing radiation with crystal

Primary act of interaction of ionizing radiation with crystal can be realized in three different types: Compton effect, photoelectric effect, or the pair creation. All these three types of interaction are schematically presented in Fig. 1.2.

Each type of the interaction has different probability, depending on the incident particle energy. In general, at the γ-rays with energy of about 0.1 MeV and below photoelectric effect dominates (see Fig. 1.3), at the energy of about 1 MeV Compton interaction is more probable, and when the energy of the incident γ-rays is above 10 MeV, the pair creation comes in action [Blasse and Grabmaier, 1994].

For NaI crystal the mass attenuation coefficient as a function of incident γ-ray is shown in Fig. 1.3(b) [Evans, 1955]. Such behavior is typical for all inorganic material.

As the excitation energy drops, the absorption coefficient grows larger (Fig. 1.4). The interaction of the incident photon occurs with the deep core electron levels of the crystal. The edges in the absorption curve around 650 eV and 5 keV correspond

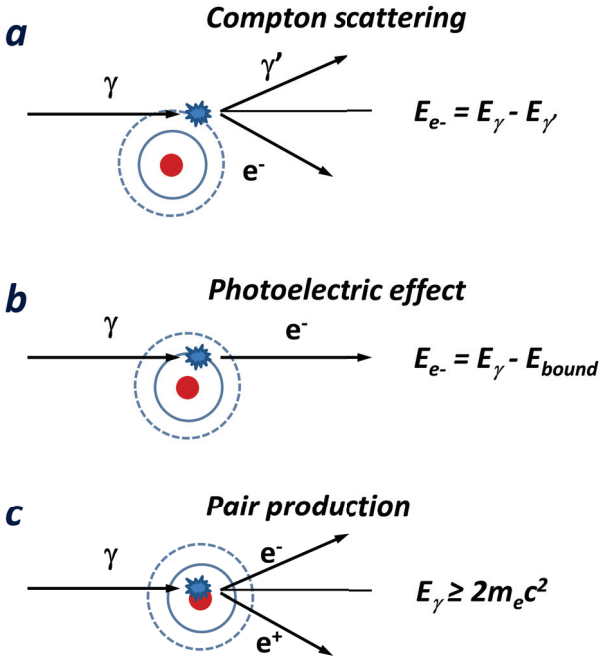

Figure 1.2: *Three different types of interaction of ionizing radiation with matter [Evans, 1955]. a – Compton effect, b – photoelectric effect, c – pair production*

to excitation of the corresponding 3d, 2p, and 2s electron shells of Cs and I atoms.

Release of an electron from an inner shell of an atom results in ionization of this atom. The atom with ionized inner shell relaxes either emitting a photon or an electron (the Auger process). A free electron (depending on its kinetic energy) can lose its energy by emitting phonons of by scattering on other electrons. The resultant secondary photons may be absorbed or scattered by analogy with primary photons. Relaxation of the hot electrons created is discussed in the following Section.

1.1.2 Relaxation of hot electrons and holes

Processes described in Section 1.1.1 result in creation of primary knocked-out electrons with some kinetic energy. Such a primary high energy electron will be propagation through the crystalline lattice, and its energy loss is caused by inelastic interaction with other electrons (so called electron-electron scattering).

Important quantitative characteristic of the fast electrons' motion in the crystal is their mean free path l_{ee} [Elango, 1991]. These is the average distance between two successive inelastic collisions with electrons of the crystal:

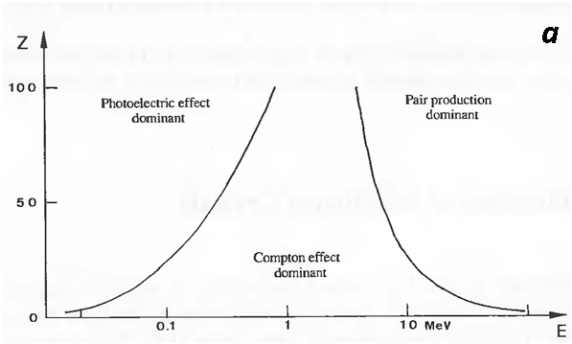

(a)

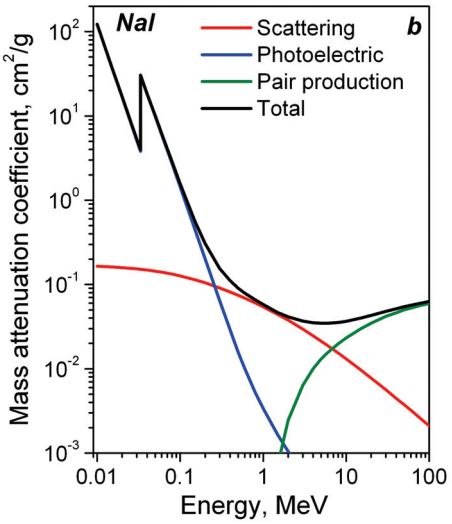

(b)

Figure 1.3: *The relative importance of the three major types of interaction of γ-rays with condensed matter. The atomic number Z is plotted linearly versus the γ-rays energy E in MeV which is plotted logarithmically (a), and calculated attenuation coefficient for NaI crystal (b)*

$$l_{ee}^{-1} = \sum_i \sigma_i N_i \tag{1.1}$$

where σ_i is the cross section of the i^{th} elementary process, and N_i is the density of electrons.

Dependence of the mean free path of electrons l_{ee} on its energy E_0 is described by a universal curve for all the solids (see. Fig. 1.5) [Ritchie et al., 1975]. It has a minimum of 100-300 eV at l_{ee} about 0.5 nm. This minimum is due to the maximum of the ionization cross sections of the valence band and the effective cross section for the creation of a plasmon in this energy region [Elango, 1991]. Ionization cross

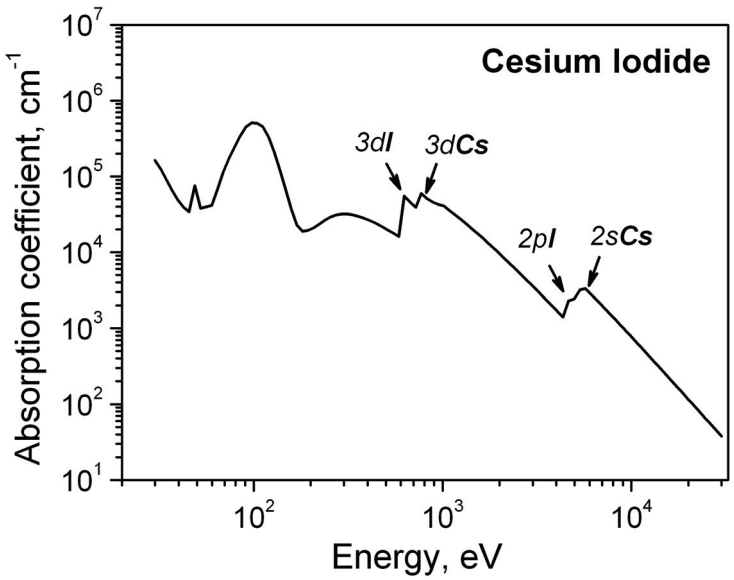

Figure 1.4: *Electromagnetic energy absorption coefficient in the X-ray energy range for CsI [xRa, 2014]*

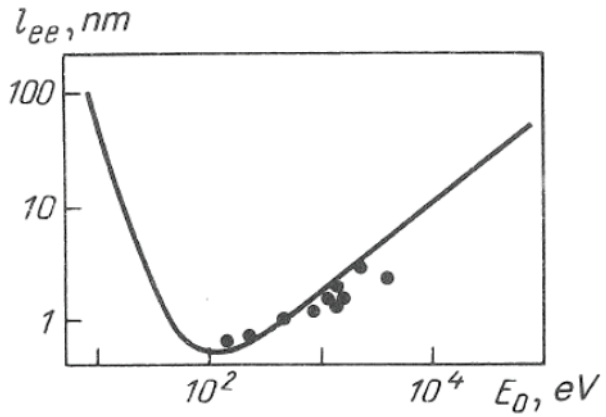

Figure 1.5: *Mean free path of electrons in the case of inelastic scattering by bound electrons in Al_2O_3 (the points are the experimental results) [Ritchie et al., 1975]*

section with valence electrons can be well described by the Bethe formula:

$$\sigma_v = \frac{4\pi e^2 n_0}{E_0 E_g} ln \frac{2E_0}{E_g} \tag{1.2}$$

where E_g is the band gap, n_0 is the number of the valence electrons per an atom, and E_0 is the initial electron kinetic energy.

Electron-electron interaction process takes place as long as the electron energy reaches the $2E_g$ scattering threshold. Below this energy creation of a new free electron is not possible. Further electron energy loss is associated with creation of

optical phonons.

1.2 Electron-phonon interaction

Modern views on the evolution of the electronic excitations suggest the important role the electron-phonon interaction on the formation of the track structure and further recombination of the electron excitations. Thanking to the works of A. Vasil'ev [Glukhov and Vasil'ev, 1995, Kirkin et al., 2012, Vasil'ev and Gektin, 2014, Vasil'ev and Michailin, 1986, Vasil'ev, 1999, Vasil'ev, 2008], theory of the key principles of electron thermalization have been developed. This Section deals with the role of electron-phonon interaction at the stages of thermalization on the spatial distribution of electrons and holes in the track.

1.2.1 Electron energy loss due to interaction with phonons

For low-energy excitations (electrons and holes, kinetic energy of which $E_k < E_g$) the main mechanism of energy relaxation is emission of phonons. This process is called electron-phonon relaxation [Elango, 1991], and the stage of the scintillation process – thermalization [Kirkin et al., 2012, Wang et al., 2011]. Electron energy loss at this stage can be analytically estimated. For the case of a single LO phonon branch electron thermalization length l as a function of the initial energy E_{e0} can be estimated as:

$$l^2_{e,LO}(E_{e0}) = \frac{1}{24} a_B^2 \left(\frac{\varepsilon_{st}}{\frac{m_e^*}{m_0}} \right)^2 th\left(\frac{\hbar\Omega_{LO}}{2k_BT} \right) Ei\left(3ln\left(\frac{4E_{e0}}{\hbar\Omega_{LO}} \right) \right) \tag{1.3}$$

where a_B is the Bohr radius, m_e^* is the electron effective mass, and m_0 is the free electron mass. According to eq. 1.3, the mean free path of the electron at the thermalization stage depends on its effective mass, and the energy of the LO phonons. Mean distance propagated by the electron as a function of the LO phonon energy is this approximation is shown in Fig. 1.6.

In general, it can be expected that in crystals with higher LO phonon energy the electron–hole separation should be smaller. This should increase the fraction of geminate e-h recombinations and minimize the energy loss.

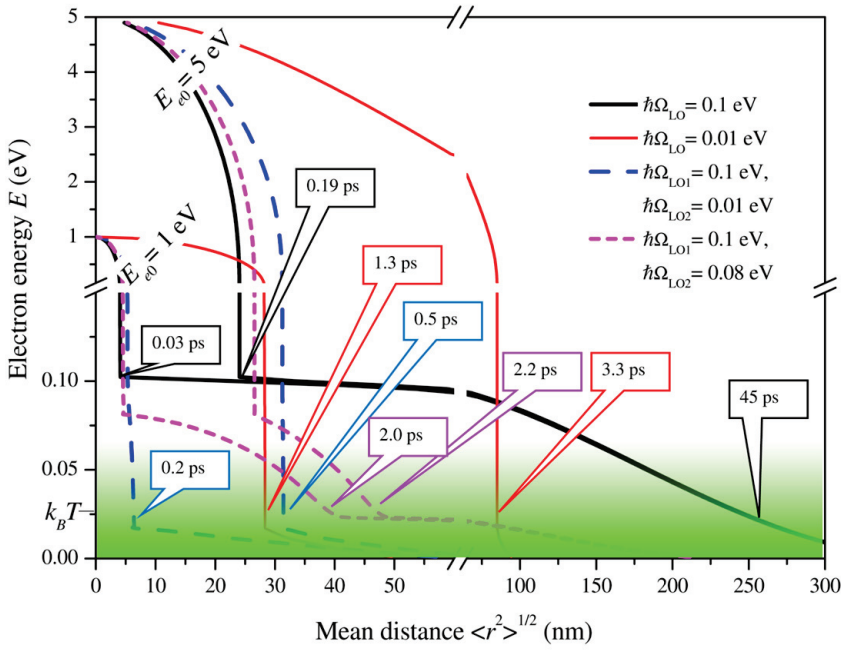

Figure 1.6: *Mean distance propagated by the electron as a function of the LO phonon energy from [Kirkin et al., 2012]*

1.2.2 Thermalization in CsI

In CsI crystals *LO* phonon energy is rather small, about 0.01 eV. This provides relatively high electron mean free path in this material. Analytical distribution function of electron thermalization distances in CsI is provided in Fig. 1.7. According to that, the average distance between genetic electrons and holes in CsI is about 180 nm.

Recombination probability of the escaped electrons with the geminate holes can be estimated using the Onsager approach [Onsager, 1938]. However, spatial distribution of the electron excitations in the track is strongly non-homogeneous. In case of relatively long thermalization distances with respect to the recombination radius significant fraction of electron-hole pairs recombines stochastically.

1.3 Energy migration and transfer

Energy transfer from the electron excitations created in the scintillation matrix to the activator ions goes mostly after thermalization stage, when the energy of electrons and holes reaches k_BT [Gridin et al., 2014c, Vasil'ev and Mikhailin, 2008].

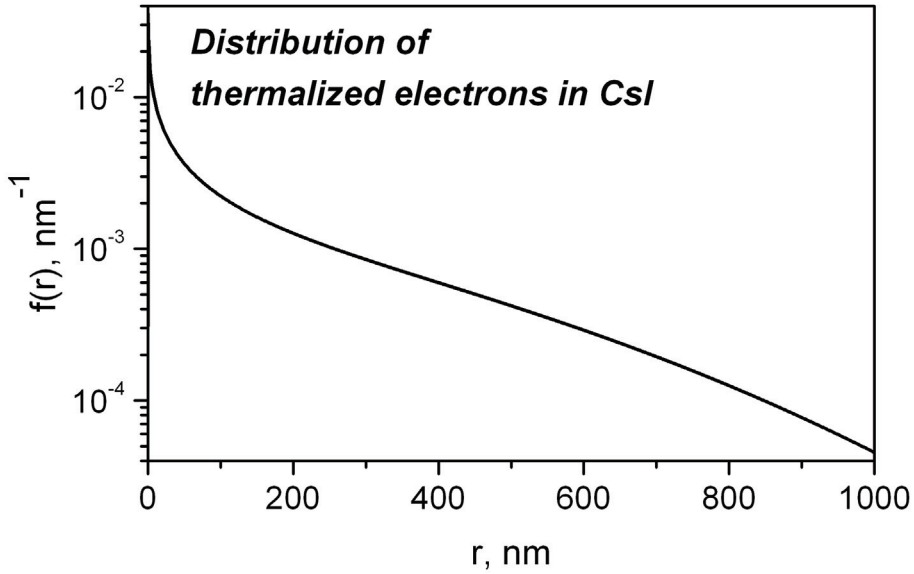

Figure 1.7: *Distribution of electron thermalization distances in CsI [Vasil'ev and Gektin, 2014]*

This consideration is true for relatively low activator concentrations (0.1 % mol. or less), when scattering of hot electrons at the activator ions is seldom. Electron-hole recombination probability at the migration stage depends on several parameters. First is the structure of the excited region, i.e. the spatial distribution of thermalized electrons and holes with respect to the recombination radius. Second is migration of correlated and separated electron-hole pairs on the way to the recombination centers.

1.3.1 Structure of the excited region

In general, scintillation track is strongly non-homogeneous in terms of the respective spatial distribution of electrons and holes. In the beginning of the track there are mostly low excitation density regions, whereas high excitation densities are typical for the final part of the track. Different spatial scales of the track with respect to the excitation energy, dimensions of the media, recombination radius, and typical distances between activator centers are presented in Fig. 1.8.

It is assumed therefore, that recombination probability of electron excitations is different along the track, and it should strongly depend on the respective spatial distribution of thermalized electrons, holes, and luminescence centers. Final electron-hole spatial distribution and formation of the track structure is achieved

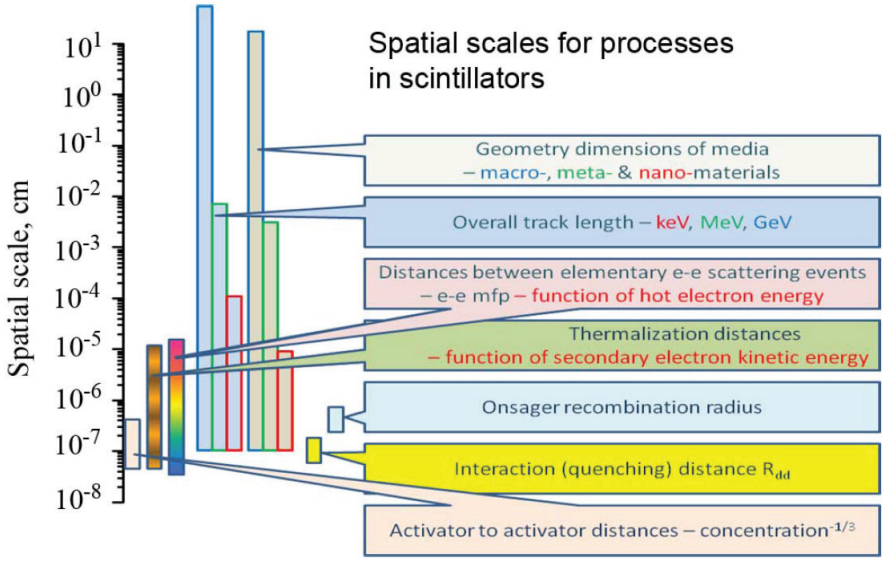

Figure 1.8: *Different spatial scales for processes in scintillators [Vasil'ev and Gektin, 2014]*

after the thermalization stage. In view of low *LO* phonon energy in CsI (0.01 eV), the average separation distance between genetic electron and hole are relatively large.

Actual structure of the excited region in inorganic crystals is not verified in an experimental way. However, there are different models of the primary electron track used to treat the e-h recombination process. Simulations of the "real" spatial distribution of electrons and holes in the track were done using the Monte Carlo method is provided in Fig. 1.9. Average concentration of charge carriers is orders of magnitude smaller than typical activator concentrations in halide scintillators. However, there are some high density clusters, where interaction of excitation (quenching) may occur. Due to the larger effective mass, holes created in the track are mostly organized in the central part.

Account of electron-hole distribution is crucial for understanding many scintillation properties such as light yield non-proportionality. However, recombination of electrons and holes occurs at some matrix defects – luminescence centers. Those can be either intrinsic or induced by an impurity. Transport of electron excitation and their capture by the luminescence center can go with some energy losses, as well. Onsager recombination radius in CsI is about 10 nm at room temperature. This means that to assure high scintillation efficiency at RT, transport of separated

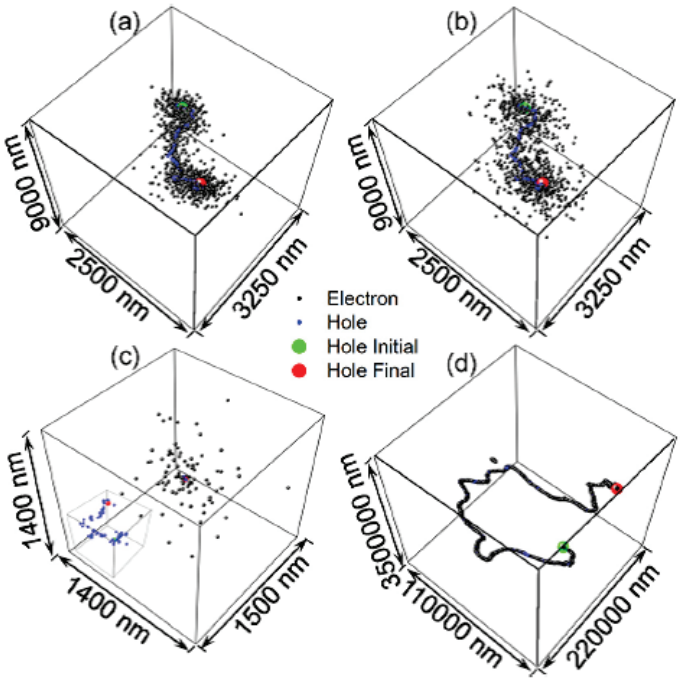

Figure 1.9: *Simulation of spatial e-h distribution in CsI after absorption of 1 keV photon [Wang et al., 2011]*

electrons and holes to the activator centers in CsI:A should be effective. Energy transfer efficiency to the luminescence centers is the subject for discussion in the following Section 1.3.2.

1.3.2 Energy transfer to luminescent centers

Given the spatial distribution of electrons and holes in the excited region, significant fraction of electrons are separated from holes much farer, that the Onsager recombination radius. On the way to recombination centers, electrons may be captured by some defects, which are always present in real crystals. Those traps can be some intrinsic defects (vacancies) or defects induced by the uncontrolled impurities. If the excitation density is much smaller that the molar fraction of the traps, such trapping should result in drop of the overall scintillation efficiency (so called migration losses). Effect of the migration losses on the luminescence quantum yield is illustrated in Fig 1.10 [Vasil'ev et al., 1985]. The model includes some electron traps in the crystal. Excitation around E_g results in creation of correlated e-h pairs only, since neither electron nor hole acquire any kinetic energy. This is why the quantum yield is always a unity. As the excitation energy growth, electron-hole separation distance

also increases . So that trapping of separated electrons should result in some drop of the quantum yield. In case Fig 1.10(a) e-h recombination distance is assumed to be much larger that the separation distance. Therefore, the excitation spectrum is flat in the region $E_g \div 2E_g$. In case Fig 1.10(b) electron-hole separation distance is about the recombination radius. Here the quantum yield somewhat drops up to $2E_g$, since separated electrons may never recombine. If the recombination radius is much smaller that the electron-hole separation distance during thermalization, only closely correlated pairs can recombine (Fig 1.10 c). Consequently, the quantum yield drops rapidly with the excitation energy increase. Increase of the quantum yield above $2E_g$ is due to multiplication of electron excitations with kinetic energy above E_g.

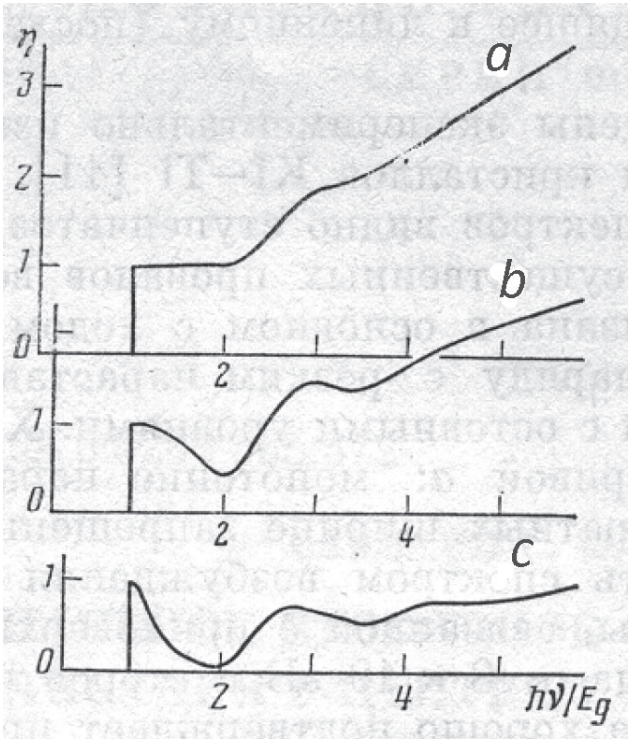

Figure 1.10: *Fluorescence quantum yield as a function of the excitation energy in a phosphor with traps: a - no migration loss, b – small migration losses, c – strong migration losses [Vasil'ev et al., 1985]*

Naturally, migration losses in efficient scintillators should be minimal. So normally luminescence excitation spectra of good scintillation materials behave similarly to *a* or *b* examples in Fig 1.10. In activated crystals energy transfer to the activator centers can go in two different ways. First, as sequential capture of electron and a hole (or vice versa): $A^+ + e^- = A^0$, $A^0 + h^+ = (A^+)^* \rightarrow h\nu$. Second, as a bound

e-h pair (an exciton): $A^+ + ex = (A^+)^* \rightarrow h\nu$. In the latter case excitons transfer their energy to the activator by means of diffusion in the crystal lattice, or non-radiative $ex \rightarrow A^+$ energy transfer may be the case. Peculiarities of energy transfer to activator center in CsI:A are discussed in Chapter 5.

1.4 Luminescence in CsI

Views on the primary processes of excitations' creation and their thermalization cannot be verified by direct experiments for extremely short time of occurrence. It is therefore necessary to analyze the later stages of radiative relaxation. Specific experiments should be chosen, that allow to understand the stage at which energy losses occur. Study of localization of the electron excitations in the crystal allows to specificity the efficiency of e-h pairs creation in the matter, and the fraction of them which recombines radiatively. This section provides a brief overview of the most important recombination centers in CsI.

1.4.1 Intrinsic luminescence in CsI

In undoped CsI crystals there are two principal channels of relaxation. First is luminescence of self-trapped excitons (STE). Its properties have been investigated in detail in [Lamatsch et al., 1970, Lamatsch et al., 1971]. This emission is intense at low temperatures, as self-trapping of holes and creation of V_k centers is efficient below 90K. A principal configuration diagram model of this emission in alkali halides (see Fig. 1.11) can be found in [Song and Williams, 1993].

Another type of intrinsic emission in CsI is so called fast intrinsic luminescence (FIL) band. It is present in pure CsI crystals, emitting at room temperature around 305 nm in nanosecond timescale under X-ray excitation. Excitation spectrum of this band, as well as its decay suggests that this emission cannot be assigned to simple STE [Belsky et al., 1994] (see Fig. 1.12).

The exact origin of this luminescent state is still not clear. It can be a localization of an exciton next to an intrinsic defect, like an anion or cation vacancy. It is natural to suppose that such defect may be present in crystal in long-living state at very low concentration. In [Belsky et al., 1997] it is suggested that the relaxation of an exciton into FIL generating state occurs only in the region of the crystal perturbed

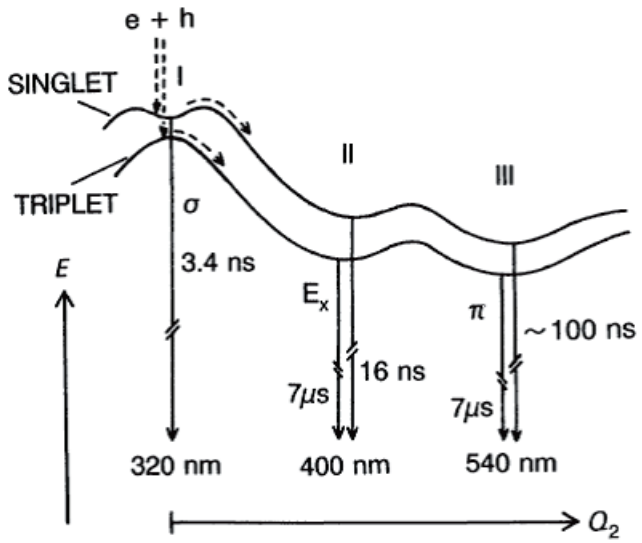

Figure 1.11: *Model of STE luminescence in RbI from [Song and Williams, 1993]*

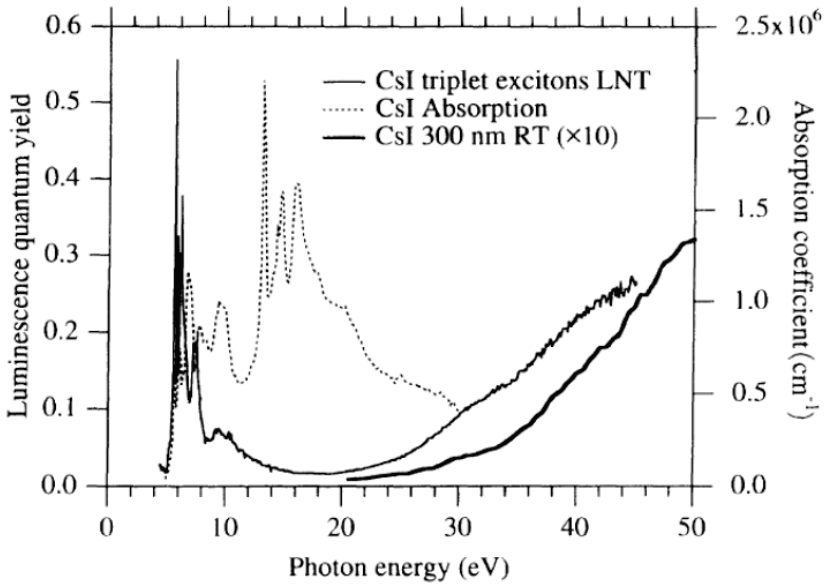

Figure 1.12: *Excitation spectra of the intrinsic emission bands in CsI [Belsky et al., 1994]*

by another electronic excitation or defect.

1.4.2 Luminescence of activator centers in CsI

In many scintillation crystals, including CsI, the intrinsic luminescence (STE band) is quenched at room temperature. To create stable at RT centers of radiative re-

laxation activator impurities are used. These impurities usually substitute for the matrix cation in the crystal lattice. In CsI lattice In^+ and Tl^+ ions (at relatively low activator concentrations) replace Cs^+ ions. The ground and the excited electron states of the activator ions are usually situated in the forbidden band of the matrix. This leads to appearance of the activator electron transitions within the band gap, which is manifested in the form of induced absorption bands in the crystal transparency region.

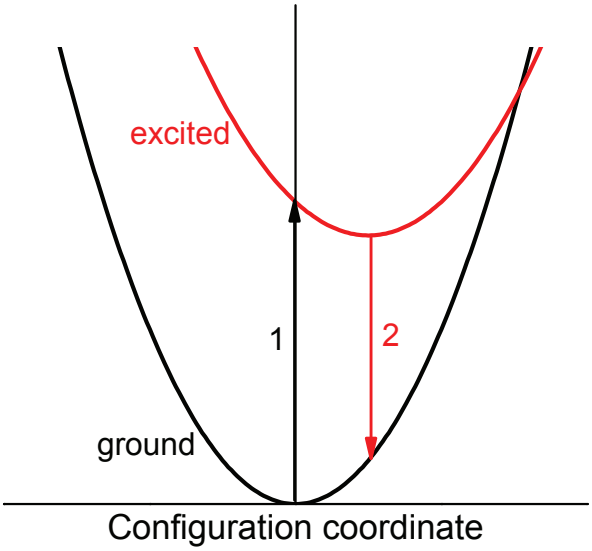

Figure 1.13: *Configuration diagram of a luminescent center*

Electron transitions involving the impurity electron states can be conveniently described using the configuration diagram (Fig. 1.13) [Blasse and Grabmaier, 1994]. Here, the lower curve corresponds to the ground state, and the upper one – to the excited state. Minimum of the excited state is shifted relative to the ground state, since the transition of the valence electron in the excited state is accompanied by a relaxation (change of position) of the surrounding ions. In this case, the distance from the center to the nearest neighbors increases. This model is based on the Franck-Condon principle, according to which electronic transitions occur so quickly that the positions of the surrounding ions do not have time to change. Therefore, in the diagram Fig. 1.13 electronic transitions corresponding to absorption (arrow 1) and the emission (arrow 2) of a photon are shown by vertical lines. Note that the energy of the emitted photon is less than the energy of the absorbed photon. This leads to so-called Stokes shift, the spectral separation of the absorption and luminescence bands. It should be also noted that the model in Fig. 1.13 is valid for

non-degenerate electron states of the activator. Generally speaking, for mercury-like ions the Jahn-Teller effect is typical, which can be manifested in fine structure of the absorption bands [Ranfagni et al., 1983]. Account of the Jahn-Teller effect leads to additional branches in the configuration diagram, depending on the degeneracy of the activator electron levels [Stoneham, 2001, Vasil'ev and Mikhailin, 2008].

In this work we use a simplification – simple potential surfaces represent the electron states of the activator ion, as our main focus will be on the effects related to the change of the activator charge state (i.e. charge transfer transitions). These are electron transitions between activator states and the matrix states. Two types of such transitions can be differed. Firstly, so-called charge transfer (CT) transitions. This is an electron excitation from the valence band to the impurity levels. In this case, the impurity ion acquires an extra electron. For the case of monovalent positively charged ion $A^+ + h\nu_{exc} \rightarrow A^0 + h_{bound}$. Potential surface of such a state can be represented using the configuration diagram model. This CT state will be represented by a parabola, which is shifted towards larger values of Q (to the right) with respect to the ground state parabola. Corresponding diagram is shown in Fig. 1.14(a). Relaxation of this state leads to a return of the center in the ground state with emission of a photon $A^0 + h_{bound} \rightarrow A^+ + h\nu_{emi}$. The relevant emission band is called the CT emission band.

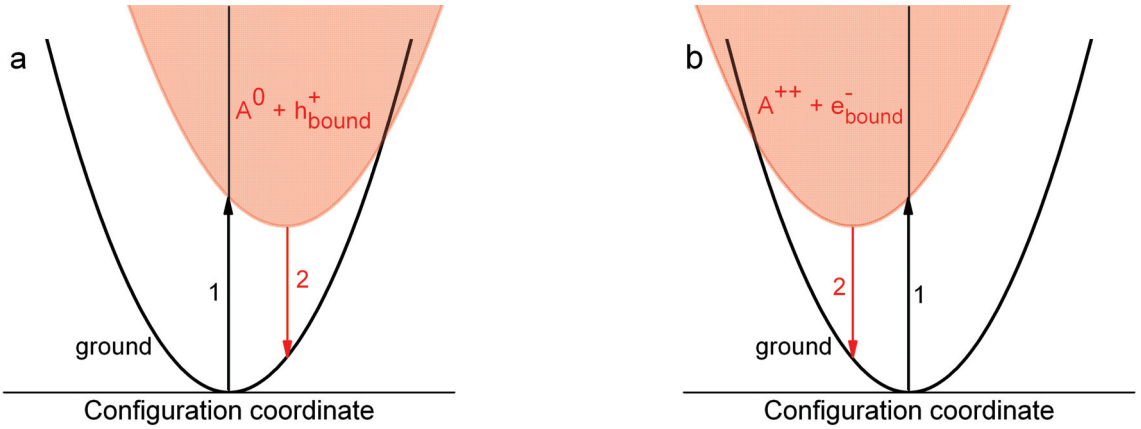

(a) (b)

Figure 1.14: *Configuration diagrams of CT ($A^0 + h^+_{bound}$) (a) and BE ($A^{++} + e^-_{bound}$) (b) states*

The second type of the charge transfer excited state occurs when electron from the activator ground state goes to the conduction band. This state is usually called

the impurity bound exciton (BE). In this case, the activator loses an electron: $A^+ + h\nu_{exc} \rightarrow A^{++} + e_{bound}$. This state should be represented by a parabola, which is shifted towards lower values of Q (to the left) with respect to the ground state parabola (Fig. 1.14 b). This state can also radiatively recombine with emission of a photon, and the corresponding emission bands is called the impurity bound exciton. In fact, this is also a type of charge transfer transition between the matrix and the impurity ion. Therefore we shall use the following notation for these two types of charge-transfer transitions.

Traditional charge-transfer state CT is indicated as $(A^0 + h^+_{bound})$, and the impurity bound exciton (BE traditional) will be indicated as $(A^{++} + e^-_{bound})$.

Possibility of implementation of one or another charge transfer state depends significantly on the typical charge states of the activator ion, as well as on the position of the activator levels relative to the band gap of the matrix. In many cases, the radiative transitions of the CT and BE are not observed. Relaxation of excited states $(A^0 + h^+_{bound})$ and $(A^{++} + e^-_{bound})$ goes without photon emission. Although such a state can still be created. In this case, the charge transfer state may play a role of a trapping centers associated with the impurity, or an intermediate excited state through which the electron excitation is transferred. Therefore, clear understanding of the impurity electron state structure can explain many of scintillators properties. Structure of the activator luminescence centers in CsI:Tl requires more detailed investigation. There are two models of thallium luminescence centers CsI. The first model is based on simple ion model of the impurity electron levels. It can be used for interpretation of many luminescence properties of CsI:Tl under intracenter excitation by UV photons [Sivasankar and Jacobs, 1985]. In addition to this model Nagirnyi and Zazubovich proposed a model of the impurity perturbed exciton [Nagirnyi et al., 1994]. In this model, the exciton is regarded as the electronic excitation of the matrix, which is distorted by the impurity. The perturbation is the stronger the closer it is to the impurity [Babin et al., 2002a, Babin et al., 2002b]. Alternatively, C. Pedrini discussed the possibility of electronic transitions involving the impurity states and the matrix, i.e. the realization of the charge transfer process in CsI:Tl [Lecoq et al., 2006]. In present work we attempt to combine these three models into one general model that would explain luminescence properties of thallium and indium in CsI matrix.

Results on the luminescence spectroscopy of CsI:In and CsI:Tl crystals as a

function of temperature for different concentrations are presented in Chapter 3. A model of activator luminescence attempting to explain the observed properties is presented, grounding on those results.

1.5 Summary

Summarizing the discussion of the scintillation stages in Chapter 1 allows stating the following physical problem. Even though the general trends in energy relaxation processes of CsI:A are known, the impact of each process is unclear. Influence of the system parameters and measurement conditions (activator concentration, temperature etc.) on the pathways of energy relaxation is also a subject for study. High efficiency of the intrinsic luminescence in pure CsI at LNT (see Table 1.1) arises the question about the origin of the energy losses in activated CsI scintillators at RT, and whether or not their light yield can be improved.

Table 1.1: *Light Yield of CsI based scintillators*

Crystal	Activator, % mol	Temperature, K	LY, photons/MeV
CsI pure	-	<80K	107 000[a]
CsI:Tl	0.1	300K	55 000[b]
CsI:Nal	0.015	300K	45 000[c]

a - [Moszynski et al., 2003], b - [Holl et al., 1988, Moszynski et al., 1997], c - [de Haas and Dorenbos, 2008]

High scintillation efficiency of STE emission in CsI pure can be in part explained by self-trapping of holes. At temperatures below the hole delocalization peak (about 90K for CsI) the thermalized holes instantly become self-trapped, awaiting an electron. Electron capture results in STE creation and its subsequent radiative recombination. Electron capture radius by the self-trapped holes R_{Ons} in this case is rather high, of the order of 100 nm (at T=30K), which is comparable to the mean free path of electrons.

However, despite high STE luminescence efficiency in CsI, light yield of activated CsI crystals at room temperature is considerably lower (Table 1.1). From general considerations described above, efficiency of the creation of electronic excitations β should not be depend significantly on the presence of the activator impurities.

Besides, given the measured light yield of pure CsI, the energy of creation of one e-h pair can be estimated as 1.6 E_g. This value is very close to the estimated fundamental limit of 1.4 E_g [Vasil'ev and Michailin, 1986]. Thus, it can be assumed that the energy loss in the activated crystals occur at stage S and Q. Hence the dynamics of energy relaxation and loss channels in CsI:A to be investigated for thermalized excitations.

Study of possible channels of energy loss in activated CsI based crystals, as well as the possibility of increasing the scintillation yield in CsI based scintillators is the aim of this work. Interactions of electron excitations at each relaxation stage usually cannot be measured directly. This is why an integrated approaches to find the solution to this problem is required.

• On the one hand, search for an alternative activator for CsI seems reasonable. This could provide more efficient radiative recombination of electron excitations in the material. There are some general criteria for the selection of the activator. Firstly, the activator defects created in the crystal should act as trapping centers of charge carriers, as well as centers of radiative relaxation. Secondly, the activator must have a high segregation coefficient in the crystal matrix, in order to reach a sufficient activator concentration. Effective recombination energy transfer from the matrix to the activator luminescence centers is also important. Overall, In^+ ions can be efficient activator for CsI.

• On the other hand, a comprehensive study of energy relaxation processes in these systems is needed. It includes the study of energy transfer processes of from the matrix to the activator, and the efficiency of the intrinsic activator relaxation channels as a function of temperature and activator concentration. Migration of electron excitations in the crystal, along with the parameters of charge trapping by the emission center should be investigated. Such studies can be carried out using spectroscopy methods. In particular, time-resolved spectroscopy under different excitation energy should be used. Thermally stimulated luminescence methods allow to obtain the parameters of the electronic excitation localization at the activator and intrinsic traps. As a consequence, CsI:Tl and CsI:In crystals were chosen for this investigation. Synthesis and basic optical properties of the CsI:A crystals grown for the investigation are described in Chapter 2. This chapter also contains a description of the experimental methods used.

Chapter 2

Materials and experimental methods

Contents

2.1 Investigated scintillation materials 22
2.1.1 Synthesis of CsI: Tl and CsI: In single crystals 22
2.1.2 Physico-chemical properties of CsI:Tl and CsI:In 25
2.2 Experimental techniques and equipment 27
2.2.1 Fluorescence spectroscopy of the activator centers 27
2.2.2 Synchrotron irradiation and VUV spectroscopy 28
2.2.3 Scintillation yield. Temperature dependence 29
2.2.4 Thermally stimulated luminescence 31
2.2.5 Experimental data treatment and mathematical modeling 32
2.3 Conclusions 32

This chapter describes the methods of synthesis of CsI:Tl and CsI:In single crystal, and their physico-chemical properties. Concentration series of CsI:In and CsI:Tl single crystals were grown from the melt by the Bridgman and the Czochralski technique. General characterization of the optical properties of the prepared samples is provided. Experimental techniques and equipment used in the investigation are discussed. Steady state fluorescence spectroscopy used for the study of luminescent properties of the activator centers in CsI:A.

2.1 Investigated scintillation materials

CsI crystals belong to the class of alkali halides. These are ionic crystals, which dictates many of their physico-chemical properties. CsI crystals are soft at 300K, and they have no cleavage planes, which makes it difficult to create a flat polished surface. Slight hygroscopicity of CsI crystals is mostly related to surface carbonization in air. Crystals of pure CsI are quite common scintillation materials thanking to the fast UV luminescence band arising when exposed to ionizing radiation. It is used in high energy physics experiments. Although scintillation efficiency of this emission is quite low at RT. A number of activator impurities can be used to create luminescence centers in CsI, such as Tl, Na, CO_3 [Sci, 2014]. Bulk CsI crystals are normally grown from the melt, using the Bridgman-Stockbarger or the Czochralski method. For present study crystals of CsI pure, concentration series of CsI:Tl, and CsI:In were grown.

2.1.1 Synthesis of CsI: Tl and CsI: In single crystals

Investigation of the activator role in energy relaxation processes requires a series of experimental samples including pure CsI and activator crystal with concentrations ranging from 10^{-4} to 10^{-1} % mol. To synthesize concentration series of CsI:Tl and CsI:In single crystals the Bridgman-Stockbarger method (the Bridgman method from here on) and the Czochralski technique were used. The crystals were grown form the melt using purified powdery CsI (5N), granulated InI (4N) and TlI (4N) as raw materials.

The Bridgman technique is a well-known and commonly used crystal growth method, which is successfully applied for synthesis of alkali halide scintillation crystals. It is technically simple and convenient for growth of experimental series of crystals in the laboratory, so it was applied for CsI:In growth. One of peculiarities of the Bridgman method is inhomogeneity of the activator distribution along the crystalline ingot. Segregation of impurity in the crystal mostly depends on its valency and its ionic radius with respect to the host ions. In case of CsI activation with indium or thallium, the activator ions substitute for cesium taking the same valency. So activator segregation in CsI:A is limited by the difference in the ionic radii between Cs^+ (1.74$\mathring{A}$) and Tl^+ (1.59$\mathring{A}$) or In^+ (1.4–1.5$\mathring{A}$) ions. Equilibrium activator distribution between the crystal and the melt (often referred as the segregation

coefficient) is defined by equation:

$$K = \frac{C_{crystal}}{C_{melt}}, \tag{2.1}$$

where $C_{crystal}$ is activator concentration in the solidified phase, and C_{melt} is its content it the liquid phase. Usually $K < 1$, this is why during the crystal growth process activator impurity is pushed into the liquid phase. Consequently, activator concentration in the melt increases. In most cases of using the Bridgman technique activator concentration in the melt cannot be controlled during the growth. In this way activator concentration in the ingot also increases as it grows up. Activator concentration along the Bridgman grown crystal can be estimated by the following equation:

$$C_{crystal} = \frac{KC_0}{(1-x)^{1-K}}, \tag{2.2}$$

where C_0 is initial activator concentration in the melt, and x is the fraction of the melt solidified. Illustration of this dependence for several K values is provided in Fig. 2.1.

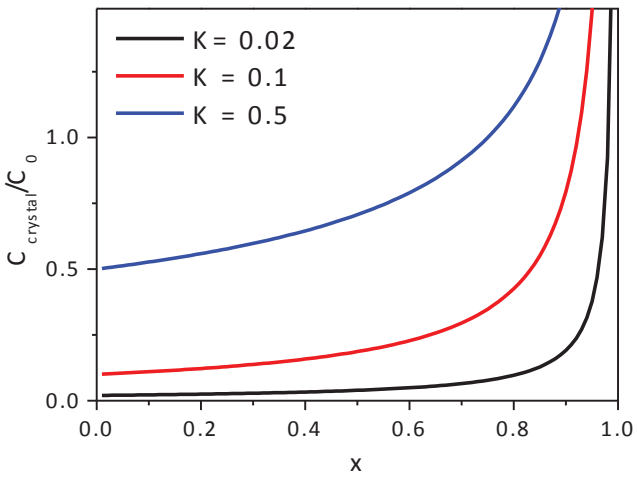

Figure 2.1: *Ratio of the activator concentration in crystal to its initial content in melt as a function of solidified fraction of the melt*

We see that in the beginning of crystallization the activator concentration does not change much, whereas at the end of the ingot it becomes larger, exceeding the initial activator fraction in the melt C_0. Relative increase of the activator content in the end of the crystalline ingot is larger for impurities with lower segregation coefficients K (see Fig. 2.1).

If the impurity is strongly non-isomorphic to the host element (usually when the difference in the ionic radii is more than 10-15%), it does not create a solid solution with the host matrix. This corresponds to the case of low K values in Fig. 2.1. In this case increase of the activator concentration leads to clusterization of the activator, like for example in CsI:Na [Rozenberg et al., 1974].

CsI:In series of crystal samples grown by the Bridgman method were obtained in the following way. Raw materials in necessary proportions were mixed together and put into quartz ampoules. Considering slight hygroscopicity of CsI, a drying procedure was applied. The ampules were put into a drying furnace and connected to a vacuum pumping system. The raw materials were being dried up with continuous heating up to 300C. After the drying procedure, the ampules with powders were vacuum sealed. Afterwards the sealed ampules were put into a growing furnace with two thermal zones, the topper of which was heated up to 670C (50C above the melting point of CsI). Pulling the ampule with the melt from the overheated topper zone to the bottom zone led to crystallization of the melt. The crystals were grown with the pulling rate of 1 mm/hour. Grown crystals were cooled down slowly, with a cooling rate of 20 K/hour, in order to avoid mechanical stress. A Bridgman grown CsI:In crystal is presented in Fig. 2.2. The grown crystals were cut into cylindrical pieces tangentially to the growth direction to make sure activator concentration is the same in within the sample.

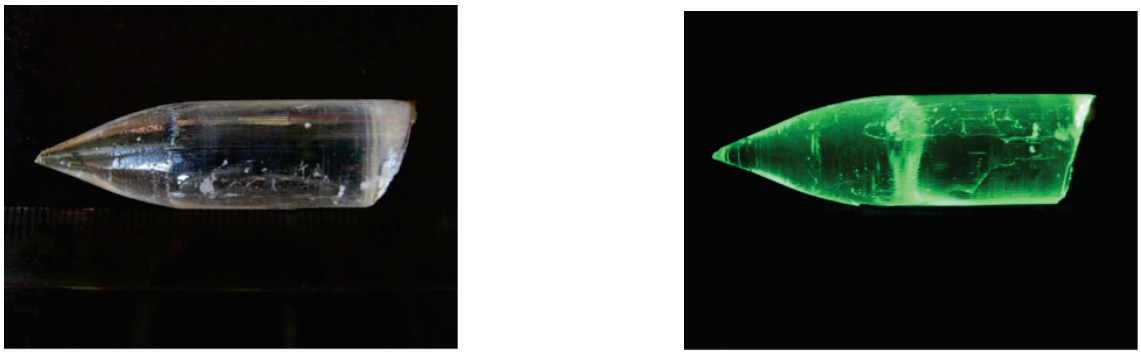

(a) (b)

Figure 2.2: *CsI:In single crystal under day light (a) and under UV light (b)*

For CsI:Tl concentration series synthesis a standard Czochralski method was used [Zaslavsky, 1999]. The experimental setup used here allows adding granulated TlI activator during the crystal growth. In this way activator concentration along the crystal can be controlled during the growth. To obtain a concentration series

of CsI:Tl the activator amount was increased after crystallization started. Consequently, the topper part of the boul contains less of Tl, and its concentration increases along the vertical axis (Fig. 2.3).

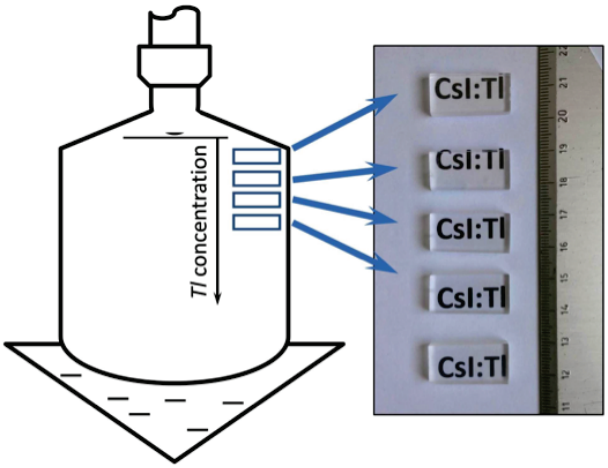

Figure 2.3: *Concentration series of CsI:Tl crystals grown by the Czochralski technique*

The crystalline ingots obtained were cut into suitable pieces by a wet wire, and polished to an optical quality. CsI:In crystals grown by the Bridgman method were cut normally to the growth axis, to assure homogeneity of the activator in each piece. Concentration of the activator in the samples was determined by inductively coupled plasma atomic emission spectroscopy.

To determine the segregation coefficient of indium in CsI, the conical part of the crystal ingot was used. It allows to assume that the activator content is more or less the same within the sample (see Fig. 2.1). The activator impurity segregation coefficient in CsI:In was found to be around 0.15. For Tl activated crystals it is known to be about 0.2-0.3. This difference can be explained by the difference in ionic radii between the two activator ions.

2.1.2 Physico-chemical properties of CsI:Tl and CsI:In

Concentration of some oxygen containing impurities in crystals can be estimated using the IR spectroscopy method. IR absorption spectra of CsI:In crystals are presented in Fig. 2.4. The measurement was done on 15-20mm long samples in order to minimize the impact of the surface defects. According to this graph, presence of CH_3^-, CNO^-, NH_4^+, NO_3^- and some other radicals can be testified. Their

concentration, however, can be estimated as $\leq 10^{-4}$ mol %, which is consistent with the purity of the initial row materials.

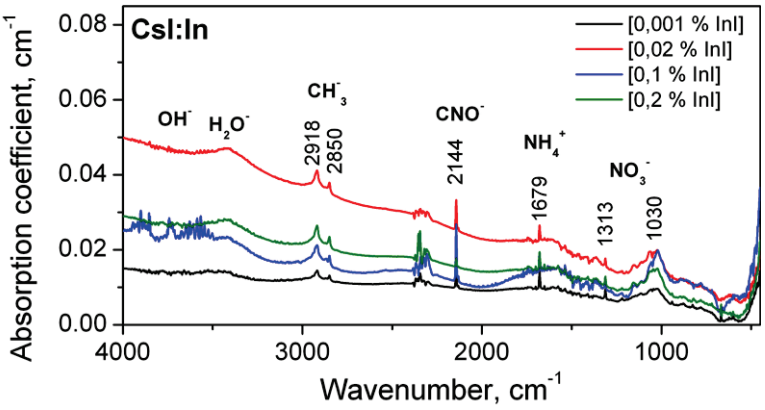

Figure 2.4: *IR absorption spectra of CsI:In crystals with different activator concentrations*

Induced absorption due to creation of color center was observed for CsI:In crystals in [Michal'chenko et al., 1966]. Radiation hardness of the CsI:In crystals grown by us has been investigated by means of absorption spectroscopy after exposure to different radiation sources. First of all it should be noted that the exposure of the samples to the day light ($> 360nm$, for 12 hours) and to UV photons (254 nm, Hg-lamp, $\sim$1 hour) does not lead to any coloration of CsI:In crystals. At the same time, exposure to X-ray irradiation induces some color centers formation in the samples with high indium content (0.03% mol. of In and above).

Absorption spectra of colored CsI:In samples manifest a set of overlapping bands in the visible and near IR regions (Fig. 2.5). The most intense bands are peaking around 518, 582-610, 800-900 nm. They were found to be unstable at RT, and slowly disappear during the crystals storage in the dark. Similar band structure in the absorption spectrum of the irradiated crystals was also observed in CsI:Tl crystals and was attributed to transitions in Tl^+ or Tl^0, localized in the vicinity of some vacancy defects [Trefilova et al., 2003]. Bands in the region of 800nm can be connected with F-type centers, distorted by the presence of the dopant ions [Chowdhury et al., 1999].

It is important to note that in CsI:In under X-ray irradiation the coloration occurs non-linearly with respect to activator concentrations. Induced absorption in CsI:In is important at 0.03% mol. of the activator or higher (see inset in Fig. 2.5).

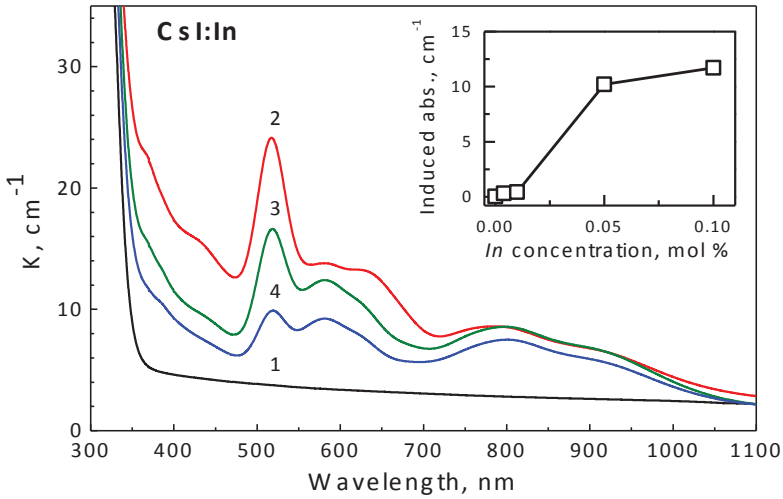

Figure 2.5: *Absorption spectra of CsI:0.05% In crystal: initial - (1), X-ray irradiated (300 Gy) - (2), after 1 day storage - (3), and after 3 days storage - (4) at room temperature. Inset: Induced absorption coefficient in CsI:In crystals at 420 nm after X-ray irradiation (300 Gy) as a function of indium concentration*

2.2 Experimental techniques and equipment

As it was mentioned in Chapter 1, comprehensive study of energy relaxation processes in CsI:A is required to understand the mechanisms of the energy loss and energy transfer. The investigation should include luminescence properties of the emission centers itself, efficiency of the energy transfer from the matrix to the luminescence centers, parameters of the charge carriers capture in CsI:A, and scintillation efficiency of the crystals. To do this investigation different fluorescence spectroscopy methods were used, including spectroscopy with time resolution, temperature variation, use of different excitation sources from UV energies to γ-rays.

2.2.1 Fluorescence spectroscopy of the activator centers

Fluorescence spectroscopy under photo excitation in the activator absorption region is used for investigation of the luminescent properties of the activator center in CsI:A. Excitation of the sample is realized using a Laser-Driven Light Source LDLS EQ-99CAL. It provides a single, continuous spectrum which covers the whole range from 200nm to 800nm. This source has larger irradiance in the UV spectral region that conventional Xe light sources. For light monochromatization double additive grating scanning monochromator Gemini 180 from Jobin Yvon was used. The spec-

trum of this excitation optical system is provided in Fig. 2.6. The calibration was done using a yellow lumogen phosphor in 190÷450nm spectral region, and a power meter for the remaining spectral range. The irradiance of the source is sufficient for CsI:A excitation in the activator absorption region (200÷360nm). For this kind of measurements polished 1-2mm thick samples were prepared. The 2nd and higher orders of diffraction were suppressed using cutoff optical filters. The emitted light from the sample was collected by Jobin Yvon-SPEX/Horiba Triax 320 Single Grating Monochromator/Spectrograph coupled with a CCD camera. This system allows taking excitation and emission maps with variable excitation energy shift.

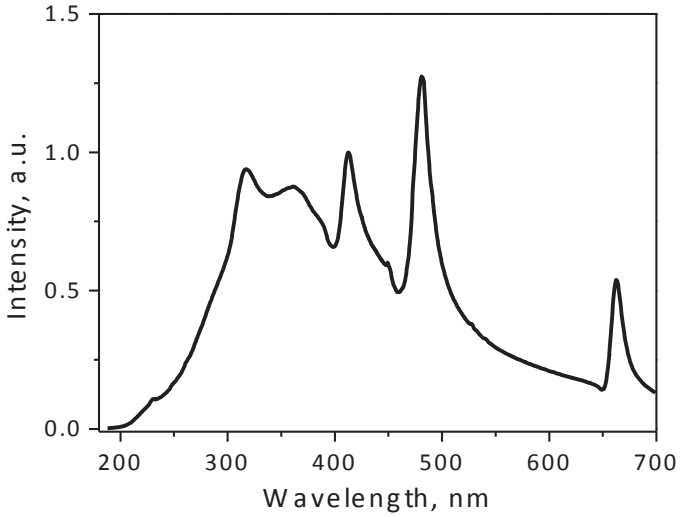

Figure 2.6: *The spectrum of the UV excitation optical system*

2.2.2 Synchrotron irradiation and VUV spectroscopy

VUV energy region is crucial for study of energy transfer processes in wide band gap insulators [Mikhailin, 1987, Mikhailin, 1995]. Analysis of the luminescence quantum yield around $E_g - 2E_g$ gives the idea about the type of energy transfer to the luminescence centers and its efficiency. Measurements of the luminescence excitation spectra were done at the SUPERLUMI setup at HASYLAB [Zimmerer, 2007](Fig. 2.7). This experimental setup provides a continuous UV – near VUV energy spectrum of synchrotron radiation.

The key aspects of measurements at SUPERLUMI station were as follows. Luminescence excitation spectra in 4eV to 30eV region were measured with aluminum diffraction grating. Sodium salicylate reference sample was measured to obtain the

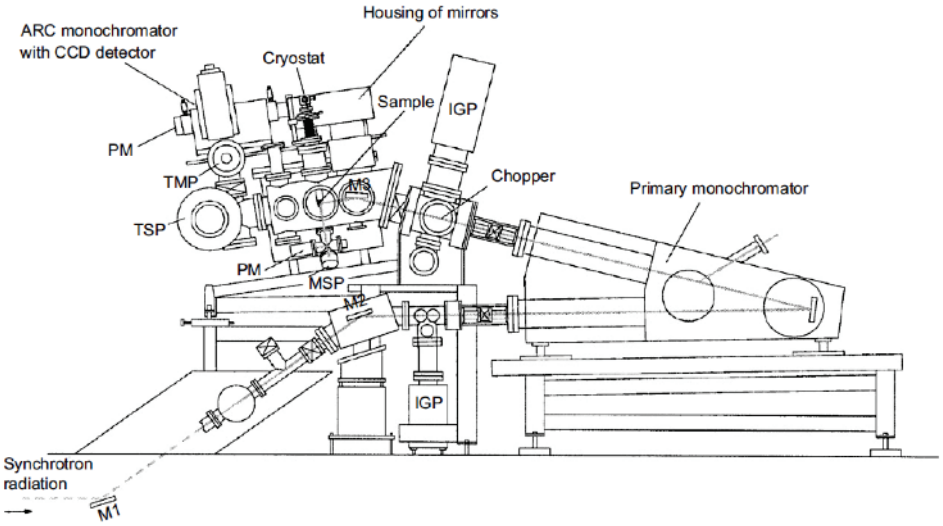

Figure 2.7: *Side view of the SUPERLUMI setup*

spectral distribution of the excitation light. Excitation in the fundamental absorption region is characterized by the absorption coefficient about $10^5 - 10^6\ cm^{-1}$. This means that electron excitations are created in the very surface layer about 10nm thick. In order to avoid the surface quenching and influence of the defects induced by polishing, CsI:A samples were cut to obtain fresh surface. Those 1-2mm thick samples were attached to the copper holder with some silver conductive paint. The setup allows working in $10 \div 350$K temperature range. SiO_2 and MgF_2 optical filters were introduced before the primary monochromator in order purify the excitation spectrum. Proper cutoff optical filters were used to avoid higher orders of diffraction in the secondary monochromator.

2.2.3 Scintillation yield. Temperature dependence

Scintillation yield measurements can be done using an ionizing radiation source, such as X-ray tube, radioactive isotopes, electron gun etc. Standard light yield measurements of scintillation crystals are typically done using ^{137}Cs radioactive isotope, emitting 662keV gamma quanta [Holl et al., 1988, Moszynski et al., 1997]. Such a technique was used for absolute light yield measurement of CsI:In (see Chapter 4). However, this method is limited in the light pulse integration time. In order to collect all the light emitted from the sample, a steady-state measurement should be done. Besides, scintillation yield measurements as a function of temperature require using some cryogenic or heating equipment. This is often inaccessible together with

standard scintillation measurement systems. On top of it, when it comes to comparison of the efficiency of two channels of radiative relaxation (as in our case, the intrinsic STE luminescence and the activator induced emission in CsI:A), luminescence spectroscopy is required. This is why X-ray excited luminescence spectroscopy method was used in this work in studies of CsI:A scintillation efficiency as a function of temperature.

X-ray excited luminescence was detected by an ANDOR Newton CCD with a Shamrock 500i spectrograph. A 150/300 diffraction grating was used. Spectral sensitivity of the Shamrock 500i spectrograph measured using the calibration source is presented in Fig. 2.8. This instrument response function allows comparing the intrinsic luminescence yield (the UV band around 340nm) with the activator luminescence yield (around 550nm in CsI:A). X-ray radiation is generated by an INEL XRG 3000 with a tungsten anode X-ray tube. The tube is operated at 35kV and 30mA. At these conditions, the radiation dose rate arriving on the samples can be estimated as ∼1 mGy/sec.

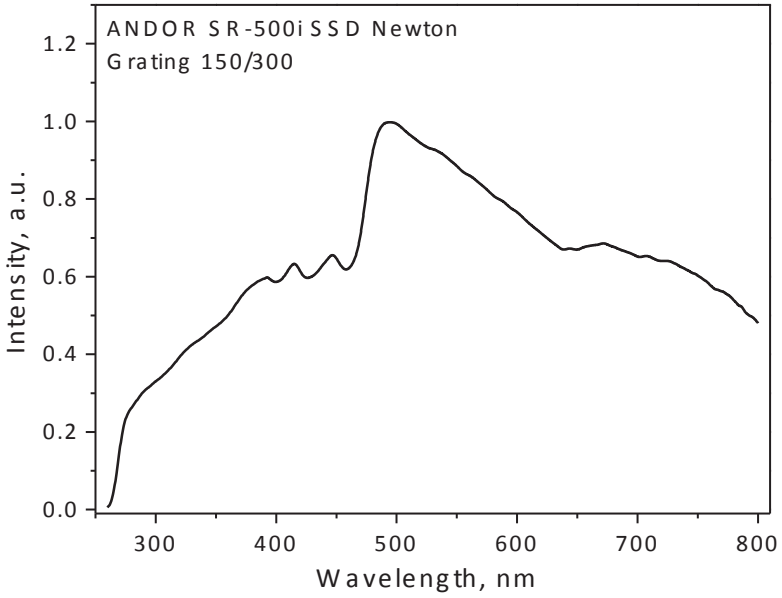

Figure 2.8: *Spectral sensitivity of the ANDOR Newton CCD coupled with Shamrock 500i spectrograph*

A closed-cycle helium cryostat was used to cool the samples. It allows measurements of X-ray excited temperature dependences between 10K and 310K. The temperature dependences of X-ray excited luminescence were measured under continuous irradiation during cooling. The cooling rate was 10K/min. Polished 1mm

thick samples were used. X-ray luminescence temperature dependences of CsI:A crystals above 300K were detected using LINKAM THMS600 Stage in the cooling mode. The cooling rate was 30 K/min. In addition, X-ray excited luminescence measurement as a function of time allows investigation of the persistent luminescence properties of CsI:A. Emission rise and afterglow measurements are done using a program-controlled shutter of the X-ray tube. These measurements verify presence of stable traps, which are important for scintillation applications.

2.2.4 Thermally stimulated luminescence

Method of thermally stimulated luminescence (TSL) is used to bring some useful information on the properties of various types of defects presented in CsI:A crystals [McKeever, 1985]. It concerns electron and hole traps associated with intrinsic or impurity induced defects in the crystal Fig. 2.9.

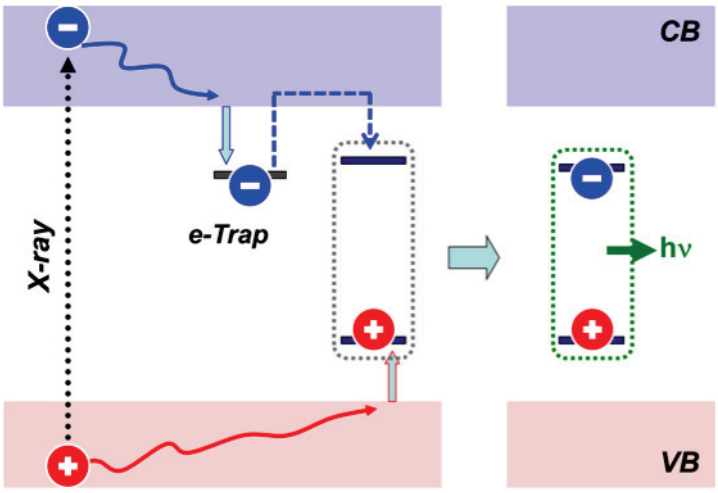

Figure 2.9: *Band model of electron trapping in a scintillator*

The important trap parameters one can obtain are the trap depth E, and the frequency factor s. Sometimes the average lifetime τ of the charge carrier at the trap can be also estimated. In present study initial rise method was used to obtain the trapping parameters for self-trapping of holes in CsI, and for activator related electron trap in CsI:Tl. This method assures quite accurate evaluation of the trap energy, when the trap is characterized by the first order kinetics [McKeever, 1985]. Parameters if the activator electron trap in CsI:In were obtained by fitting the corresponding glow peak with the May-Partridge general order kinetics expression for the TSL emission intensity.

2.2.5 Experimental data treatment and mathematical modeling

The experimental data obtained in the form of tables was processed and visualized graphically using data visualization software. The data treatment included: 1) account of the background and the dark noise of the instruments, 2) correction of the spectra using the instrumental response function, 3) extraction of the system parameters and characteristics by fitting of the experimental curves.

Radiation times of emission centers were obtained by fitting the luminescence decay curves with the expression of the radiative decay:

$$y = y_0 + A\ exp\left(\frac{-t}{\tau}\right), \tag{2.3}$$

where τ is the radiation time.

To get the peak maximum positions as well as full widths at half maximum (FWHM) of emission bands were fitted with Gaussian curves:

$$y = y_0 + \frac{A}{w\sqrt{\pi/2}} exp\left(-2\frac{(x-x_c)^2}{w^2}\right), \tag{2.4}$$

where $w = \frac{FWHM}{\sqrt{ln(4)}}$.

Trap parameters of activator centers in CsI:In were obtained by fitting the glow curve with the general order kinetics equation [McKeever, 1985]:

$$I(T) = n(0)s^{"} exp(\frac{-E_A}{kT}) \left[1 + \left(\frac{(b-1)s^{"}}{T'}\right) \int_{T_0}^{T} exp(\frac{-E_A}{kT})dT\right]^{b(b-1)} \tag{2.5}$$

where b is kinetic order, $n(0)$ – concentration of filled traps, s – frequency factor, E_A – trap depth, k – Boltzmann constant, T – temperature, T' – heating rate.

Mathematical modeling of energy relaxation processes in the systems under study was carried out in the "Mathematica 8" computational software. Numerical solution of the system of rate equations was found using NDSolve built-in algorithm.

2.3 Conclusions

Concentration series of CsI:In and CsI:Tl single crystals were grown from the melt using the Bridgman and the Czochralski methods, respectively. Activator concentration is ranging between 10^{-4} and 10^{-1} % mol. Presence of some oxygen containing

impurities was testified by IR spectroscopy means, however their concentration is $\leq 10^{-4}$% mol in the crystals. Color centers absorbing in the UV and VIS spectral regions can be induced in CsI:In under exposure to X-ray irradiation. These centers are unstable at RT, and their concentration is dependent on the activator content.

A comprehensive set of experimental methods has been chosen to investigate the energy relaxation and energy loss mechanisms in CsI:A scintillation materials. Fluorescence spectroscopy method under UV excitation is chosen for investigation of the activator centers properties in CsI:A. VUV spectroscopy under synchrotron irradiation is aimed to reveal the energy transfer efficiency form the crystalline matrix to the activator centers in CsI:A. Steady state and time resolved X-ray luminescence spectroscopy can provide information on the scintillation efficiency as a function of temperature and time. TSL analysis gives important information about the traps for charge carriers.

Use of all these methods together should allow obtain the necessary information of the electron excited states and their dynamics in CsI:A.

Chapter 3

Luminescent properties of In- and Tl- activated CsI crystals

Contents

3.1 Optical properties of Tl-like activator ions 36
3.1.1 Tl-like activator energy levels 36
3.1.2 Absorption spectra of Tl^+ and In^+ in CsI 37
3.2 Activator luminescence of CsI:In and CsI:Tl crystals . . 39
3.2.1 Excitation spectra from 200nm to 350nm at 15K 39
3.2.2 Time resolved spectroscopy 42
3.2.3 Temperature dependence of activator emission intensity . 43
3.3 Electron structure of the activator luminescence centers in CsI:In and CsI:Tl 46
3.3.1 Activator levels positioning in the forbidden band 46
3.3.2 Configuration diagrams of luminescent centers 48
3.4 Activator ionization in CsI:A 52
3.5 Conclusions 56

This chapter presents a spectroscopic study of the activator-related luminescence in CsI:In and CsI:Tl crystals. Even though both activator ions have the same s^2 electron configuration, their luminescent properties were found to be significantly different. To explain this difference, positions of the activator levels in the forbidden band of the crystal are considered. Electron transitions in the activator-induced luminescence centers of CsI:A are discussed using the configuration diagram model involving charge transfer states.

Thallium induced luminescence in CsI scintillator is quite intense under X-ray or γ-ray irradiation at 300K. Its scintillation efficiency explains use of CsI:Tl crystals in various scintillation applications. However, the origin of the 550nm emission band is still unclear. There are several models of emission centers suggested to explain radiative transition in CsI:Tl. In particular, the intense visible emission was ascribed to intracenter radiative relaxation of Tl ions [Masunaga et al., 1966, Sivasankar and Jacobs, 1985]. Accumulation of the experimental data on the fluorescence spectroscopy of CsI:Tl crystals led to a conclusion that the properties of the luminescence centers cannot be described using the simple ion model. The two visible emission bands were attributed to relaxation of Tl-perturbed self-trapped on-center and off-center excitons [Nagirnyi et al., 1994]. Still there has not been a configuration diagram model suggested so far, which would describe the electron transition in the activator induced centers of CsI:Tl.

Indium activated CsI crystals are much less investigated. Both Tl^+ and In^+ activator ions in CsI have equivalent electron configuration s^2, and one can expect them to have similar structure of emission centers. Comparative study of CsI:Tl and CsI:In spectroscopic properties is the key for the general understanding of the Tl-like luminescence centers structure in CsI:A.

3.1 Optical properties of Tl-like activator ions

3.1.1 Tl-like activator energy levels

Substituting for Cs^+ cation in CsI lattice, Tl- like ions have a valency of A^+ with the electron configuration s^2. For a free ion such electronic configuration is characterized by singlet ground state ^1S, singlet and triplet excited states ^1P and ^3P. The latter in result of the spin-orbit coupling is split into three excited electron levels: $^3P_0$, $^3P_1$ and $^3P_2$. Typical electron structure of a free Tl-like ion is shown in Fig. 3.1. In activator absorption spectra (as well as in activator luminescence excitation spectra) of crystals doped with Tl-like ions fine structure of the absorption bands is sometimes observed [Ranfagni et al., 1983]. This splitting of the degenerate levels associated with the Jahn-Teller effect, which is stronger for lighter ions.

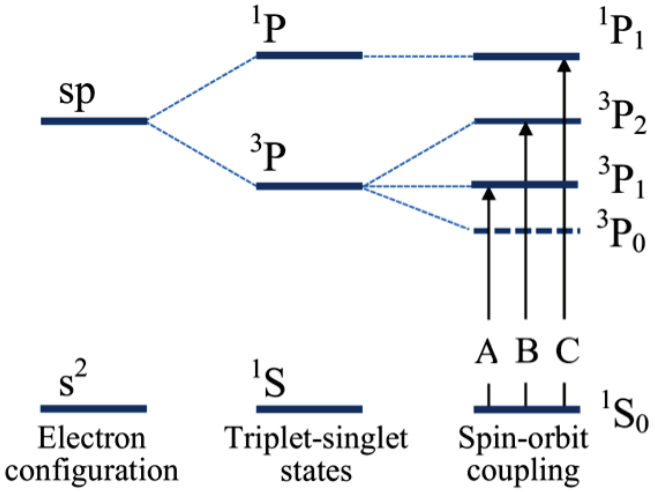

Figure 3.1: *Electron transitions in Tl-like ions according to [Ranfagni et al., 1983]*

3.1.2 Absorption spectra of Tl^+ and In^+ in CsI

The optical properties of thallium-like impurities in alkali-halide crystals were investigated in [Ranfagni et al., 1983] based on the absorption spectra. The only spin-allowed transitions are ${}^1S_0 \rightarrow {}^1P_1$ (C-band in the absorption spectrum). Electronic transitions ${}^1S_0 \rightarrow {}^3P_0$, and ${}^1S_0 \rightarrow {}^3P_2$ are spin-forbidden, and are forbidden for the total angular momentum J selection rule. However, the latter transitions (B-band in the absorption spectrum) are often observed in the absorption spectra as a weak band. The lowest energy absorption band (A-band) corresponds to ${}^1S_0 \rightarrow {}^3P_1$ transitions. They are spin-forbidden, but this band is quite intense due to the spin-orbit interaction, mixing the triplet and the singlet states.

Activator absorption spectra of CsI:In and CsI:Tl with different activator concentrations measured at 300K are shown in Fig. 3.2. The measurement was done using SPECORD 40 spectrophotometer. Polished $1 \div 2$mm thick samples were used. Practically all the researchers agree that CsI:In and CsI:Tl absorption around 4.0-4.8eV corresponds to electron transitions in the activator ions. It should be noted however, that the absorption spectrum of CsI:Tl crystal measured at LHeT contains up to 6 separate bands [Masunaga et al., 1966]. Maximum of the lowest energy absorption band (A-band) is shifted from 300nm to 290nm as temperature goes down from 300K to 10K. The maxima of the other bands do not significantly shift.

In the majority of Tl-like ions absorption spectra the C absorption band is the most intense, like in case of CsI:In (Fig. 3.2). However, in the absorption spectra of CsI:Tl absorption intensity at the C-band is comparable to that of the A-band.

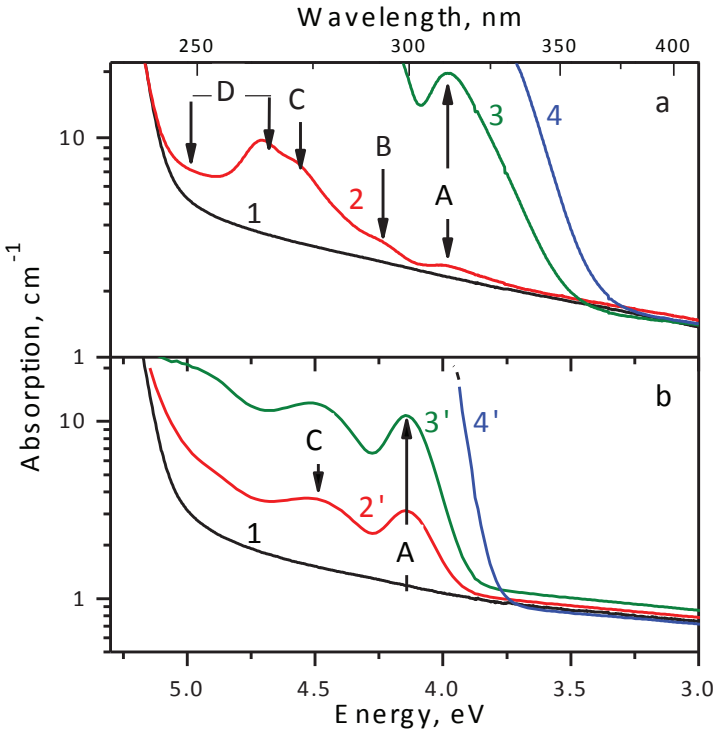

Figure 3.2: *Absorption spectra of CsI pure (curve 1);*
CsI:In (a): 2 - 10^{-4}% In, 3 - 0.005% In, 4 - 0.045% In;
CsI:Tl (b): 2' - 10^{-4}% Tl, 3' – 5×10^{-4}% Tl, 4' - 0,021% Tl

It is reasonable to assume that in the latter case there is stronger mixing with the singlet state or with the matrix states.

Electron transitions in the activator absorption is summarized in Table 3.1. Origin of the activator induced absorption at higher energies (around 4.8-5.3 eV) is less clear. There can be a few possible explanations to these transitions. First, transitions between the impurity ion and the matrix states (the charge transfer transitions discussed in Section 1.3) [Ranfagni et al., 1983], and activator ionization. Second, in this region transitions in CsI host are also possible (the Urbach tail), in presence of the impurity defects. Absorption of excitons perturbed by intrinsic or impurity defects can be also expected in this region.

When it comes to the activator emission, there is no satisfactory model of activator luminescence centers in CsI:Tl. One of the difficulties is that excitation of CsI:Tl crystal in the A-band gives rise to a set of bands in the luminescence spectrum, containing at least 4 bands [Nagirnyi et al., 1995, Nagirnyi et al., 1994, Sivasankar and Jacobs, 1985]. Therefore, it is concluded that the luminescent properties of CsI:Tl crystal cannot be explained only in terms of the activator ion electron

Table 3.1: *Activator transitions in CsI:In and CsI:Tl for LHeT based on [Masunaga et al., 1966, Sivasankar and Jacobs, 1985]*

Crystal:Ion	Band	Transition	WL, nm	Energy, eV	Selection Rules
CsI:In	A	${}^1S_0 \rightarrow {}^3P_1$	305	4.07	Spin forbidden
	B	${}^1S_0 \rightarrow {}^3P_2$	290	4.28	Spin forbidden, J-forbidden
	C	${}^1S_0 \rightarrow {}^1P_1$	270	4.59	Allowed
	D	CT	230-260	4.77-5.40	
CsI:Tl	A	${}^1S_0 \rightarrow {}^3P_1$	293	4.23	Spin forbidden
	B	${}^1S_0 \rightarrow {}^3P_2$	∼280	∼4.43	Spin forbidden, J-forbidden
	C	${}^1S_0 \rightarrow {}^1P_1$	275	4.50	Allowed

transitions. Still, there are several approaches to explain the origin of the visible and UV emission bands in CsI:Tl. In particular, according to the model of activator perturbed self-trapped exciton [Nagirnyi et al., 1994], the luminescence bands in the visible spectral region (peaking around 2.25eV and 2.55eV at LHeT) can be related to electron transitions in the on-center and off-center STE configurations perturbed by the impurity ion. Another model dealing with charge transfer state was first proposed by C. Pedrini [Lecoq et al., 2006]. According to him, the intense 2.25eV visible luminescence of CsI:Tl can be related to radiative recombination of either CT or BE state. Comparative investigation of emission centers in CsI:In and CsI:Tl by means of UV-VIS luminescence spectroscopy was done as a function of temperature for samples with different activator concentration. Analysis of CsI:In and CsI:Tl luminescence properties is presented in the following sections.

3.2 Activator luminescence of CsI:In and CsI:Tl crystals

3.2.1 Excitation spectra from 200nm to 350nm at 15K

In order to investigate the properties of the activator luminescence centers in CsI:A UV –VIS emission spectroscopy measurements were done as a function of temperature and the activator concentration. Fluorescence spectroscopy maps of CsI:A measured at 15K (Fig. 3.3) provides the most complete information on the elec-

tronic transitions in the activator centers.

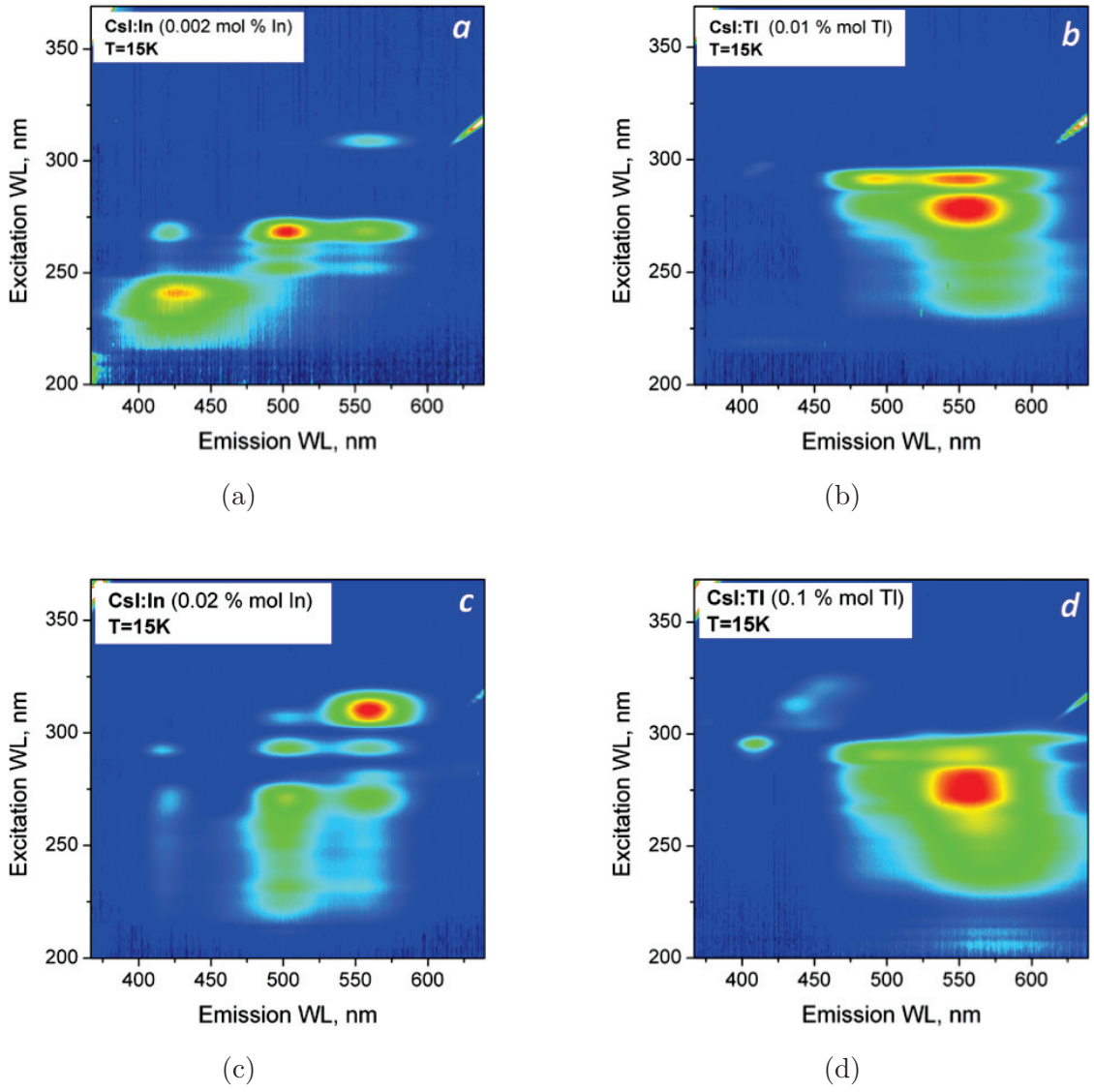

(a) (b)

(c) (d)

Figure 3.3: *Fluorescence spectroscopy maps of CsI:In (a, c) and CsI:Tl (b, d) activator emission under 200-360nm excitation at 15K*

Comparison of the fluorescence spectroscopy maps (Fig. 3.3) points to the following common features of CsI:Tl and CsI:In emission centers. Both activators produce two visible emission bands (peaking around 500nm and 550nm for CsI:In, and at 500nm and 560nm for the CsI:Tl), and there is also a UV band around 400-420nm. The observed set of three main UV and VIS bands in CsI:In and CsI:Tl is in agreement with observations of other researchers [Masunaga et al., 1966, Nagirnyi et al., 1995, Nikl et al., 1993, Simkin et al., 1984, Sivasankar and Jacobs, 1985,

Sivasankar et al., 1985]. However excitation of these bands is different for each of the activators.

In case of CsI:In crystals (Fig. 3.3 a,c) electron transitions are consistent with the scheme of the electron levels in Tl-like ions (Fig. 3.1). Excitation with low energy photons (around 310nm) gives rise to low energy emission band only (the 550nm emission). Increase of the excitation energy reveals the band at around 490nm, and the band around 420nm in CsI:In crystals (Fig. 3.3 a,c). Broad emission band around 400-450nm in slightly doped CsI:In sample (Fig. 3.3 a) excited only around 220-250nm is unrelated to the activator transitions. It could be caused by presence of some uncontrolled impurity traces such as CO_3^{2-}.

In case of CsI:Tl crystals (Fig. 3.3 b,d) all the three main emission bands are excited around the lowest energy A-absorption band at 295nm. In addition, emission band peaking around 400nm is excited only in the A-band of the activator absorption spectrum. When excitation energy is increased, only the two visible bands (490nm and 550nm) are present, but no band at 400nm.

Besides, increase of the activator concentration to 0.1% mol (see Fig. 3.3 d) leads to appearance of some additional emission bands in CsI:Tl. In particular, there are two band around 520nm and 600nm arising under excitation at the low energy side of A-band. Band around 600nm was also observed in [Sivasankar and Jacobs, 1985]. It was ascribe to $(Tl^+)_2$ dimer in view of sensitivity to thermal treatment of the sample. The weak band around 350nm in CsI:Tl emission was observed in [Nagirnyi et al., 1994] and [Nagirnyi et al., 1995] under excitation at the A absorption band. In Fig. 3.3 (d) it is clearly seen that the excitation energy of this band is shifter to longer wavelengths. It is excited at around (315-320)nm. Another group of band are emitting around (450-460)nm when excited at 320 nm. Their origin could also deal with creation of complex Tl-containing clusters. Otherwise, this emission can be related to radiative transitions from $^3P_0$ activator level to $^1S_0$ ground state.

Let us consider excitation spectra for each emission band separately. Simple 2-dimentional excitation spectra can be obtained integrating the segments of the emission spectra for all the excitation energies ranging from 200nm to 360nm (Fig. 3.4 a, b). This figure shows that CsI:Tl emission band peaking at 400nm (Fig. 3.4 b) is excited only around 297nm. While excitation of 490nm and 560nm activator luminescence bands occurs almost along all the activator absorption range. In the case of CsI:In (Fig. 3.4 a) activator luminescence bands 500nm and 550nm excited at

all the absorption bands, starting from the A-band (308nm at 15K). However, the 400nm emission band is excited starting only from the B absorption band (290nm in CsI:In). Besides, 400nm emission band excitation is quite efficient at C- and D-absorption bands as well.

3.2.2 Time resolved spectroscopy

Fluorescence spectroscopy measurements of CsI:In and CsI:Tl emission gives the information about the decay time of the emission bands (Fig. 3.5). Here the fluorescence is monitored depending on time delay after an excitation pulse.

For CsI:In crystal fluorescence spectra with time resolution (Fig. 3.5 a) were obtained at SUPERLUMI station described in Section 2.2.2. Entire integration time (Total) makes up to 200ns, whereas in the Fast component the time gate was about 20ns after the excitation pulse. Emission band at 420nm in CsI:In contains larger fraction of Fast component than the other bands. Therefore in view of its fast decay time it can be associated with fully allowed radiative transitions $^1P_1 \rightarrow ^1 S_0$ in In^+ activator ion.

Time resolved fluorescence spectra of CsI:Tl (Fig. 3.5 b) were measured under pulsed Nd:YAG laser excitation. An Intensified CCD camera with a delay generator was used for detection. As one can see from the Figure, excitation around C absorption band gives rise to two visible emission bands at 490nm and 550nm. Emission band around 400nm is not manifested in this spectrum, which is consistent with its excitation spectrum (Fig. 3.4 d,f). In this case the time gate for the Fast component is set to (10-100)ns after the excitation pulse. Emission band around 550nm contains mostly fast decay component. The Slow (150-2000)ns and the UltraSlow (2000-10000)ns components are composed of the both 490nm and 550nm bands. Intensity ratio of these two bands does not significantly change from Slow to UltraSlow. High impact or the Fast decay component in 550nm band indicates allowed transitions. This result is important for building a configuration diagram for CsI:Tl (see Section 3.3.2).

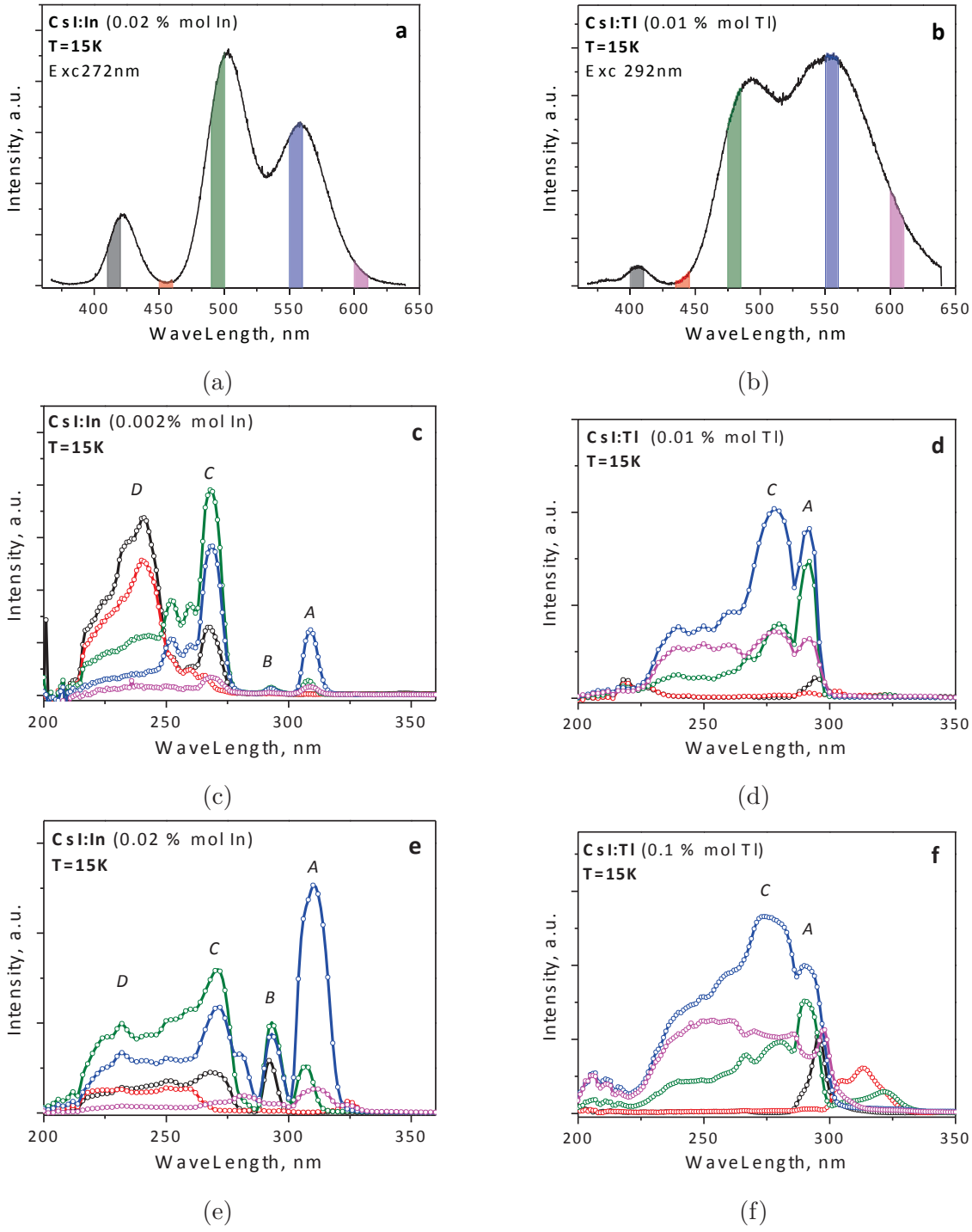

Figure 3.4: *Activator luminescence spectra of CsI:In under 272nm excitation (a), and CsI:Tl under 292nm excitation (b) measured at 15 K. Excitation spectra of CsI:In activator luminescence (c, e) and CsI:Tl crystal (d, f) for the respective segments of the emission bands*

3.2.3 Temperature dependence of activator emission intensity

As noted above, emission spectra of CsI:Tl and CsI:In crystals under A-band excitation and C-band excitation are significantly different. In CsI:Tl 400nm emission

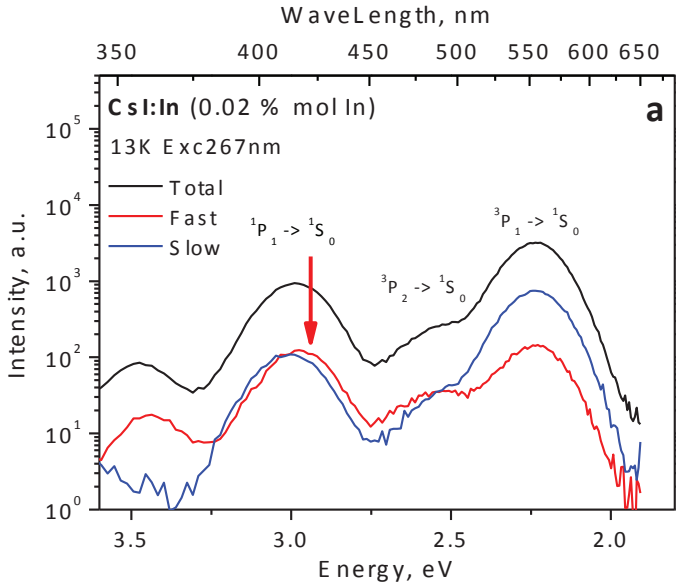

(a)

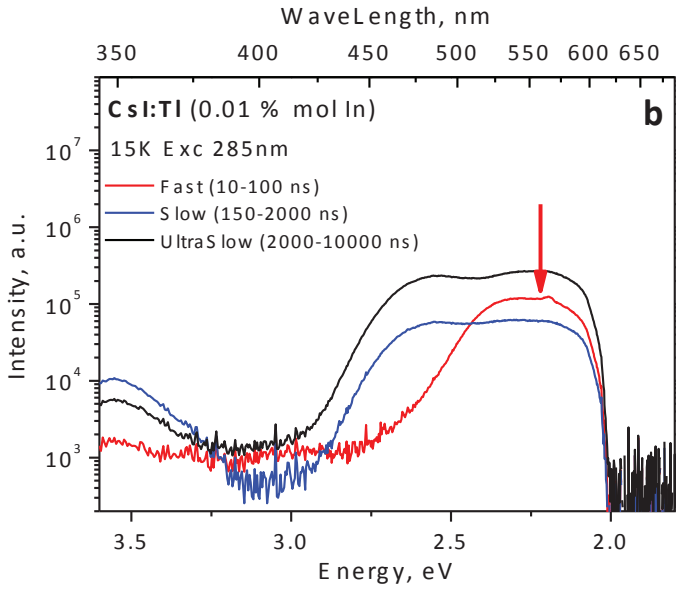

(b)

Figure 3.5: *Time resolved emission spectra of CsI:In (a) and CsI:Tl (b) under excitation around C absorption band. Red arrows point at the bands with fast decay component*

band is pronounced only if excited at the low energy edge of the A absorption band (see Fig. 3.4 d, f). On the contrary, A-band excitation in case of CsI:In gives rise to visible luminescence bands at 500 and 550 nm (Fig. 3.4).

Let us consider temperature dependence of the activator band emission intensity of both systems under A-band and C-band excitation. Corresponding CsI:Tl and

CsI:In emission spectra under A-band excitation as a function of temperature are presented in Fig. 3.6 (a,b). As temperature goes down from 300K to 15K, the intensity of 400nm emission in CsI:Tl starts increasing (Fig. 3.6 a). The 400nm band reaches its maximum intensity at around 100K. Then with further temperature decrease it starts quenching. In the case of CsI:In (Fig. 3.6 b), quenching of visible emission (bands 500nm and 550nm) is also observed when approaching the LHeT.

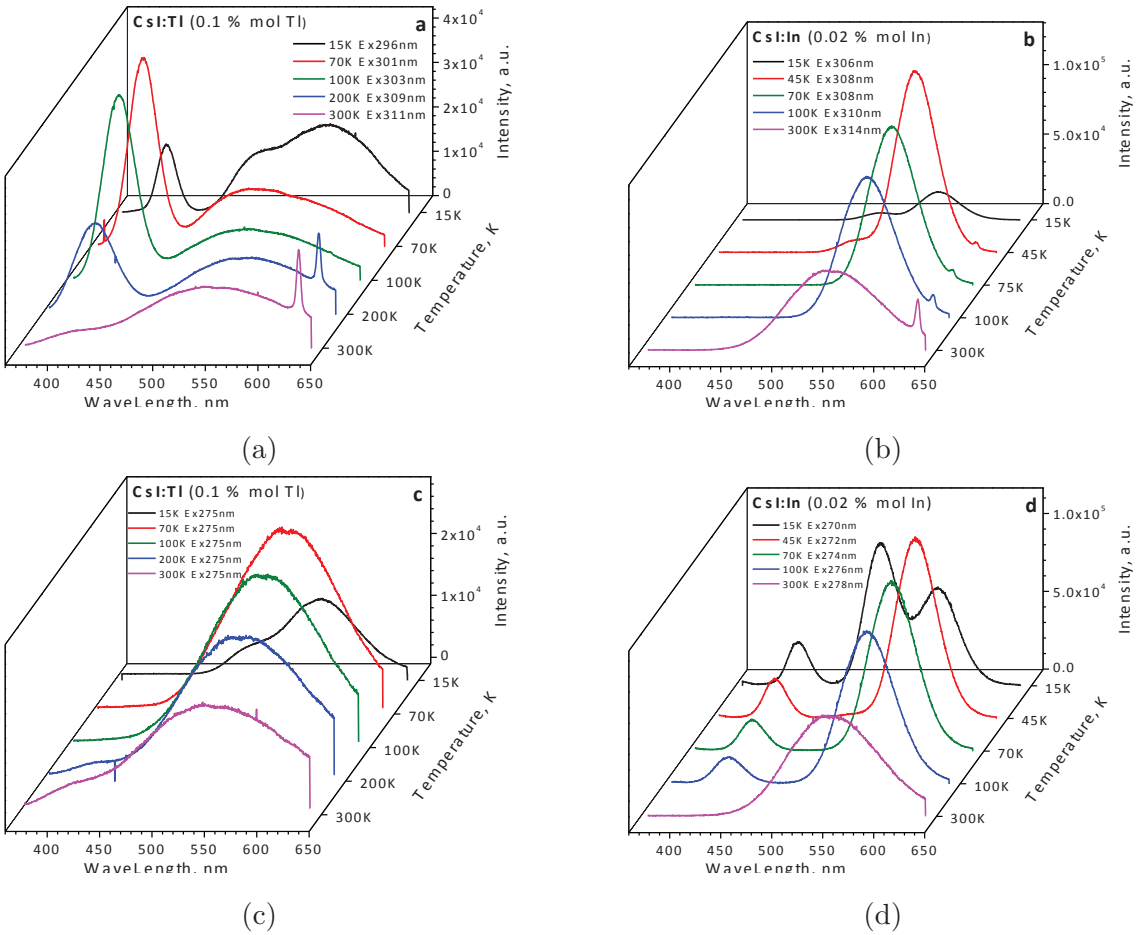

Figure 3.6: *CsI:Tl (a,c) and CsI:In (b,d) emission spectra as a function of temperature*

Spectral composition of CsI:Tl and CsI:In emission under excitation at C-band are also quite different (Fig. 3.6 c,d). In CsI:Tl emission spectra only visible emission is present. At 15K two bands peaking at 490nm and 550nm can be clearly distinguished (Fig. 3.6 c), but no band at 400nm is present. In CsI:In emission spectra (Fig. 3.6 d) at low temperatures 420nm band arises. At 15K all the three main bands are observed, around 420nm, 490nm and 550nm. Indium emission intensity at C-band excitation does not drop at 15K, in contrast with A-band excitation.

Radiative transitions in CsI:A, as well as decrease of the activator emission intensity at low temperatures can be explained using the model of configuration diagrams (see Section 4.4.).

3.3 Electron structure of the activator luminescence centers in CsI:In and CsI:Tl

3.3.1 Activator levels positioning in the forbidden band

Relative positions of the excited electron state and the ground state of the activator ions can be determined based on the activator absorption spectra. Activator levels positioning relative to the band gap of the crystal is less obvious. Nevertheless, let us try to propose a scheme of the activator electron levels in CsI based on the experimental results available. In the case of CsI:In A, B and C absorption bands are clearly manifested in the absorption spectra at LHeT [Sivasankar et al., 1985] (Fig. 3.7 a).

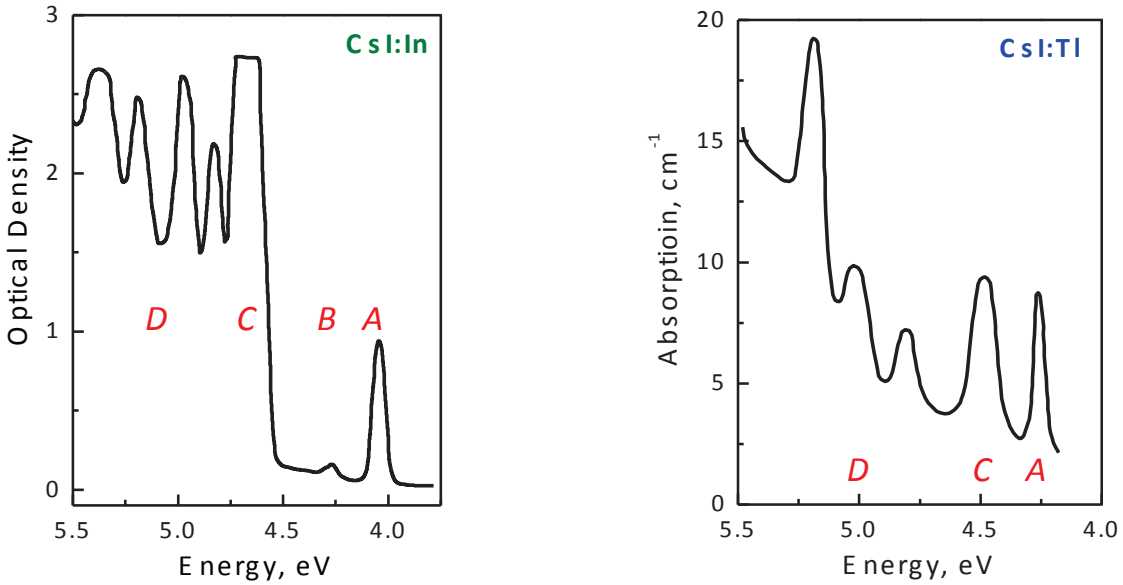

(a) (b)

Figure 3.7: *CsI:In (a) and CsI:Tl (b) absorption spectra measured at LHeT from [Masunaga et al., 1966, Sivasankar et al., 1985]*

The D-band in the absorption can be related to electron transitions from the activator to the conduction band of the matrix (charge transfer transitions). Keep

in mind that the C-band in the absorption spectra of CsI:In is related to ${}^1S_0 \rightarrow {}^1P_1$ transitions. Thus, ${}^1P_1$ indium level should be directly under the bottom of the conduction band of CsI (Fig. 3.8 a). In the case of CsI:Tl activator absorption spectrum contains at least 6 separate bands [Masunaga et al., 1966]. The entire absorption spectrum in this case is situated on a pedestal (Fig. 3.7 b). Besides, in CsI: Tl crystals A-band has a complex structure.

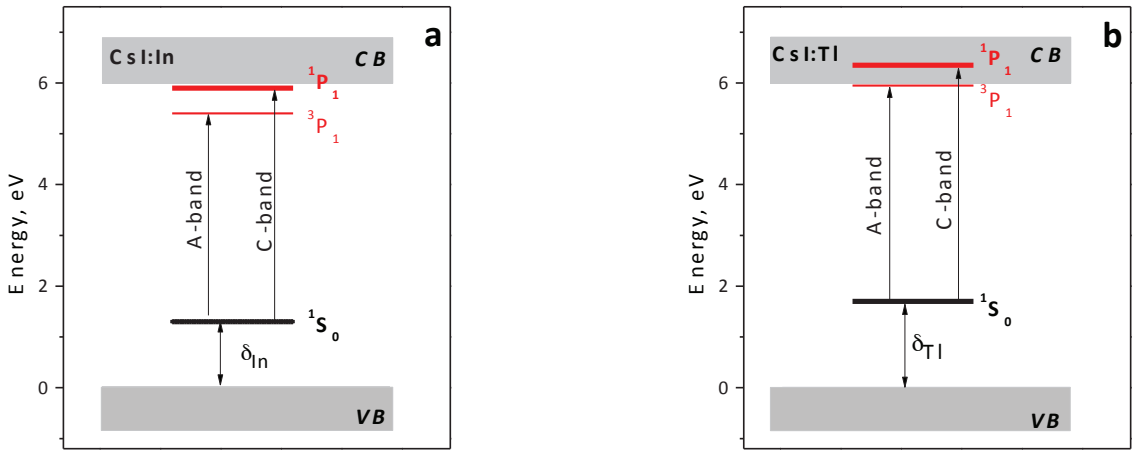

(a) (b)

Figure 3.8: *Band diagrams of activator electron levels of In^+ (a) and Tl^+ (b) ions relative to forbidden energy gap of CsI*

So there are several key arguments that excited Tl^+ levels are overlapping with the conduction band of CsI, which are based on the absorption and fluorescence spectroscopy data:

• Absorption spectrum of CsI:Tl (Fig. 3.7 b) has an intense pedestal starting with the lowest energy A absorption band. Indium related absorption bands for example are resolved much better (Fig. 3.7 a). Besides, Tl^+ ions in different host matrixes with larger band gap have well resolved absorption bands at LHeT, too [Ranfagni et al., 1983].

• Absorption coefficients of A and C bands in CsI:Tl absorption spectra have close values (see Fig. 3.7 b, and Fig. 3.2 b), even though ${}^1S_0 \rightarrow {}^3P_1$ transition corresponding to A-band is spin forbidden. Besides C band in thallium absorption spectra is broader that A-band. This fact suggests an overlap of the activator level corresponding to C band transitions with the states of the conduction band.

• According to fluorescence spectroscopy measurements (Fig. 3.3 and Fig. 3.4) A band has complex structure. CsI:Tl excitation at the low energy side of this

band leads to 400nm emission band only. Slight increase of the excitation energy gives rise to the two visible bands at 490nm and 550nm, whereas 400nm emission disappears completely. This observation suggests that $^3P_1$ thallium level should be exactly under the very bottom of the conduction band of CsI.

These considerations allow positioning of the excited $^3P_1$ Tl^+ state at the bottom of CsI conduction band. Positions of Tl^+ electron levels in CsI are shown in Fig. 3.8 b.

Distance to the activator levels from the top of the valence band is provided in Table 3.2. Thus, the Tl^+ $^1S_0$ ground state lever appears to be higher, that the one of In^+. Indeed, Tl^+ ion has an extra electron shell given the $6s^2$ electron configuration (compared with $5s^2$ electron configuration of In^+). Consequently, thallium ground state should be higher in energy than the one of indium.

Table 3.2: *Positions (in eV) of In^+ and Tl^+ levels from the top of the valence in Fig. 3.8*

Activator	E_g (CsI)	$^1S_0$	$^3P_1$	$^1P_1$
In^+	6.0 eV (CsI)	1.3	5.4	5.9
Tl^+	6.0 eV (CsI)	1.75	5.95	6.25

It is worthy to note here that activator $^3P_1$ levels have different energy depth in CsI:In and CsI:Tl (Fig. 3.8). This is consistent with the parameters of electron capture by the activator centers. As shown in Section 4.2, parameters of the electron capture activator centers can be determined from the glow curve analysis.

As excited activator levels in CsI:A are situated closely to the conduction band, activator ionization can be expected under UV excitation. Spectroscopic effects testifying activator ionization in CsI:A are discussed in Section 3.4.

3.3.2 Configuration diagrams of luminescent centers

As can be seen from Fig. 3.3, CsI:In and CsI:Tl crystals have a similar set of emission bands, arising under UV excitation in the activator absorption region. In the visible region there are two emission bands peaking around 500nm and 550nm. There is also emission band at 400nm, intensity of which increases as temperature goes down. Nevertheless, excitation spectra of these emission bands are different for CsI:In and CsI:Tl crystals. In particular, 400nm emission band of CsI:Tl can be excited only at

the low energy edge of the A absorption band. In the case of CsI:In 400 nm emission is excited mainly around the C absorption band. Excitation at the A-band in CsI:In crystals gives rise mainly to the activator emission band at 550nm.

In addition, as one can see in Fig. 3.6, there are some peculiarities in temperature dependence of the luminescence intensity under A-band excitation. In particular, CsI:In integrated intensity does not change considerably as temperature goes from 300K down to the LHeT. However, at T = 15K (see Fig. 3.6 b) visible emission intensity decreases sharply. In the case of CsI:Tl (see. Fig. 3.6 a) with temperature decrease, redistribution of intensity between the UV (400nm) and visible (500nm and 550nm) luminescence bands occurs. At 300K, 400nm band of CsI:Tl is virtually absent. There is only the intense visible luminescence band at around 550nm. Further, as temperature goes down, 400nm band intensity starts to increase. This increase is accompanied by a slight drop of the visible emission band. At LHeT (15K) 400nm band emission intensity of CsI:Tl falls down again. This goes with a certain increase of the visible emission bands.

These essential peculiarities of luminescent properties in CsI:Tl and CsI:In activator centers can be explained using a diagram of configuration curves. Corresponding configuration diagrams for CsI:In and CsI:Tl radiative transitions are presented in Fig. 3.8. Let us focus on the interpretation of activator-induced electron transitions in CsI:A using the diagrams in Fig. 3.9.

When it comes to CsI:In crystals, the activator induced electron transitions can be explained using the simple ion model (see Fig. 3.9 a). When CsI:In crystals are excited with photons of 310nm (A absorption band), $^3P_1$ electron state of the activator ion is filled. Radiative relaxation of this state (radiative transition to the ground state) gives rise to 550nm luminescence band. In this case, if temperature is high enough, thermally activated filling of $^3P_2$ level is also possible. Radiative electron transition from this excited state to the ground state results in emission of 490nm photons. Both of these bands are pronounced at low temperature in CsI:In luminescence spectra (Fig. 3.3 a,c). Non-radiative transition from $^3P_2$ to $^3P_1$ is also possible. As a result, excitation at the B absorption band gives both 490nm and 550nm emission bands. Further increase of the excitation energy activates the electron transitions to $^1P_1$ excited level (C absorption band). In CsI:In luminescence spectra there is also a band with a maximum around 400nm. It can be associated with $^1P_1 \rightarrow ^1 S_0$ activator relaxation. This band has mostly fast decay component

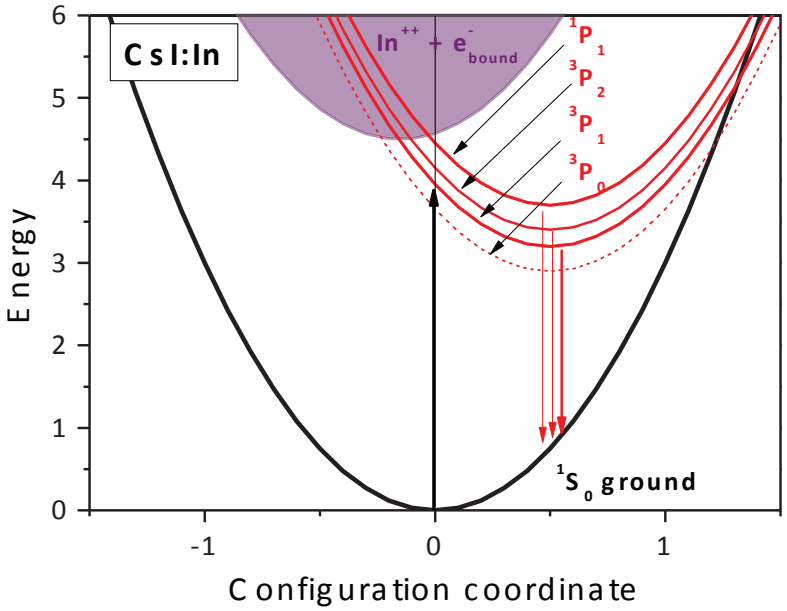

(a)

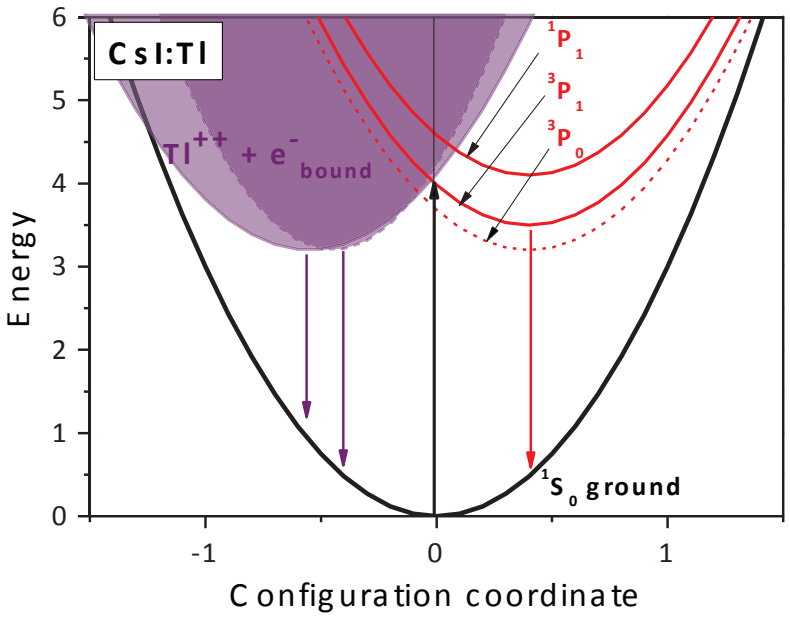

(b)

Figure 3.9: *Configuration diagrams for CsI:In (a) and CsI:Tl (b)*

(see Fig. 3.5 a), this is why it is reasonable to associate 400nm emission band with that allowed transition. The long-wavelength (visible) emission under direct optical excitation $^1P_1$ level is observed, probably, due to non-radiative relaxation to the lower energy states $^3P_2$ to $^3P_1$.

Excited electron state $^3P_0$ is also filled from higher electron levels. Since radiative transitions from this state to $^1S_0$ ground level are forbidden (see Table 3.2), this kind of transitions ($^3P_0 \rightarrow^1 S_0$) is not observed at sufficiently high temperatures.

It should be noted that 450nm emission band can be observed in CsI:In crystals at 10-15K (see Fig. 3.4 c). This band is excited exclusively at around 325nm. This excitation energy is lower than the A band. A similar luminescence is observed in CsI:Tl crystals (see Fig. 3.4 d). It is more pronounced in crystals with higher activator concentration. This emission can be ascribed to radiative relaxation of $^3P_0$ electrons. Account of this electron state can also explain the emission intensity decrease of CsI:A at low temperature (see Fig. 3.6 a,b). Potential minimum of $^3P_0$ level must be located below the other electron excited levels (see. Fig. 3.9 a,b). Then, if temperature is low enough, thermally activated transition to a higher energy level ($^3P_1$) would not be possible. Thus, $^3P_0$ level can be considered as a trapping state. The activator becomes a trapping center at low temperature. In CsI:Tl crystals time-resolved spectroscopy measurements done under laser excitation at the A-band revealed an extra-long component in luminescence decay of 450nm band. This result confirms the assumption that $^3P_0 \rightarrow^1 S_0$ forbidden transitions are responsible for 450nm emission band.

Now let's try to apply the configuration diagram model to describe the electron transitions of CsI:Tl crystals. Account of the activator ion electron states is not sufficient here. In particular, it does not allow to describe the excitation spectra of the main luminescence bands. Overlap of Tl^+ levels with the conduction band of CsI (Fig. 3.8 b) implies that activator ionization is possible under excitation in the activator absorption region. In case of CsI:Tl the configuration diagram should include some additional electron stats. Account of the impurity bound exciton state is shown in Fig. 3.9 (b). Use of a charge-transfer state for CsI:Tl bright visible activator emission band at 550nm was first suggested by C. Pedrini [Lecoq et al., 2006]. Although it should be noted that the model of self-trapped exciton perturbed by the activator [Nagirnyi et al., 1994, Nagirnyi et al., 1995] can be taken as a type of CT state - impurity bound exciton. Figure 3.9 (b) shows that in addition to the activator levels a charge transfer state is introduced. This excited state is a hole captured be the activator centers, and the bound electron in the conduction band ($Tl^{++} + e^-_{bound}$). Note that the ionization of the impurity ion leads to some relaxation of its surroundings, so that the distance from Tl^{++} to the nearest neighbors (first

configuration sphere) is reduced. Hence the corresponding parabola in the configuration diagram is shifted towards lower values of the configuration coordinates. It is also supposed that the free electron created as a result of thallium ionization belongs to the electron levels of the conduction band of CsI. This is why a singlet (σ) and a triplet (π) configuration of the ($Tl^{++} + e^-_{bound}$) state can be expected. Those are presented as two overlapping parabolas in Fig. 3.9 (b).

Let us consider the electron transitions of activator center for the case of CsI:Tl, according to the configuration diagram (Fig. 3.9 b). When the crystal is excited at the A-band, $^3P_1$ activator level is filled, as well as the BE state ($Tl^{++} + e^-_{bound}$). Radiative relaxation of $^3P_1$ state gives rise to 400nm emission band. Relaxation of the singlet ($Tl^{++} + e^-_{bound}$) is responsible for 550nm luminescence, whereas the triplet BE state is assigned to 490nm emission band. Depending on temperature, both of these electron states can be populated, since they are thermally coupled. At sufficiently low temperatures transitions from the singlet BE state (490nm luminescence band) become evident. Excitation energy increase leads to activator ionization, creating an electron in the conduction band. If the electron kinetic energy is high enough, it can escape from its birthplace (Tl^{++} center). Diffusion of such free electrons can introduce some long component in the luminescence decay. Activator ionization in CsI:A is discussed in Section 3.4.

In addition, at LHeT electrons from the higher levels will relax down to the lowest $^3P_0$ energy level. Radiative transitions from that level to the ground state are forbidden (see Table 3.2). This leads to the emission intensity decrease for the 400nm band at low temperature (as shown in Fig. 3.6). Thus, the configuration diagram in Fig. 3.9 (b) can satisfactorily describe luminescent properties of CsI:Tl. Radiative CsI:In and CsI:Tl transitions are summarized in Table 3.3. Note that those emission bands ascribed to intracenter transitions have basically the same full width at half maximum. Only the bands ascribed to radiative relaxation of impurity bound excitons ($Tl^{++} + e^-_{bound}$) are significantly broader than the others.

3.4 Activator ionization in CsI:A

As Fig. 3.8 shows, the excited electronic levels of CsI:A are located just below the conduction band, or overlap with it. In this case, it is reasonable to expect some effects associated with activator ionization.

Table 3.3: *Energies of CsI:In and CsI:Tl radiative transitions shown in Fig. 3.9*

Activator	Transition	Energy, eV	WL, nm	FWHM, eV
In^+	$^1P_1 \rightarrow ^1S_0$	3.0	400	0.175
	$^3P_2 \rightarrow ^1S_0$	2.55	490	0.185
	$^3P_1 \rightarrow ^1S_0$	2.2	550	0.185
Tl^+	$^1P_1 \rightarrow ^1S_0$	3.0	400	0.162
	$Tl^{++} + e^-_{bound}(\sigma)$	2.55	490	0.248
	$Tl^{++} + e^-_{bound}(\pi)$	2.2	550	0.311

Under UV excitation in the activator absorption region activator ionization is possible in case that the excitation energy is high enough. In this way an electron will be separated from the activator, and transferred to the conduction band ($A^+ + h\nu \rightarrow A^{++} + e^-_{free}$). If in this case the electron remains bound with the A^{++} center, a stable excited ($A^{++} + e^-_{bound}$) can be created. At the same time the free electron in the conduction band (if its kinetic energy is sufficient) can overcome the capture radius of ionized activator center A^{++}. Such processes can lead to appearance of slower decay component in the luminescence kinetics.

In the case of CsI:In there are two experimental facts observed, indicating the possibility of activator ionization under UV excitation. Firstly, these are the emission decay curves under photo-excitation, which were found to be dependent on the photon energy. Activator luminescence decay curves of CsI:In crystal under pulse deuterium lamp excitation at 300K are shown in Fig. 3.10.

Fig. 3.10 (a) shows that increase of excitation energy up to 230nm (5.39eV) gives a long component in the decay kinetics of the activator luminescence. One should also note that some additional rise time appears in the decay kinetics of the activator luminescence under 230nm excitation (Fig. 3.10 b). Similar change in the decay kinetics as a function excitation energy was observed for cerium ionization in $LiYF_4 : Ce$ crystal in [Belsky et al., 2013].

Appearance of emission rise in the decay kinetics can be explained as follows. When activator ionization takes place, free electrons are created in the conduction band. This electrons initially have certain kinetic energy E_{kin}. Such a free electron goes away from its birthplace (ionized center In^{++}) on a distance $l(E_{kin})$ [Kirkin et al., 2012]. Capture of the escaped electron is limited by the radius of

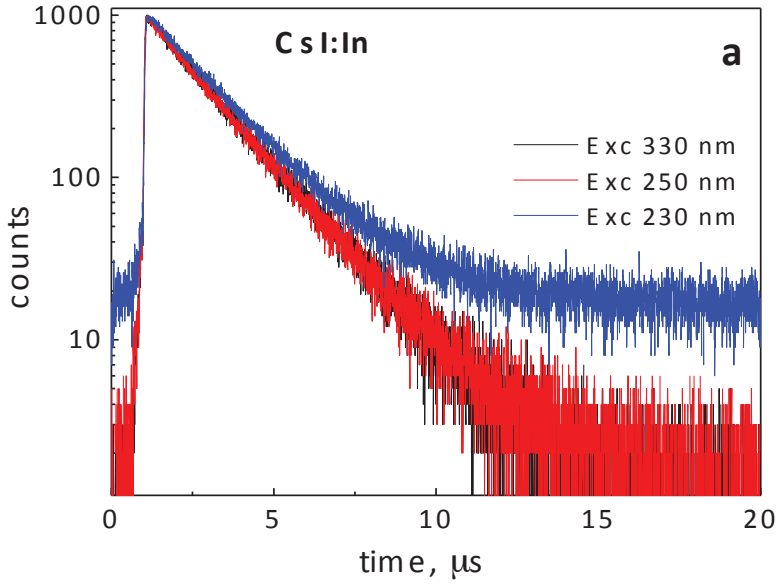

(a)

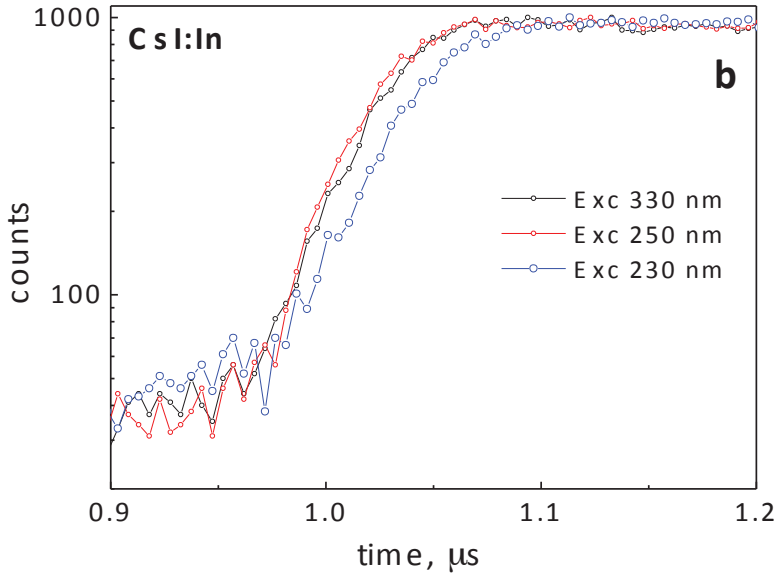

(b)

Figure 3.10: *CsI:In 550nm luminescence decays (a) and rise profiles (b) depending on the excitation wavelength at 300K*

Coulomb interaction R_{Ons} between e^- and In^{++}. If during its thermalization time the electron flies away from the charged activator center at a distance, which is greater than the radius of interaction, there will be no instant recombination. Such escaped electrons will diffuse through the crystal lattice, and their capture by some charged activator center will be delayed in time. This delay in recombination causes the rise and the slow decay component in the luminescence kinetics.

Second evidence of indium ionization in CsI is the experimental observation that the temperature dependences of activator luminescence intensity are dependent on the excitation energy (Fig. 3.11). It is reasonable to assume that the capture radius of an escaped electron the ionized activator center R_{Ons} is reversely proportional to temperature. This follows that with temperature increase the probability of electron capture goes down. Then, the temperature stability of the activator luminescence will be better in case of direct activator excitation, and the emission should start quenching earlier in case of ionization. This is the pattern observed for CsI:In crystals (Fig. 3.11). For thallium doped samples emission intensity temperature dependence was found to be the same independently of the excitation energy.

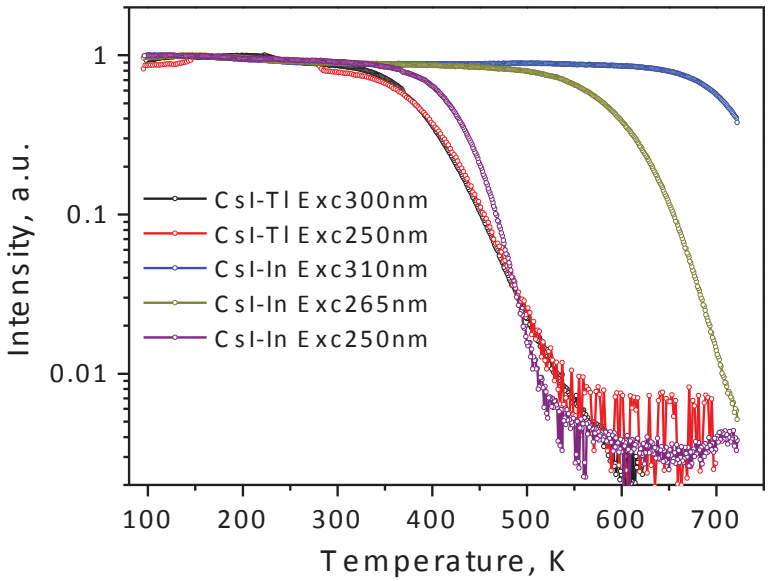

Figure 3.11: *Temperature dependence of integrated activator emission intensity of CsI:A as a function of excitation wavelength*

According to Fig. 3.11, CsI:Tl temperature dependences under 300nm and 250nm excitation are almost equivalent. The difference in temperature dependences between the two activators can be related to the positions of the excited levels with respect to the conduction band. In case of CsI:Tl under excitation at the A-band (300nm) thermal escape of electrons in the conduction band is already possible. This is because $^3P_1$ level is just at the bottom of the conduction band. Therefore, increase of the excitation energy does not result in any change of temperature dependence. It is possible that this effect determines the lower thermal stability of thallium luminescence yield compared with that of indium (see Section 4.4).

Qualitatively relaxation of electron excitation at ionized activator centers can be

described by a configuration diagram with a spatial coordinate. A simplified model is shown in Fig. 3.12.

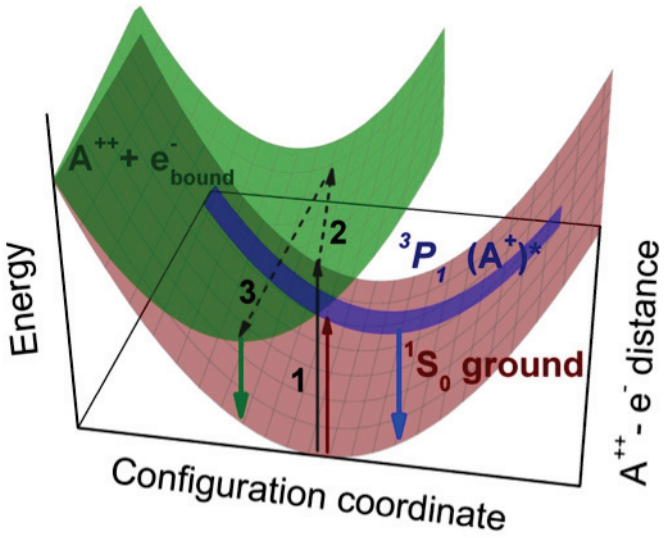

Figure 3.12: *Configuration diagram of activator relaxation in CsI:A with account of the spatial coordinate*

Figure 3.12 shows that in the case of activator ionization there is a free electron created in the conduction band (arrow 1). Its kinetic energy is equal to the exciting photon energy minus the ionization threshold. This free electron depending on its initial kinetic energy E_{kin}, can escape at a certain distance $l(E_{kin})$ [Kirkin et al., 2012] (as indicated by arrow 2). If at the end of thermalization it remains within the radius of the A^{++} Coulomb capture, it will return to the place of birth (arrow 3). This configuration of the ionized activator center and the electron forms a BE state ($A^{++} + e^{-}_{bound}$), followed by its radiative recombination. Electron's free path can be higher than the capture radius. Then this electron will be migrating through the lattice for a while. Corresponding statistical delay in recombination will be manifested in form of emission rise and some slow decay component in the luminescence kinetics.

3.5 Conclusions

Set of fluorescence spectroscopy measurements described in this Chapter allows to make some important conclusions about the properties of the activator luminescence

in CsI:A crystals. Since the electron structure of the Tl-like activator ions is similar, the major parameter to determine the luminescence properties is the positions of the activator electron levels with respect to the forbidden band of the crystal.

• Band model of the Tl^+ and In^+ non-relaxed activator levels in CsI has been suggested. According to the model, In^+ ground level and the excited electron levels lay within the forbidden band, whereas Tl^+ excited electron levels are supposed to be overlapping with the conduction band (Fig. 3.8). This model allows to explain the differences in luminescence properties of the systems.

• Comparative analysis of CsI:In and CsI:Tl luminescent properties allowed to suggest a configuration diagram model of activator luminescent centers in CsI:A. In case of CsI:In crystals simple ion model can be applied to describe the radiative transitions. To explain the activator luminescent properties in CsI:Tl account of activator levels only is not sufficient. Intense Tl-induced emission bands around 490nm and 550nm are assigned to radiative recombination of an impurity bound exciton state ($Tl^{++} + e^-_{bound}$) in CsI:Tl (Fig. 3.9 b). In CsI:In crystals presence of a similar bound exciton is also possible, although this kind of charge transfer state does not take part in the radiative transitions (Fig. 3.9 a).

• Ionization of the activator in CsI:A under excitation below the band gap was investigated. Evidence of activator ionization in CsI:In is pronounced in luminescence decay change and luminescence temperature quenching as a function of the excitation energy (Fig. 3.11). Luminescence temperature profile of CsI:Tl was found to be independent on the excitation energy, which is consistent with the positions of Tl^+ excited electron levels in the conduction band. A configuration diagram model of the activator relaxation in CsI:A with account of spatial coordinate between the ionized center and the escaped electron was suggested to explain ionization of the activator (Fig. 3.12).

The model of the activator electron states suggested in this Chapter allows to explain the properties of electron capture by In^+ and Tl^+ activator ions. Parameters of the activator electron traps can be obtained from the TSL glow curves analysis, as presented in the following Chapters.

Chapter 4

Scintillation properties of CsI:In and CsI:Tl crystals

Contents

4.1 Light yield and energy resolution 60
4.1.1 Pulse height spectra of scintillation response 60
4.1.2 Non-proportionality of the light yield and the energy resolution 64
4.2 Time response of scintillation 65
4.2.1 Microsecond decay and integraion time 65
4.2.2 Afterglow in millisecond scale 66
4.3 Temperature stability of the activator luminescence . . 68
4.3.1 Low temperature range – competition with self-trapping . 68
4.3.2 High temperature range – influence of deep traps 69
4.3.3 TSL diagrams of CsI:Tl and CsI:In 71
4.4 Persistent luminescence in CsI:A 72
4.4.1 Emission rise and afterglow under X-ray irradiation . . . 73
4.4.2 Role of the activator electron traps 76
4.5 Conclusions 78

This chapter is devoted to investigation of CsI:In scintillation properties in comparison with those of CsI:Tl crystals. Scintillation yield of CsI:In is measured as a function of the activator concentration, integration time and temperature. Presence of slow millisecond-second decay component was found in CsI:In scintillation pulse, limiting its light yield by 50% measured with 10μs integration gate. Activator-related glow peak at 240K was found in CsI:In TSL. Persistent luminescent properties (emission rise and afterglow) of CsI:A crystals under X-ray excitation are investigated in terms of the role of the activator traps.

As noted in Chapter 1, scintillation efficiency of CsI:Tl at 300 K is about half of the STE luminescence yield in pure CsI below LNT. Supposing that the quantum efficiency Q of the activator luminescence centers in CsI:Tl is close to unity, the energy loss in the activated crystal can be linked to non-radiative relaxation of the excitations at the migration stage S. Fraction of such migration losses may be limited by the parameters of electron and hole capture by the activator centers. It is reasonable to assume that more effective alternative activator for CsI can be found. This activator impurity should lead to the creation of luminescence centers with different parameters of electron and hole capture. Indeed, as it was shown in Chapter 3, the excited electron states of indium ions in CsI lay much deeper in the forbidden band (see Fig. 3.8). From general considerations, such an arrangement of electron levels makes indium a deeper trap for electrons than thallium.

For the time of research scintillation properties of CsI:In crystals had not been studied. Possibility to obtain an alternate CsI-based scintillator with a nontoxic activator was also a motivating factor for this study. This chapter presents the results of CsI:In scintillation properties investigation in comparison with a standard CsI:Tl scintillation crystal. By the standard scintillator CsI:Tl we mean here a crystal with the optimal activator concentration, grown by the modified Czochralski method at ISMA (see Chapter 2).

4.1 Light yield and energy resolution

4.1.1 Pulse height spectra of scintillation response

The Light Yield (LY) measurements of crystal scintillators depend on many experimental conditions. One of the important parameters is the integration time of the scintillation pulse. Under direct excitation of luminescent centers luminescence decay is usually exponential, and the decay time is determined by the luminescence center radiation time. Under X-ray or γ-ray excitation the scintillation decay curve often deviates from the single exponential law. The deviation from the mono-exponential law can manifest either in increase or decrease of the decay time. When scintillation crystal is excited by high-energy photons (e.g. X-rays or γ-rays) the shape of the scintillation pulse depends on the relative spatial distribution of the electron excitations and the luminescence centers, as well as on presence of traps.

Exposure of scintillation crystals to ionizing radiation can result in increase of the rise time and appearance of the slower (compared to the radiation time) decay component in scintillation decay. In particular, in ionic crystals presence of the slow decay component is due to diffusion of the spatially separated electron-hole pairs on their way to the recombination centers [Belsky et al., 2013].

Acceleration of the decay kinetics is usually associated with the processes of non-radiative relaxation (for example, the excitation density quenching) [Kirm et al., 2009, Pedrini et al., 1993, Williams et al., 2011]. Also luminescence decay acceleration can be observed due to nonradiative energy transfer from donor to acceptor [Förster, 1948]. In this case the decay kinetics of donors accelerates, and the decay kinetics of the acceptor has some rise time.

Scintillation light yield of inorganic scintillation can depend strongly on the integration gate time of the scintillation pulse. Pulse height spectra of CsI:In and CsI:Tl crystals measured with different peaking times are presented in Fig. 4.1 a,b. Channel number corresponding to a photo-peak position here is proportional to the number of light photons emitted by the scintillators for an unit incident energy. This value is referred as light yield further. Full width at half maximum of a photo-peak, divided by its maximum position, is called the energy resolution. Insets in Fig. 4.1 a,b present the photoelectron numbers measured versus peaking time for tested CsI:In and CsI:Tl crystals. We see that with increase of the integration time (peaking time here) the scintillation yield increases approaching some stationary level. For CsI:In these curves are weakly dependent on In concentration. Still, neither CsI:Tl nor CsI:In reaches full saturation even at 24 μs peaking time.

In view of presence of the extra slow component in CsI:In scintillation decay, there are reasons to expect some significant increase of CsI:In light yield with increase of integration time. Since peaking times above 30 μs were unavailable, we measured CsI:In light yield relative to CsI:Tl etalon (0.1 % mol of Tl). Concentration dependence of CsI:In LY in comparison with CsI:Tl can be seen in Fig. 4.2. The light yield of CsI:In measured at 30 μs peaking time does not exceed 45-50% from CsI:Tl. At the same time, the relative X-ray luminescence yield of CsI:In is around 80% of what CsI:Tl emits.

As it is shown in Fig.4.2, scintillation yield of CsI:In crystals measured with the ^{137}Cs γ-source reaches saturation at around (0.005-0.01) % mol In. Further increase of the activator content doesn't lead to significant increase of the light

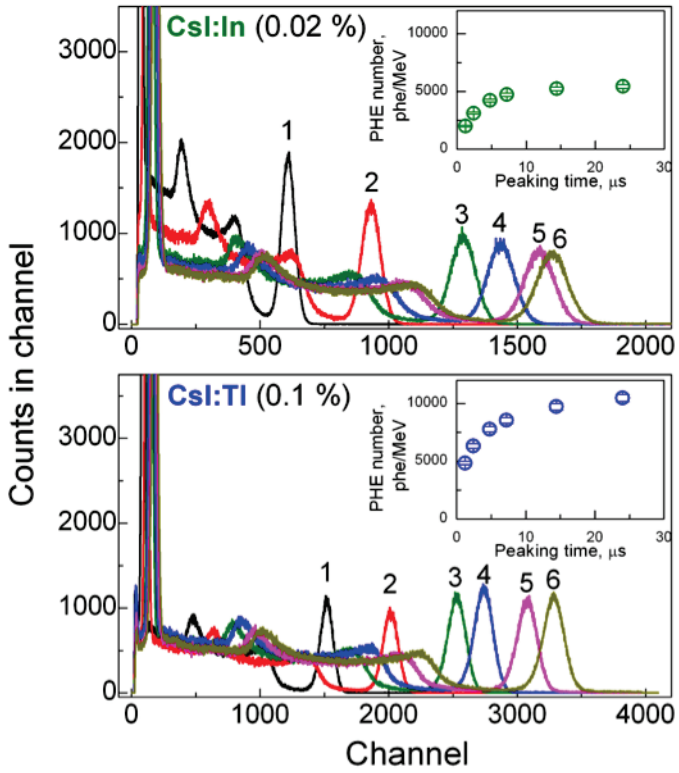

Figure 4.1: *Pulse height spectra of CsI:In (a) and standard CsI:Tl (b) measured with different peaking times under ^{137}Cs γ-excitation of 661.6 keV. Insets - photoelectron number as a fucntion of the integration gate*

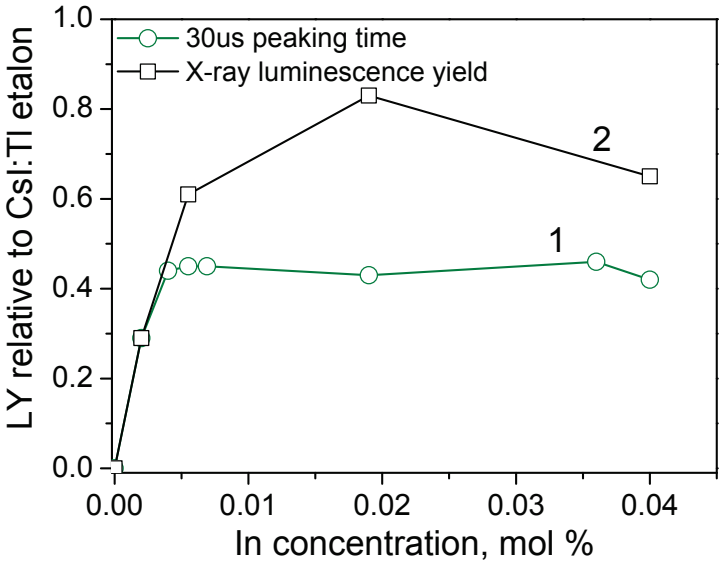

Figure 4.2: *CsI:In light yield depending on the activator concentration, relative to a CsI:Tl etalon scintillation detector measured under the same conditions. Squares – X-ray luminescence yield. Circles - γ-excitation by ^{137}Cs with 30 μs peaking time*

yield. This low saturation threshold is important from the point of view of potential applications, since in highly doped CsI:In crystals (with In concentrations around 0.03 % mol and above) creation of color centers was observed [Grabmaier, 1984, Gwin and Murray, 1963, Hamada et al., 2001, Kudin et al., 2005, Trefilova et al., 2002]. Absorption bands induced by these centers overlaps with the activator emission, resulting in decrease of the scintillation yield.

Absolute light yield measurements of CsI:In and CsI:Tl crystals were performed at the National Centre for Nuclear Research, (Otwock-Swierk, Poland) by Prof. Moszynski and coworkers. Single photoelectron peak method was used as described in [Gridin et al., 2014a, Moszynski et al., 1997]. For three CsI:In samples tested with activator concentration ranging from 0.005 to 0.04 mol % the absolute light yield was found to be 27000 ±1000 photons/MeV. The total energy resolution of tested CsI:In and CsI:Tl samples were measured with the XP5212 spectroscopy photomultiplier due to its high blue sensitivity of 12.2 μA/lm blue. Basic scintillation properties of CsI:In (the absolute light yield and the energy resolution) are arranged in Table 4.1. The results of measurements (assuming similar emission spectra for CsI:Tl and CsI:In) collected in Table 4.1 are in a good agreement with the relative LY measurements presented in Fig 4.2.

Table 4.1: *Light yield and energy resolution of tested CsI:In and optimal CsI:Tl crystals*

Crystal	Activator, % mol	LY, photons/MeV [a]	Energy resolution, % [b]
CsI:Tl	0.10	64 000 ± 2000	5.3 ± 0.2
CsI:In #1	0.005	27 000 ± 1000	11.0 ± 0.8
CsI:In #2	0.001	27 000 ± 1000	8.5 ± 0.3
CsI:In #3	0.04	26 000 ± 1000	9.2 ± 0.3

[a]Measured with calibrated XP2020Q PMT, QE = 0.083 for CsI:Tl

[b]Measured with XP5212 with a high blue sensitivity of 12.2 μA/lm blue

The best energy resolution of 8.5% was obtained for a sample containing 0.01 mol % indium. It should be noted that Bridgman method, applied for the synthesis of crystals of CsI:In, does not provide a uniform distribution of the activator impurities in the crystal ingot. Therefore, optimization of the crystal growth techniques may give a certain improvement of the activator homogeneity, resulting in better energy resolution.

As one can see from the light output measurements results above, the lower the light output of crystals CsI:In in comparison with CsI:Tl may be associated with presence of the millisecond scintillation decay component in indium doped crystals. To confirm this hypothesis, decay kinetics of CsI:In and CsI:Tl crystals were measured under pulsed X-ray excitation. The results are provided in Section 4.2.

4.1.2 Non-proportionality of the light yield and the energy resolution

Non-proportionality of the light yield versus gamma ray energies correlates with the scintillators response to the local deposited energy ($-dE/dx$) [Bizarri et al., 2009], and it is related to the spatial distribution of electron excitations along the γ-ray track. Investigation of this parameter is an important part of evaluation of potential level of energy resolution in the scintillator. The non-proportionality is defined here as the photoelectron yield measured at specific gamma ray energy relative to the photoelectron yield at 662 keV gamma peak. Fig. 4.3 (a) shows a comparison of the non-proportionality characteristics measured for the CsI:In #2 and CsI:Tl crystals and Fig. 4.3 (b) - corresponding them energy resolutions.

As we see form Fig. 4.3 (a), both CsI:Tl and CsI:In non-proportionality curves have a typical shape for alkali halide crystals [Mengesha et al., 1998]. Light yield of both scintillators tends to steadily grow with excitation energy decrease, reaching a broad maximum around 20-50 keV. The yield of CsI:In crystals is more sensitive to the excitation energy change, than CsI:Tl. Around 50 keV excitation energy range, relative light yield of CsI:Tl sample gains at around 15 % compared with 662 keV excitation, whereas CsI:In #2 gains about 20-25 %.

Energy resolution of both CsI:Tl and CsI:In crystals increases with excitation energy decrease (Fig. 4.3 b). A much poorer energy resolution of CsI:In in this respect is observed. Intrinsic resolution of the CsI:In #2 crystal of 7.4 % is about 50 % poorer than that of CsI:Tl of 4.9 %. Although the non-proportionality characteristic of CsI:In #2 sample is somewhat poorer than that of CsI:Tl, it does not explain so large difference in the intrinsic resolution between the two scintillators.

As it was mentioned earlier, rather high energy resolution of CsI:In crystals can be related to nonhomogeneous activator distribution. The Bridgman crystal growth

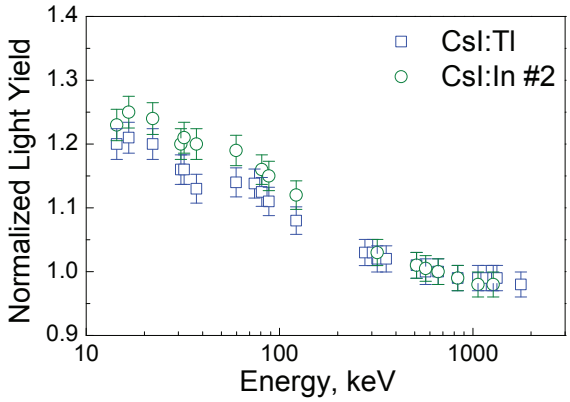

(a)

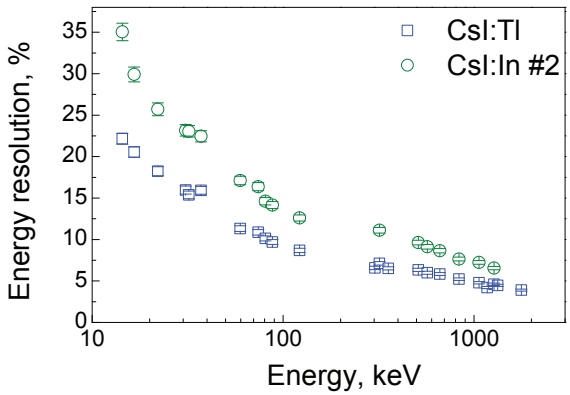

(b)

Figure 4.3: *Light yield (a) and energy resolution (b) depending on excitation energy for CsI:Tl and CsI:In #2 crystals*

technique used for synthesis of experimental CsI:In samples does not provide uniform impurity distribution (see Chapter 2).

4.2 Time response of scintillation

4.2.1 Microsecond decay and integraion time

Luminescence decay curves for CsI:In #2 and CsI:Tl crystals visible emission measured under pulsed 30 keV X-ray excitation are presented in colour lines in Fig. 4.4. Corresponding decay curves under UV 300 nm pulsed excitation for 550 nm emission are shown in Fig. 4.4 in black lines. Exponential fit of the latter decays gives 570 ns and 1950 ns of radiation decay time for CsI:Tl and CsI:In #2 respectively. These values were found to be almost independent on the activator concentration. In Fig. 4.4 we see that first, both in CsI:Tl and in CsI:In the decay kinetics becomes

longer under X-ray irradiation compared with the 300 nm excitation. And second, the relative fraction of the longer decay component of CsI:In is much higher, than in CsI:Tl.

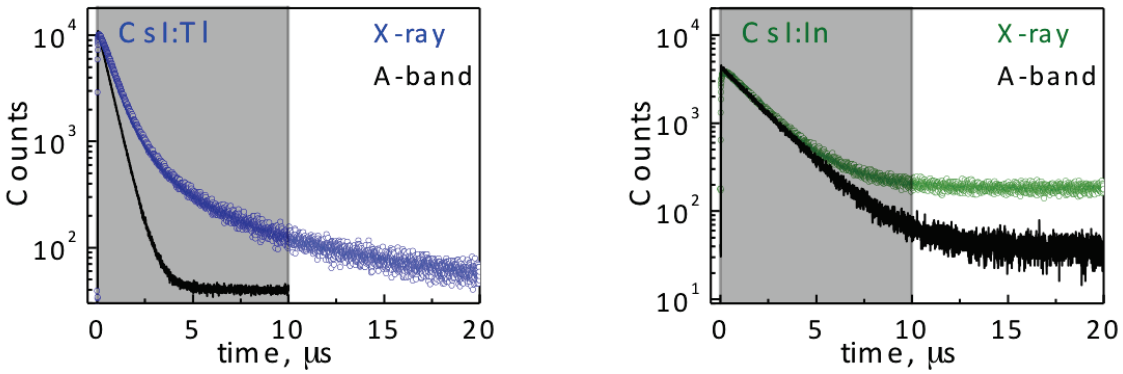

(a) (b)

Figure 4.4: *Scintillation decay of CsI:Tl (a) and CsI:In #2 (b) crystals measured under pnoto excitation (black) and under pulsed X-ray excitation (coloured) at 300K*

A qualitative idea of the slow decay component contribution in the total scintillation yield can be obtained from Fig. 4.5. The dependence of the summarized luminescence intensity on the integration gate (Fig. 4.5) was acquired by integrating the photon counts in Fig. 4.4 over the time scale. Here we see that by 30 μs of integration CsI:Tl total light intensity is approaching the saturation level, whereas CsI:In emission goes on growing up. This means that the emitted scintillation light is more spread in time in indium doped crystals, and it cannot be accumulated with integration times about 20-30 μs.

4.2.2 Afterglow in millisecond scale

Kinetic properties of scintillation pulse are dependent not only on the excitation energy and the type of the ionizing particles, but also on the exposure time to the irradiation. Measurements of scintillation afterglow are normally done after continuous (of the order of seconds) irradiation by X-rays. This reflects the ability of the media to store part of the energy in form of electron excitations in the timescale of hundreds ms. This effect can be an additional explanation for the scintillation yield difference between Tl and In doped CsI crystals. Corresponding kinetics for both types of scintillators are shown in the Fig. 4.6.

As we see in Fig. 4.6, CsI:In afterglow curves are all quite similar regardless the

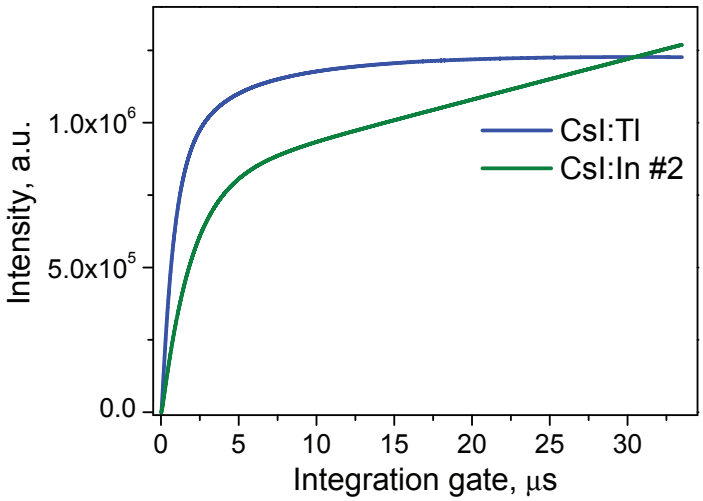

Figure 4.5: *CsI:Tl and CsI:In integrated luminescence intensity as a function of the integration gate (based on Fig. 4.4)*

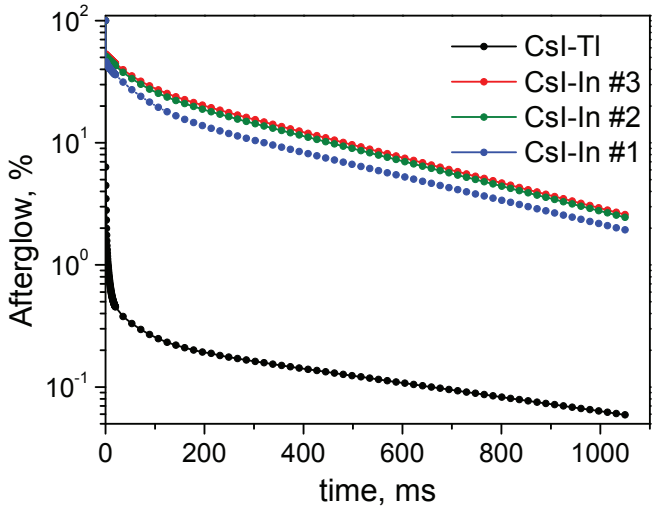

Figure 4.6: *Afterglow curves of CsI:Tl and CsI:In samples , measured after 2 seconds of X-ray 130kV irradiation at 300K*

activator concentration. But the difference between these curves and the curve of CsI:Tl is very large. CsI:In afterglow level at 100 *ms* is about 15-20 %. One can see that afterglow level for CsI:In is an order of magnitude higher than the typical value for CsI:Tl (0.5-0.8 %). It is clear that significant part of the excitation energy is stored at some traps, which are stable around room temperatures.

4.3 Temperature stability of the activator luminescence

4.3.1 Low temperature range – competition with self-trapping

Temperature stability of the scintillation intensity may be crucial for certain applications. Temperature dependences of the yield were measured for photo- and X-ray luminescence. In this way it is possible to collect all photons emitted in 350-690 nm range independently on decay time. Both crystals emit in the visible band around 550 nm which agrees with spectral sensitivity of common photomultipliers and Si-photodiodes.

Now let us compare the scintillation yield for CsI:In with that of CsI pure and CsI:Tl in the low temperature range from 10K to 300K. Taking into account the concentration dependence of the scintillation output CsI:In (Fig. 4.2), samples with 0.01-0.04 mol % of *indium* should be chosen. Furthermore, given the presence of slow decay component in the scintillation pulse, it makes sense to compare the measurements done in the steady state mode (with no integration gate). Therefore, we shall match the CsI:In X-ray luminescence temperature dependence at 10-300K with the corresponding curves for CsI:Tl and CsI pure (Fig. 4.7).

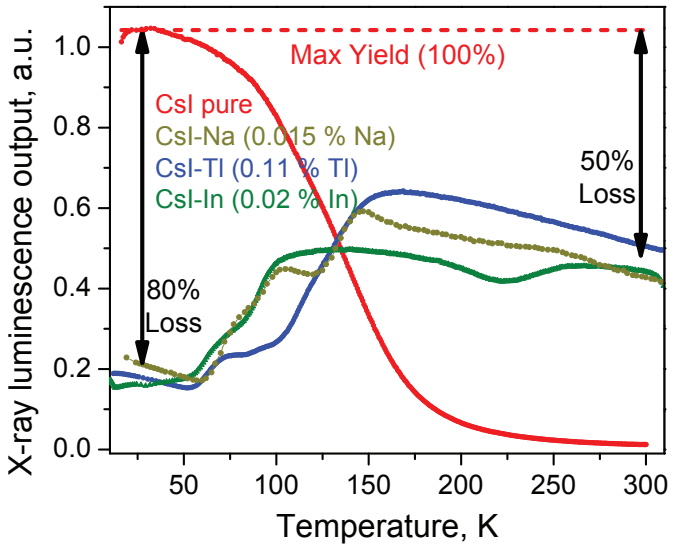

Figure 4.7: *Scintillation yield temperature dependences of CsI pure, CsI:Tl, CsI:Na, and CsI:In under X-ray excitation*

According to Fig. 4.7, at around room temperatures CsI:In scintillation yield is close to the output of CsI:Tl and CsI:Na standard scintillators. As we can see,

scintillation efficiency of the activated CsI:A crystals is about 50 % of the STE luminescence yield of CsI pure at low temperatures. These results are consistent with the absolute light yield measurements [Holl et al., 1988, Moszynski et al., 2005, Moszynski et al., 1997, Moszynski et al., 2003]. Furthermore, at low temperatures (10-60K) activator luminescence yield is only about 20 % of the maximum. Those energy losses in CsI:A at low temperature range (10-60K) are present in all CsI:A scintillators measured (Fig. 4.7) independently on the activator. They can be related to self-trapping of holes below 90K in CsI. As soon as temperature is below the self-trapping point, thermalized holes become instantly self-trapped in CsI lattice, limiting their mobility and transport to the activator centers. Although the profiles of the curves in Fig. 4.7 are different for different activators. Competition of the activator and the intrinsic channels of relaxation as a function of the activator concentration and temperature is investigated in detail in Chapter 5.

4.3.2 High temperature range – influence of deep traps

Temperature dependences of CsI:In and CsI:Tl emission in the high temperature range from 300K to 700K are presented in Fig. 4.8. The dependences were measured while cooling down the samples, in order to avoid the impact of TSL. First, let's note significant difference between the shapes of the luminescence yield curves under photo- and X-ray excitations. Decrease of X-ray luminescence yield of CsI:Tl below 150K is related to trapping of electrons on Tl^{+} ions (see TSL glow peaks around 120K in Fig. b). The valley around 150-400 K at CsI:In X-ray temperature curve can be also explained by trapping of "escaped" electrons by In^{+} centers.

Temperature quenching of the Tl-related luminescence is quite similar both under photo- and X-ray excitation, closely following the Mott's law. This fact suggests the thermally activated non-radiative transition of the relaxed excited activator state to the ground state to be the main mechanism of the thermal quenching in CsI:Tl. According to the configuration diagram of activator relaxation in CsI:Tl suggested in Chapter 3, this should be the BE state $Tl^{++} + e^{-}_{bound}$ (see Fig. 3.9 b). Activation energy of non-radiative transition from $Tl^{++} + e^{-}_{bound}$ to $^{1}S_{0}$ ground state corresponds to the crossing point between the two corresponding parabolas.

In CsI:In temperature quenching starts at about 600-650 K contrasting with 350-400K in CsI:Tl. The experimental setup used did not allow us reaching the

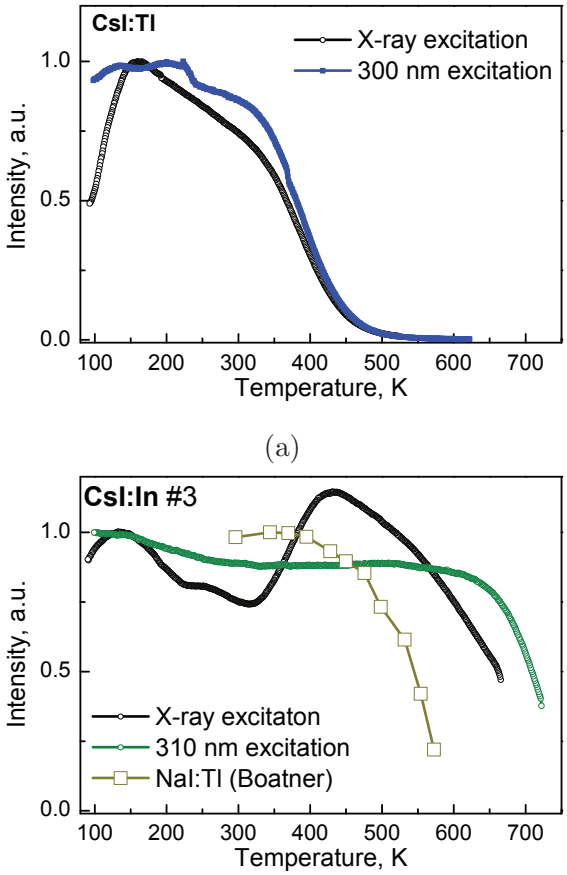

Figure 4.8: *Temperature dependences of CsI:Tl (a) and CsI:In #3 (b) luminescence yield under X-ray excitation, and excited in A absorption band, and NaI:Tl scintillation yield temperature dependence from [Boatner et al., 2013]*

temperature of CsI:In complete thermal quenching. However, non-radiation electron transition here occurs between the electron states of In^+ ion. Crossing point between the parabolas of $^3P_1$ excited state and $^1S_0$ ground state corresponds to activation energy of the non-radiative relaxation (see Fig. 3.9 a). Different nature of excited states of In^+ and Tl^+ activators can explain the difference in temperature stability of CsI:In and CsI:Tl.

Scintillators with high temperature stability play the key role in well logging, where conventional NaI:Tl is still the dominating option [Boatner et al., 2013]. Thermal stability of NaI:Tl crystals allows using them up to 450-470K, that is not enough for current geophysical needs. CsI:In with emission thermal stability up to 600-650K could be a good alternative in case its performance is improved. Some technological efforts to suppress afterglow and improve energy resolution could be made in order

to obtain more efficient temperature stable CsI:In scintillator.

It should be noted that the temperature dependences for each activator have its characteristics structure. Nevertheless, the general patterns of energy relaxation in crystals of CsI:A must be the same. None of the activators used allows to achieve maximum yield in CsI at RT. In order to explain the energy losses in CsI:A at room temperature, as well as at the temperature of LHeT, it is necessary to produce a general model of the energy relaxation in this scintillation system. This model should take into account all main electron excited states in CsI and their role in the function of temperature and the activator concentration. This aspect of the problem is treated in Chapter 5.

4.3.3 TSL diagrams of CsI:Tl and CsI:In

Afterglow in scintillation crystals is normally caused by trapping of charge carriers by some intrinsic or impurity defects. One of the most efficient techniques for charge carrier's traps investigation is the thermally stimulated luminescence (TSL) method. In the frame of this study TSL spectra were measured after X-ray irradiation at 10K. Typical TSL diagrams for both In- and Tl- doped CsI are shown in Fig. 4.9.

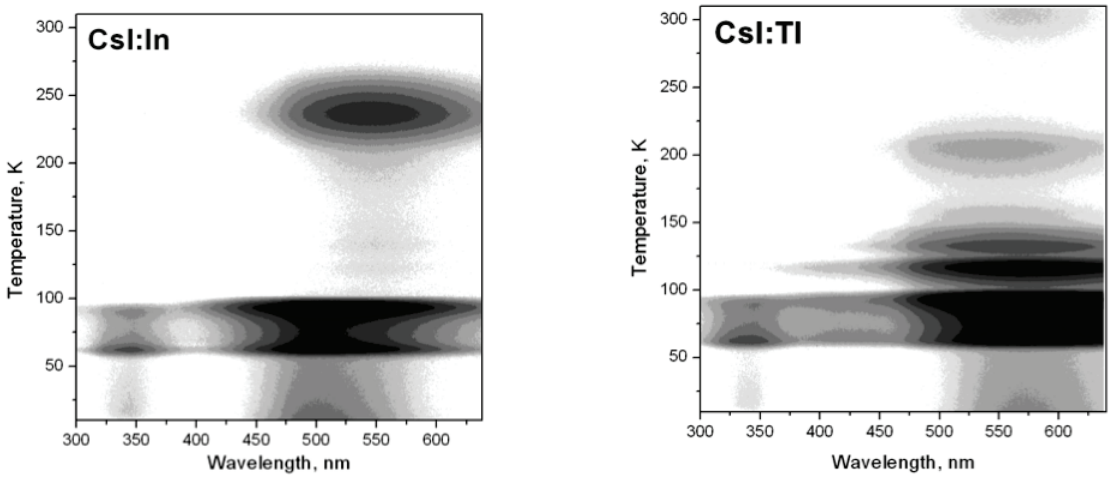

(a) (b)

Figure 4.9: *TSL diagrams for CsI:In #3 (a) and CsI:Tl (b) crystals measured after X-ray irradiation at 10K*

Two low temperature peaks (60K and 90K) are typical for CsI crystals regardless the activator impurity type [Martinez et al., 1964]. They correspond to release of

self-trapped holes (STH) with their consecutive recombination at activator ions.

Let us focus on the activator related glow peaks in the both systems. The intense peak around 115K in CsI:Tl corresponds to release of electrons from Tl^0 centers, and recombination of these electrons at Tl^{2+} centers. The less intense glow peak at 135K can be connected either with presence of Na^+ impurity in the crystal, or with complex Tl centers of electron capture [Barland et al., 1981, Brecher et al., 2006]. The weak peak at 215K in CsI:Tl is frequently attributed to presence of impurities, and is thought to be responsible for millisecond afterglow in CsI:Tl [Kudin et al., 2009].

When it comes to CsI:In, apart for the two intrinsic peaks at 60K and 90K there is only one intense symmetric peak around 240K. Its relative intensity is dependent on the activator concentration, which leads to the conclusion that this peak is related with e^- or h^+ capture by the activator. Based on the band diagram of the activator energy levels (Fig. 3.8), we assume that the 240K glow peak in CsI:In corresponds to an electron trap. However, independently on the 240K peak origin, it is clear that such a stable trap will lead to millisecond decay components, reflected in the CsI:In afterglow in Fig. 4.6. TSL curves in 300-700K range are presented in the following Section.

4.4 Persistent luminescence in CsI:A

Afterglow and bright burn (luminescence hysteresis) are usually attributed to charge carrier traps stable at room temperature. For example, in CsI:Tl scintillator afterglow is observed in the time range of the order of 10-100 ms after exposure to X-ray irradiation. It is associated with the presence of impurity traps of charge carriers, which is manifested in the TSL curves as peaks at 200-220K. Nature of these traps is assumed to be associated with presence of divalent cations or oxygen-containing impurities in the crystal [Kudin et al., 2009]. Several works report use of some co-dopant to reduce these effects [Bartram et al., 2008, Brecher et al., 2006, Kudin et al., 2009]. However, the influence of activator-induced traps remains unclear. Present Section is focused on this aspect in $Tl-$ and $In-$ doped CsI.

4.4.1 Emission rise and afterglow under X-ray irradiation

It was shown above that CsI:In crystals have a strong luminescence afterglow in the millisecond time range. Intense TSL peak in CsI:In at 240K (Fig. 4.9) indicates the energy storage by the activator traps. On this basis, it was suggested that the observed afterglow is due to the trapping of electrons activator centers.

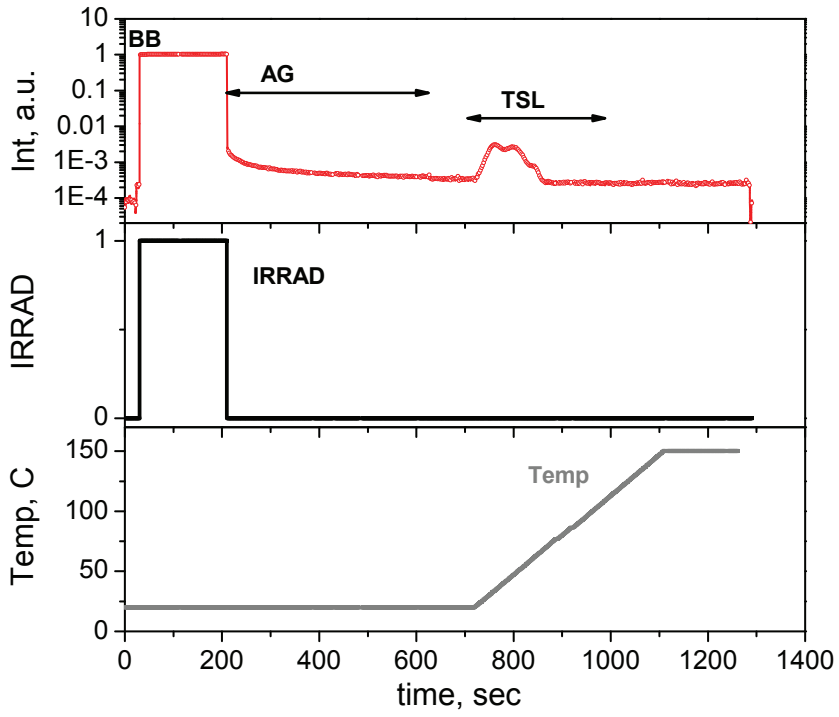

Figure 4.10: *TSL signal after irradiation at 300K reveals presence of stable traps*

The luminescence rise and afterglow were measured at 300K under steady-state X-ray excitation. A software-controlled shutter in front of the X-ray source window controls the irradiation. Fluorescent signal was detected using EMI9789 photomultiplier tube. Activator emission was allocated using cutoff filters. Polished crystalline samples were installed in the camera Linkam Heating Stage (attached to the sample holder with silver conductive paint). This allows heating of the samples before measurement to empty all the traps, as well as obtain TSL curves.

A principal scheme of the afterglow and luminescence rise measurement is shown in Fig. 4.10. After 30 seconds of the experiment the shutter opens the X-ray source and the sample becomes exposed to the irradiation. Activator luminescence intensity of the crystals increases for some time. The intensity rise curves are different in CsI:Tl and CsI:In crystal. As can be seen from Fig. 4.11 (a), CsI:In luminescence intensity grows much slower with time than in the case of CsI:Tl. In addition, the

luminescence curve of CsI:In contains faster and slower rise components.

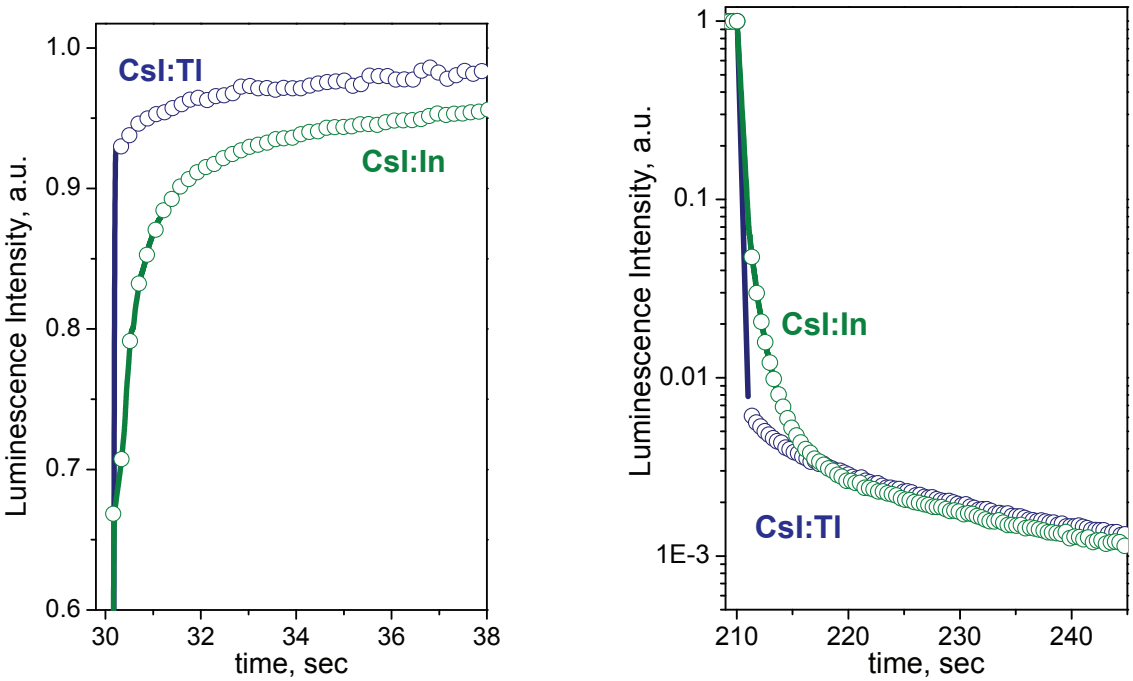

(a) (b)

Figure 4.11: *CsI:A emission rise (a) and afterglow (b) profiles under continuous X-ray irradiation at 300K*

It can be also noted that the luminescence rise profile starts at about 0.9-0.95 of maximum intensity for CsI:Tl sample, and about 0.65-0.7 in the case of CsI:In. During the next 180 seconds samples are being irradiated with the X-rays. During this time, the luminescence intensity reaches some saturation level. After that the X-ray source shutter is shut down and the afterglow signal is being measured as a function of time. Afterglow curves in logarithmic coordinates are shown in Fig. 4.11 (b). There are also two components. The faster afterglow component is present in the both CsI:A crystals. In the case of CsI:In in the time range of a few seconds the afterglow level is about 1-10%. Comparison of the afterglow of CsI:Tl and CsI:In a time scale of 1000 ms is given in Fig. 4.6.

Subsequent linear heating the samples up to 450K indicates the presence of some energy stored in the crystals. It is revealed in the form of TSL peaks at 320K and 370K (Fig. 4.12). Note that the TSL intensity of these peaks is 2-3 orders lower than the X-ray luminescence intensity. This may indicate a low concentration of the traps which are responsible for the high-temperature TSL peaks. In addition, these peaks

are observed in all TSL curves of CsI:A crystals (Fig. 4.12). TSL intensity of these peaks is not significantly dependent on the activator concentration. Consequently, they can be related to some uncontrolled crystal defects (not related to the activator impurity). In [Kolotilin and Shtanko, 1984] 340K TSL peak is associated with the thermal destruction I_3^- centers of the anion-cation-anion structure. Formation of such defects, according to [Luschick and Luschick, 1989], may occur as a result of non-radiative STE decay. Creation of cationic vacancies with interstitial cations or anion vacancies with interstitial anion is suggested.

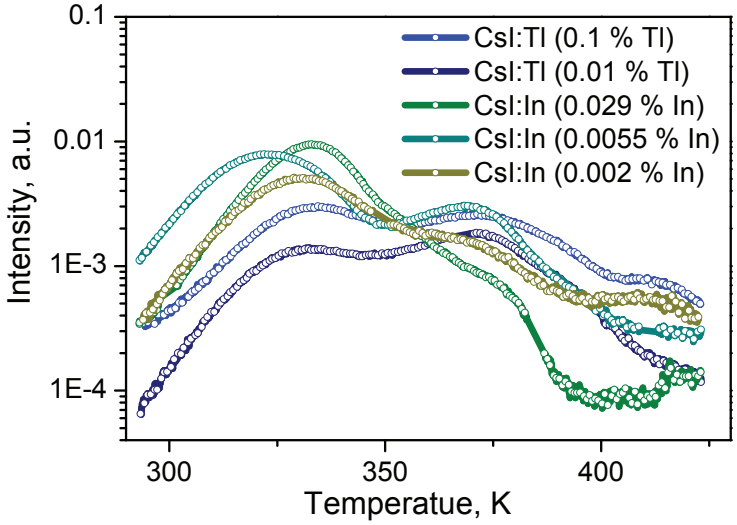

Figure 4.12: *TSL glow curves of CsI:A crystals as a function of the activator concentration. TSL intensity is normalized by the X-ray luminescence yield*

These processes can be written in the form of the following reaction: $e^0 \rightarrow e_s^0 \rightarrow v_c^- i_a^0 + v_a^+ i_c^0$. After charge exchange these centers can be converted into $(X_3^-)_{aca}$ centers having the $(v_c^- e^+ i_a^0)$ structure as remarked in [Luschick and Luschick, 1989]. Nevertheless, the nature of these traps is not clearly defined, and their properties require additional studies, which are beyond the scope of this work. Here, we rely on the fact that these trapping centers are not induced by the activator. Therefore, we will refer to the traps corresponding to TSL peaks around 320-360K as intrinsic. Thus, there are three main processes occurring under irradiation of CsI:A crystals. Firstly, capture the correlated electrons and holes by the activator centers (direct excitation of the activator). Secondly, capture of separated charge carriers by the activator traps which are stable at RT. As can be seen from the luminescence rise curves (see Fig. 4.11 a), these traps are being filled slowly enough under X-ray irradiation. Thirdly, it is filling of the activator trapping centers. The latter process

is clearly pronounced for CsI:In. It can be assumed that filling of the activator traps with electrons and holes (e.g. creation of A^{++} and A^{0} centers) is not complete. It should go until a certain equilibrium concentration of charged activator centers is reached. Obviously, trapping parameters of the activator centers (lifetime of a charge carrier on that center) determine the fraction of the energy stored on the activator traps.

4.4.2 Role of the activator electron traps

In this Section role of the activator on the luminescence rise and the afterglow in CsI:A is investigated. In order to do that, capture by the intrinsic traps should be avoided. For luminescence rise measurements the experiment is organized the way that capture of charge carriers by the intrinsic traps is negligible. For this purpose CsI:A samples were warmed up to empty all the traps, and after a sequence of X-ray irradiations (180 seconds each) was done, decreasing time interval between the irradiations (Fig. 4.13). In this case after switching off the irradiation (0 value in the Irradiation profile) electrons are released from the activator centers, hence those are unstable traps at RT. Whereas the stable intrinsic traps should remain mostly filled with electrons. It should be noted that the afterglow curves are expected not to change, effected by both activator and intrinsic traps.

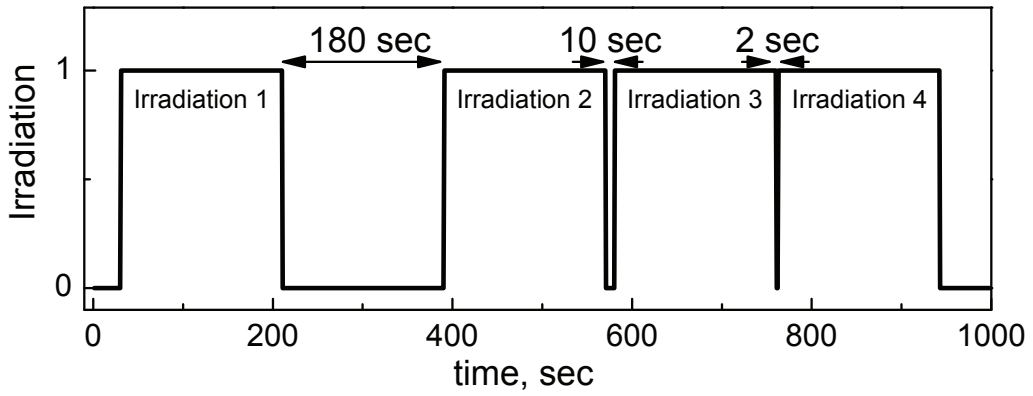

Figure 4.13: *Experimental procedure of emission rise measurement with filling of the intrinsic traps in CsI*

To reveal the role of activator traps on luminescence rise time in CsI:A let us focus on comparison to curves for one sample CsI:Tl and CsI:In with a similar activator concentrations. Fig. 4.14 shows the luminescence rise curves of CsI:Tl (0.01% mol) and CsI: In (0.0055% mol) when the X-ray source is switched on. The irradiation

was carried out according to the scheme shown in Fig. 4.13. Luminescence intensity of the crystals increases sharply when the X-ray source is switched on, and it takes a few tens of seconds to reach a steady level.

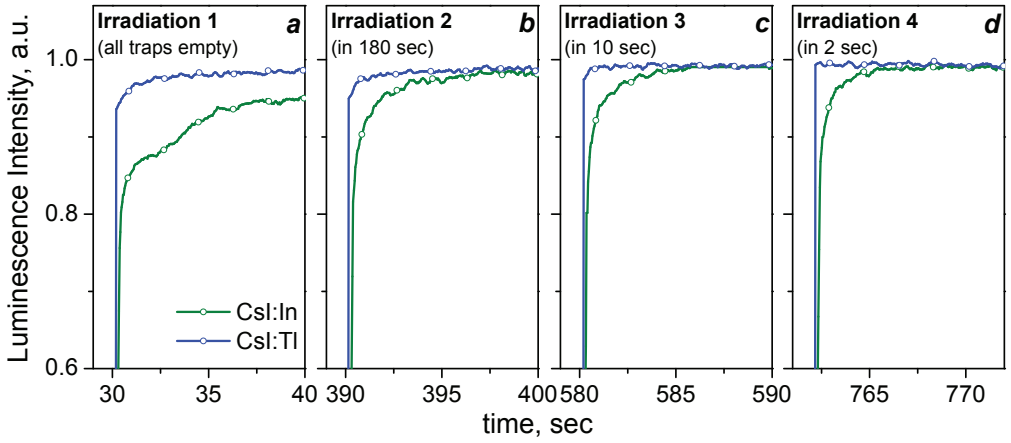

Figure 4.14: *Emission rise profiles for CsI:Tl (0.01 % mol) and CsI:In (0.0055 % mol). The curves are normalized to the maximum intensity*

Irradiation 1 was done on the samples previously warm up to 450K. In this case intrinsic and activator traps are supposed to be empty. Thus when the X-ray is switched on the intrinsic traps (TSL peaks 320-360K) are being filled, and electrons are being captured by the activator centers as well. As a consequence, luminescence rise curve in Fig. 4.14 (a) has a significant contribution of the slow component. The next *Irradiation 2* is done after relaxation for 180 seconds (see Fig. 4.14 b). Contribution of the slow component observed in the emission rise profile is significantly reduced. Further decrease of the relaxation time between irradiations of CsI:Tl and CsI:In samples does not result in any important change of rise time (Fig. 4.14 c, d). In general, in the case of CsI:Tl under all the irradiation conditions applied the slow rise component predominates. At the same time, for CsI:In even after a very short relaxation time for 2 seconds (see Fig. 4.14 (d)) some emission rise is observed for a few seconds. All the scintillation properties of CsI:A crystals investigated in this Chapter allow to suggest a model of energy relaxation, which would explain the common features of the activator luminescence in CsI:A. This is done in Chapter 5 of the present work.

4.5 Conclusions

Scintillation properties of new CsI:In were investigated as a function of activator concentration, integration time, and temperature jointly with CsI:Tl etalon sample. Comparison of CsI:In properties with CsI:Tl classical scintillator results in the following resume of CsI:In scintillation properties:

• Light yield of CsI:In scintillators is strongly dependent on the integration time. Absolute light yield of CsI:In crystals was found to be 27 000 photons/MeV measured with the integration time of 24 μs . The light yield value is about 50% of CsI:Tl. However, measurements of X-ray excited luminescence yield (current mode) of CsI:In crystals show similar to CsI:Tl efficiency. This fact suggests presence of a millisecond component in CsI:In scintillation decay.

• Energy resolution of CsI:In under 662 keV ^{137}Cs γ-ray excitation is about 9% (in comparison with 6% for CsI:Tl). As excitation energy decreases, this parameter in CsI:In deteriorates faster than that in CsI:Tl. Measured light yield non-proportionality curves for CsI:In and CsI:Tl crystals were found to be quite similar (Fig. 4.3 a). Therefore higher energy resolution in CsI:In can be related to non-homogeneity of the activator distribution in the crystals.

• Activator effect on persistent luminescence properties of CsI:A is investigated. A slow component is observed in the scintillation decay kinetics under pulsed X-ray excitation and in the afterglow measurements. Rise of CsI:In scintillation pulse under X-ray excitation takes seconds at 300K, and is almost absent in CsI:Tl crystals. The persistent luminescence in CsI:In is caused by trapping of free electrons at the activator centers. Corresponding glow peak is pronounced in the TSL glow curves. Deep electron trapping level associated with In^+ is consistent with the model activator level positions in the forbidden band, suggested in Chapter 3.

• Temperature stability of CsI:In scintillation yield was found to be remarkably high. X-ray luminescence temperature quenching of CsI:In starts at around 600K, whereas the activator emission intensity of CsI:Tl drops starting from 350K. This difference between the two activator can be ascribed to different nature of the excited states: BE state in CsI:Tl, and activator excited $^3P_1$ state in CsI:In. Its temperature stability makes CsI:In a promising material to use in high temperature applications, such as well logging.

Scintillation efficiency of CsI:In at 300K (taking into account the delayed light)

was found to be the same as in CsI:Tl or CsI:Na (Fig. 4.7). Moreover, temperature profile of X-ray excited luminescence yield in indium doped CsI is quite similar to other activators. This fact suggests that the energy losses in CsI:A crystals are independent on the activator and have some intrinsic origin. Model of energy relaxation in CsI:A crystals with account of the intrinsic (STE) and activator channels is discussed in the following Chapter.

Chapter 5

Relaxation of electron excitations in CsI:In and CsI:Tl crystals

Contents

5.1 Electron excitations in CsI pure and CsI:A and their interaction 82
5.1.1 Excitation of STE luminescence in CsI 83
5.1.2 Activator excitation channels in CsI:A 84
5.2 Kinetic model of energy relaxation in CsI:A 89
5.2.1 General scheme of electron excitations 90
5.2.2 Mathematical modeling of energy relaxation 91
5.2.3 System parameters determination and numerical solution 94
5.2.4 Comparison of simulation and experiment 98
5.3 Model of the luminescence rise and the afterglow with account of the activator traps 108
5.4 Conclusions 113

This chapter deals with the processes of energy relaxation in CsI:Tl and CsI:In crystals. A general model of energy relaxation in CsI:A is suggested. At low temperatures in CsI holes start self-trapping which gives rise to the intrinsic channel of relaxation-emission of self-trapped excitons (STE). Activator impurity doping creates an additional competing channel of relaxation. Efficiency of these two channels is strongly dependent on temperature and the activator concentration. The model is used to explain energy losses in CsI:A scintillators.

As it was shown in Chapter 4, energy losses in CsI:A are about 50% at RT, and can reach up to 80% at LHeT (see Fig. 4.7). Another important experimental fact is that the amount of this loss is not dependent on the activator type (at least among tested Na^+, Tl^+ and In^+ activator ions). At temperatures below 100K (as self-trapping of holes comes in action), competition between intrinsic and activator induced channels of radiative relaxation is observed. Relative impact of each cannel into the total scintillation yield depends strongly on the activator concentration. Such behavior is observed for both In- and Tl-doped crystals. In general, at low temperatures (20-50K) we observe decrease of STE luminescence efficiency with increase of the activator concentration. This is accompanied by some increase of the activator luminescence intensity. Reasonable explanation to the energy losses observed in CsI:A is required. Beside of that, it follows from Chapter 4 that scintillation yield of CsI:A crystals strongly depends on the integration time. Standard integration times of the order of 10 μs are not sufficient for CsI:In. The activator induced electron trap was found to be the reason of the emission rise and the afterglow.

The goal of the present chapter is to develop a kinetic model of energy relaxation in CsI:A. This model should include the most important electron excitations in activated CsI, as well as possible interaction between them.

5.1 Electron excitations in CsI pure and CsI:A and their interaction

At this point, there are 3 experimental facts which require explanation. First, it is the high efficiency of STE emission in CsI pure at LHeT. Second, energy loss of 50% in activated CsI based scintillation crystals at RT. Third, up to 80% energy loss in CsI:A at LHeT. The first fact suggests high efficiency of e-h pair creation (β) in CsI. This efficiency does not significantly depend on temperature, nor on the activator concentration (see Chapter 1). Consequently, one can assume that the origin of the energy losses should be at the migration stage of the scintillation process (S). Quantum efficiency of luminescent centers (Q) is a function of temperature, so it should also be taken into account. In the following sections let us consider the efficiency of luminescence centers in CsI:A, and interactions between the electron excitations.

5.1.1 Excitation of STE luminescence in CsI

Let us first discuss the features of e-h recombination in undoped CsI crystal. As noted in Chapter 1, according to the absolute light yield measurements, STE luminescence in pure CsI crystal is extremely efficient. Due to low energy of *LO* phonons (about 0.01eV) electron thermalization distance in CsI should be quite long [Gridin et al., 2014c, Kirkin et al., 2012, Vasil'ev and Gektin, 2014]. This would provide a relatively small fraction of geminate e-h recombinations. Apparently, significant fraction of electron-hole pairs recombine stochastically, providing high efficiency of STE emission. This fact suggests a small contribution of the migration energy loss, because most of the excitations created eventually recombine.

One can get the idea of energy transfer efficiency from the matrix to the luminescence centers from the luminescence excitation spectra in UV – near VUV region. Luminescence excitation spectrum of 340 nm STE emission band in pure CsI crystal at 10 K is presented in Fig. 5.1. In this case the efficiency of electron capture by self-trapped holes can be characterized. One can compare the intensity of the luminescence excitation of STE along $E_g \div 2E_g$ region.

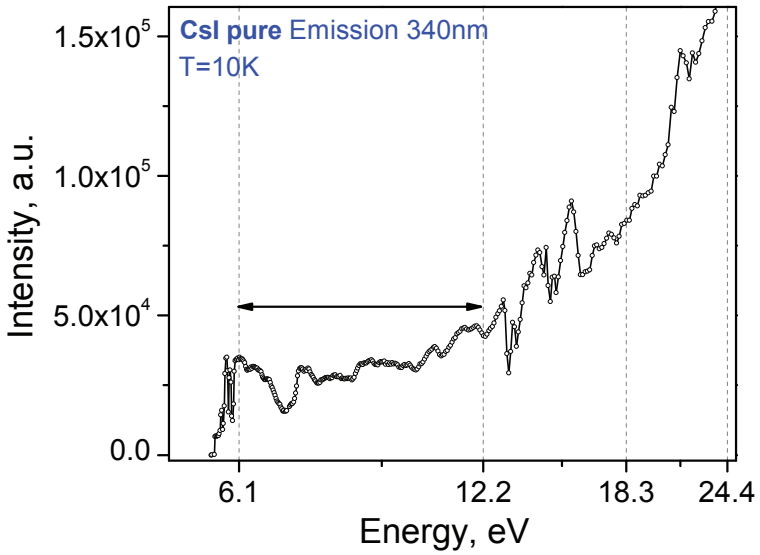

Figure 5.1: *CsI pure STE 340 nm band excitation spectrum at 10K*

Excitation of the crystal at around Eg (∼6.1 eV in CsI) results in creation of correlated electron-hole pairs. Such geminate pairs will form STEs and recombine radiatively. Increase of the excitation energy above E_g leads to creation of electrons in the conduction band and holes in the valence band with some kinetic energy. Consequently, the thermalization length of the charge carriers also increases. This

means that the average distance between geminate thermalized electron and hole becomes larger. Further, these thermalized electrons and holes will be diffusing through the crystal lattice until they interacts with each other to form a STE. Otherwise, in real crystal they can be captured by some traps – defects of the crystal lattice. If such trapping occurs, it can also be followed by non-radiative recombination. So the contribution of migration losses is expected to increase with increase of the distance between the electrons and holes. Therefore, increase of the excitation energy (if the migration energy losses are in action) will lead to decrease of the luminescence quantum yield. However, as we see from Fig. 5.1, the quantum yield of STE luminescence in pure CsI does not drop in $E_g \div 2E_g$ region. This suggests that the measured high light yield of CsI pure intrinsic emission characterizes the efficiency of e-h pairs production in the crystal.

5.1.2 Activator excitation channels in CsI:A

Certain assumptions about the mechanism of energy transfer to luminescence centers and about efficiency of this transfer can be made based on the analysis of the activator luminescence excitation spectra in the UV-VUV energy region, too.

Fig. 5.2 presents excitation spectra of the activator luminescence of CsI:Tl (a) and CsI:In (b) crystals within the region from 4 to 20 eV at 300K and 10K. Here E_a – is the edge of activator excitation, E_g – is the energy of band-to-band transitions, which is about 6.1 eV at 10K in CsI. The excitation spectrum of CsI:Tl activator luminescence presented in Fig. 5.2 (a), at 300K is similar to the spectrum presented in [Belsky et al., 1998]. Comparison of the luminescence quantum yield in the activator absorption region ($E_a \div E_g$) with the excitation intensity around $E_g \div 2E_g$ at 300K confirms high efficiency activator luminescence in CsI:Tl (Fig. 5.2 (a)).

Excitation directly at the excitonic absorption bands (around E_g) results in creation of correlated e-h pairs which recombine as excitons mostly. Activator luminescence quantum yield under excitation in this region characterizes efficiency of excitonic energy transfer to activator. Increase of the excitation energy above E_g leads to separation of electron-hole pairs created. In this case activator centers are excited due to consecutive capture of separated charge carriers. Increase of the activator quantum yield of CsI:A with the excitation energy increase (Fig. 5.2 a, b) suggests competition with the intrinsic STE recombination channel. Energy trans-

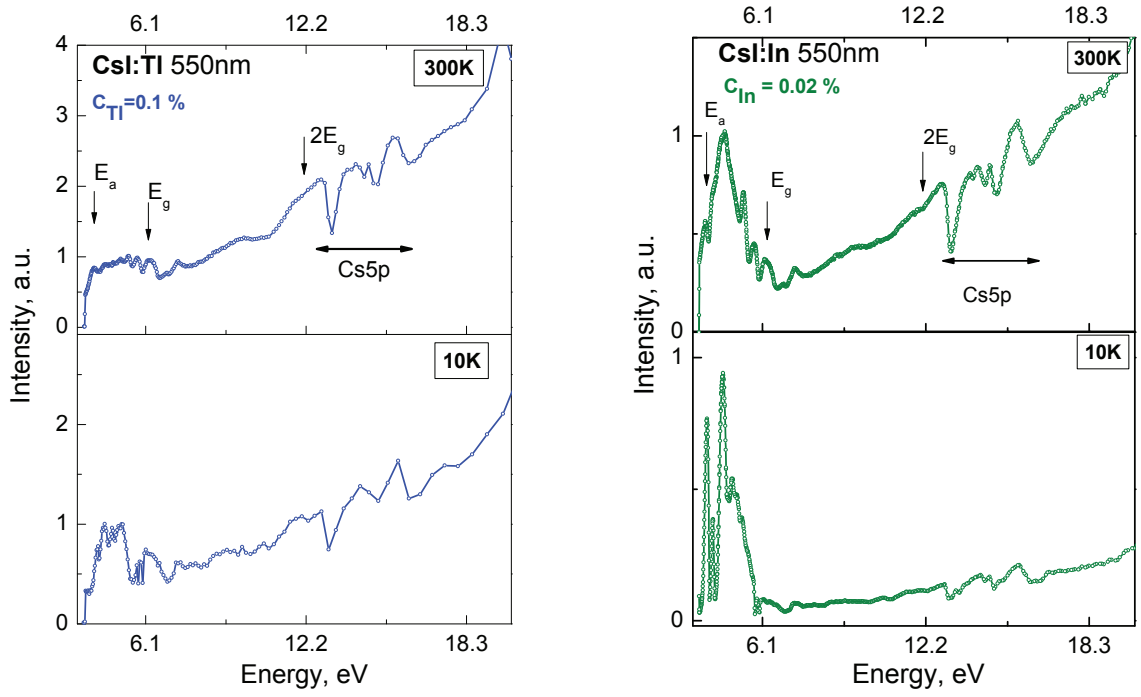

(a) (b)

Figure 5.2: *Excitation spectra of the activator emission 550nm in CsI:Tl (a) and CsI:In (b)*

fer from excitons to the activator centers in CsI:A is less efficient than capture of separated carriers. Efficiency of the energy transfer to the luminescence centers is lower at 10K than at RT, probably due to effective self-trapping of holes below LNT.

Let us consider the electron excited states in CsI:A. It is supposed that Tl^+ and In^+ activator ions in CsI can capture either an electron or a hole as a first carrier. Activator related electron trap is pronounced as TSL glow peak in CsI:A. In case of CsI:Tl the intense peak at 115K is related to electron release form Tl^0 centers, followed by their recombination with Tl^{++} centers. Similar explanation was suggested in Section 4.3 for 240K glow peak in CsI:In.

Beside of that, at $T < 90K$ self-trapping of holes occurs in CsI. Such a self-trapped hole (V_k center) has an effective positive charge, so it can capture a free electron. This process results in creation of STEs [Song and Williams, 1993]. Depending on temperature, this STE excited state can radiatively or non-radiatively recombine.

Charge carriers capture by activator and intrinsic centers in CsI:A can be discussed in detail based on the TSL glow curves. TSL glow curves for CsI:A with

different concentrations of the dopant are presented in Fig. 5.3. For CsI:Tl the peaks at 60K and 115K increase progressively with the dopant concentration (Fig. 5.3 a) relative to the peak at 90K. Similar dependence of TSL peaks intensity in CsI:Tl was mentioned in [Babin et al., 2002a].The intensity of TSL peak around 240K in CsI:In is also concentration dependent (Fig. 5.3 b).

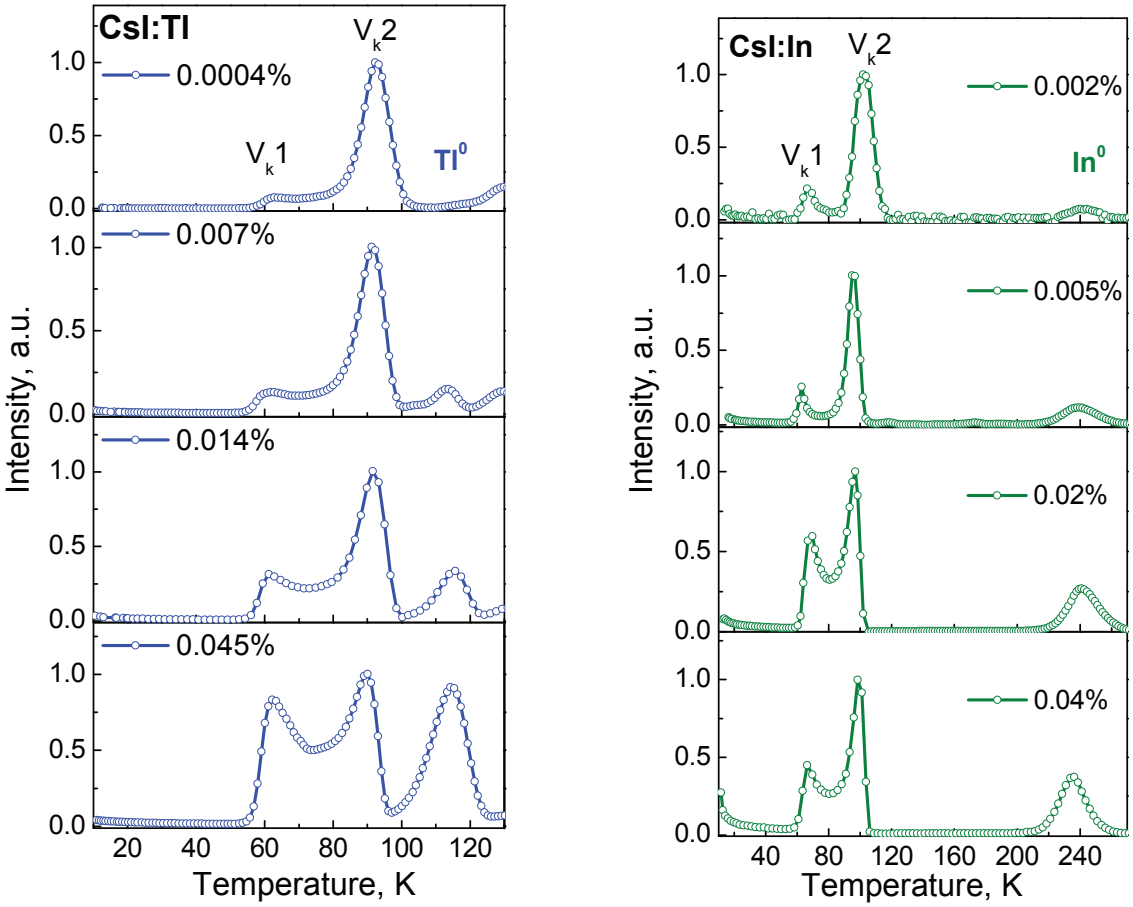

(a) (b)

Figure 5.3: *TSL glow curves of CsI:Tl (a) and CsI:In (b) crystals with varying dopant concentration*

The features of excitations localization and migration should be considered as a function of temperature. There are two diffusion mechanisms of self-trapped holes in CsI. First is the hopping diffusion, when one of the halides involved in the creation of V_k center remains at its site, and the second one changes for the neighbor one. Such jump is accompanied with 90^0 rotation of the V_k center. TSL peak at 60 K is connected with holes' recombination, moving in such way. Second is diffision of delocalized (free) holes which corresponds to the glow peak at 90K.

The model of delocalization and migration of the carriers in CsI:A (based on literature data and our results) can be represented as follows. Under X-irradiation at 10K e-h pairs are created, and the charge carriers get captured. We suppose that an electron can localize only at the activator ($A^+ + e \rightarrow A^0$) site. A hole can become self-trap ($h \rightarrow STH = V_k$), or localize at the luminescence center ($A^+ + h \rightarrow A^{++}$). We shall note that under X-irradiation the probability of STH creation should be much higher than that of A^{++} formation, because V_k centers can be formed in any cell of the lattice ($n_{V_k} = n_{I_2} = 10^{22} cm^{-3}$ in CsI), while $n_{Tl} = 10^{19} cm^{-3}$. The mechanism of V_k hopping diffusion is activated at 60K and their recombination at A^0 centers (electron captured by the activator ion) occurs, and the capture of holes at A^+ ($A^+ + h \rightarrow A^{++}$) is also possible. The thermal de-trapping of holes and their migration to A^0 (as they are negatively charged) occurs at 90K. Because of this, the released holes are captured at A^+ ions with the formation of A^{++}, when migrating, should be less probable. The peak at 115K in CsI:Tl is a result of electrons release from Tl^0 and capture by Tl^{++}. Given such model, delocalization of the holes from activator centers should occur at a higher temperature. However, this delocalization is not pronounced as an intense TSL peak because all the Tl^0-centers have already been destructed at 115K.

In Cs:In, apart the two main low-temperature TSL peaks, the intense concentration dependent peak around 240K is observed. Probably it is connected with the capture of e^- or h^+ at the activator with the following delocalization. We suppose that the model of the capture mechanism and excitations relaxation, similar to that proposed for CsI:Tl crystal, can be used in case of CsI:In.

Let us consider the possibility of non-radiative energy transfer from STE to activator in CsI:Tl and CsI:In. Necessary condition for non-radiative d-d energy transfer between the STE and the activator in CsI:A is the overlap of the activator absorption spectrum with the STE emission band. In fact, the probability of dipole-dipole energy transfer is proportional to the overlap of the emission and absorption spectra [Agranovich and Galanin, 1982, Förster, 1948, Vasil'ev and Mikhailin, 2008]. As can be seen from Fig. 5.4, for both activators the overlap of the excitation spectra of the STE emission band at 3.6 eV is very weak. However, as shown in the inset Fig. 5.4, the activator absorption spectrum of CsI:A overlaps with 4.25eV on-center STE band. Reabsorption of this emission band by the activator results in the char-

acteristic valleys at the energy of band maximum. Thus, the non-radiative energy transfer from the STE to the actuator is possible due to the overlap of the activator absorption with the 4.25 eV on-center STE band. If we refer the model of the exciton relaxation, shown in Fig. 1.11 in [Song and Williams, 1993], on-center and of-center states are thermally coupled. If the energy barrier between the on-center and off-center minima is small enough, populating of the higher exciton level II from lower energy level III is possible. Indeed, in [Belsky et al., 1992] emission around 4.25 eV was observed under pulsed X-ray excitation even at room temperature and above.

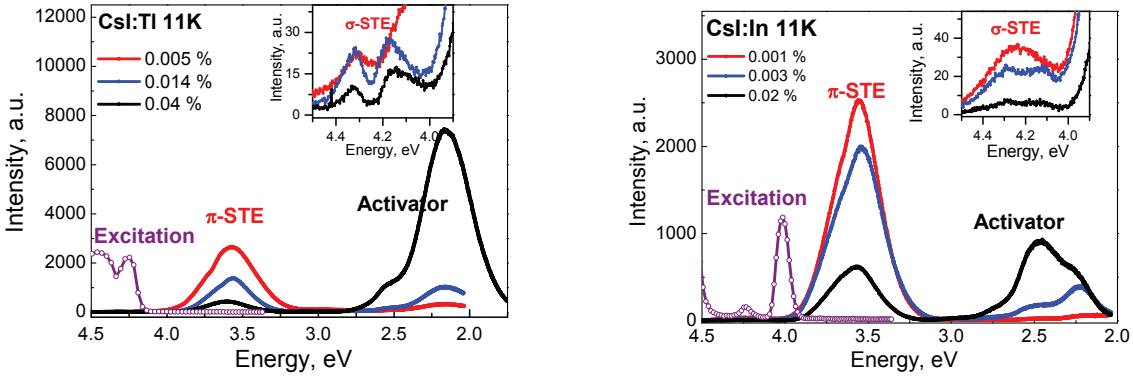

(a) (b)

Figure 5.4: *Overlap between activator absorption and STE luminesce bands at 11K: X-ray luminescence spectra of CsI:Tl (a) and CsI:In (b) –solid lines, excitation spectra of 550 nm emission band – empty circles*

Strictly speaking, in order to confirm the fact of non-radiative transfer between the STE and the activator centers, luminescence decay measurements of the STE emission band as a function of the activator concentration are necessary. Such experiments were not conducted during this study, though.

Summarizing the discussion of the scintillation process in CsI:A crystals in this Chapter, evolution of electron excitations can be presented as a diagram in Fig. 5.5. Thickness of the branches corresponds to concentration of holes (h, red lines), electrons (e, green), excitons and self-trapped excitons (ex and STE, dark yellow), self-trapped holes (STH, dark red), excited states of activator (A^*, blue), activators with captured electrons (A^-, blue-green) and holes (A^+, blue-red). Bifurcations of lines correspond to different processes mentioned in the flowchart. Gray line corresponds

to non-radiative quenching of excitations. The flowchart is subdivided into three parts, corresponding to the cascade of carriers (β), efficiency of energy transfer to the luminescence center (S), and quantum efficiency of the luminescence centers itself (Q).

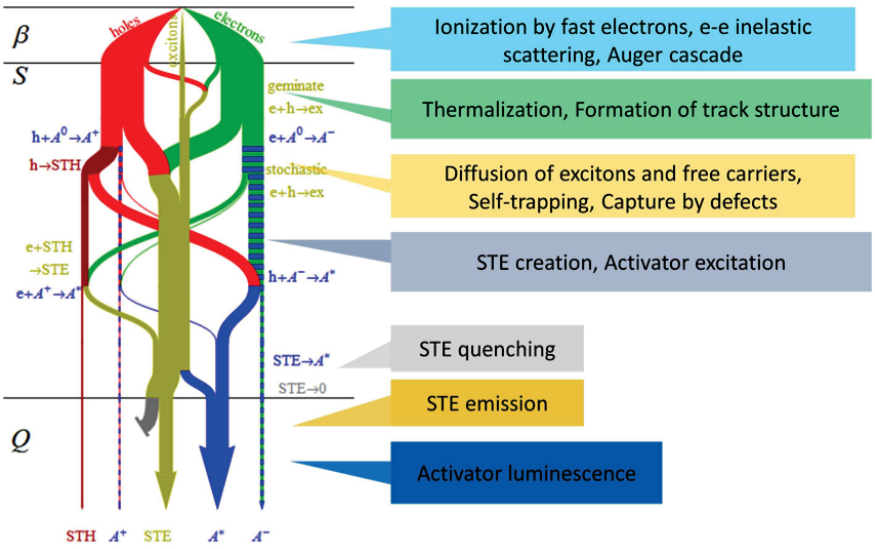

Figure 5.5: *Pathways of electron and hole recombination with production of excitons and capture by activators in CsI:A [Gridin et al., 2014c]*

Even though the general trends in energy relaxation processes of CsI:A are known, the impact of each process (thickness of each branch) is unclear. Influence of the measurement conditions and parameters should be investigated.

5.2 Kinetic model of energy relaxation in CsI:A

For a correct and complete description of the scintillation processes in CsI:A a general model of energy relaxation should be suggested. It should take into account all the most important features of the luminescence centers and the system parameters. As described in Chapter 1, thermalization of the electron excitations is followed by the migration stage (S term in eq. 1). During this stage localization of electron excitation takes place at some capture centers. Then once excited luminescence centers are formed, there can be some interaction between them. This interaction may include the energy transfer or emission quenching. Otherwise radiative recombination of the excited centers occurs (Q term in eq. 1). All these processes are closely related, and depends strongly on the parameters of the system:

peculiarities of the luminescence centers and traps of charge carriers. Most of the energy relaxation calculus approaches use simplified models of electron excitations in CsI:A, or calculate only the interactions during the first picoseconds of thermalization [Kerisit et al., 2008, Wang et al., 2012]. In this section a detailed description of the final energy relaxation stage is provided, which includes all the activator charge states, as well as the intrinsic relaxation channel in CsI:A.

5.2.1 General scheme of electron excitations

Based on the experimental data analysis presented in the Chapter 3, Chapter 4, and Section 5.1, the general model of energy relaxation in CsI:A is described in Fig. 5.6. Under exposure to ionizing radiation, free electrons and holes are created. These charge carriers can participate in creation of the following electron excitations. Firstly, these are actually free electrons e^- (electrons in the conduction band) and free holes h^+ (holes in the valence band). Free holes can become self-trapped, they can as well be captured by neutral activator centers A^+ or by charged activator centers A^0. The latter case leads to formation of excited activator centers $A^0 + h^+ \rightarrow (A^+)^*$. Free electrons e^- can be captured by STH to form a self-trapped excitons $STH + e^- \rightarrow STE$. Another possibility is electron capture by the activator cents $A^+ + e^- \rightarrow A^0$, or $A^{++} + e^- \rightarrow (A^+)^*$.

It is supposed here, that the excited activator state $(A^+)^*$ (in the temperature range 10-300K that we consider) undergoes radiative relaxation with the characteristic radiation time τ_A: $(A^+)^* \rightarrow A^+ + h\nu$ 550nm. STE, depending on temperature, can give either radiative ($STE \rightarrow h\nu$ 340nm), or non-radiative relaxation ($STE \rightarrow h\Omega$). Both this processes are indicated in Fig. 5.6. It is important to note here, that only two relaxation channels are introduced in the suggested Model: (1) STE, which can radiatively of non-radiatively recombine, and (2) activator emission. No impurity centers of relaxation are used.

Captured charge carriers, when the thermal energy is enough, can be released and go back the corresponding allowed band: $A^0 \xrightarrow{kT} A^+ + e^-$, or $A^{++} \xrightarrow{kT} A^+ + h^+$, and for self-trapped holes $STH \xrightarrow{kT} h^+$. It should be also accounted, that a certain fraction of excitations is instantly bond in excitons (so called direct creation of excitons) [Vasil'ev and Gektin, 2014].

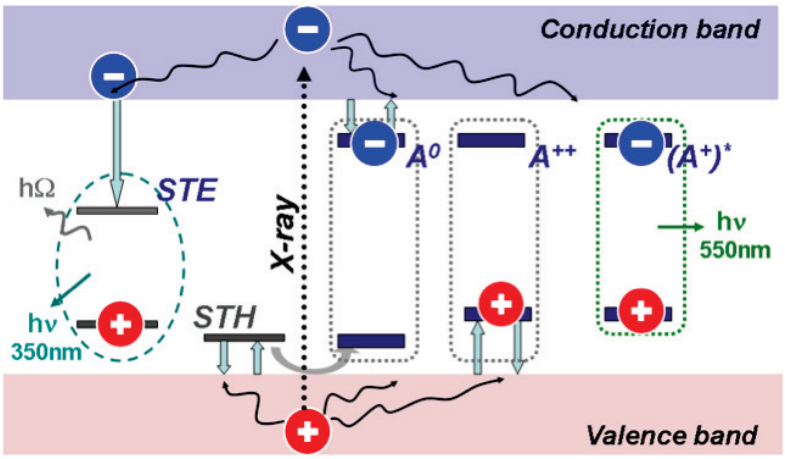

Figure 5.6: *Band model of electron excitations in CsI:A which contains:*
1) free electrons (electrons in conduction band)
2) free holes (holes in the valence band)
3) self-trapped holes (STH)
4) self-trapped excitons, i.e. electrons trapped by STH ($STH + e^- = STE$)
5) electrons trapped by activator ions ($A^+ + e^- = A^0$)
6) holes trapped by activator ions ($A^+ + h^+ = A^{++}$)
7) excited states of the activator centers $(A^+)^*$, *which is created if either an electron is trapped by* A^{++} *center* ($A^{++} + e^- = (A^+)^*$), *or if a hole is trapped by* A^0 *center* ($A^0 + h^+ = (A^+)^*$)

5.2.2 Mathematical modeling of energy relaxation

For mathematical modeling of energy relaxation presented in Fig. 5.6 a system of rate equations was composed (see eq. 5.1). This approach to describe the luminescence kinetics crystal phosphors was initially developed in the 60th by Antonov-Romanovskiy and Fok [Antonov-Romanovskiy, 1966, Fok, 1964]. For some simplified cases the analytical solutions were obtained. Recently, the method of kinetic modeling of energy relaxation processes was used to describe energy relaxation processes in scintillation crystals [Moretti et al., 2014, Savon et al., 2012]. In the latter works, mathematical modeling is done using numerical method to solve the equations.

This system of equations eq. 5.1 describes change in time for concentration of free electrons n_e, free holes n_h, those holes which are self-trapped in vicinity of A^0 centers n_{TH}, the rest of self-trapped holes n_{STH}, electrons captured by activator centers n_{ce}, holes captured by activator centers n_{ch}, self-trapped excitons STE, and

excited activator centers n^*.

System of rate equations

(1) $\frac{dn_e(t)}{dt} = \alpha(t)(1 - r_{ex}) - \beta_{0e}n_e(t)(n_{cc} - n_{ce}(t) - n_{ch}(t)) + s_e n_{ce}(t)exp(\frac{-A_e}{kT}) - \beta_{he}n_{ch}(t)n_e(t) - \beta_{STE}n_e(t)(n_{STH}(t) + n_{TH}(t))$

(2) $\frac{dn_h(t)}{dt} = \alpha(t)(1-r_{ex})-\beta_{STE}n_h(t)(n_{hh}-\beta_{TH}n_h(t)(n_{hh}-n_{TH}(t))-\beta_{0h}n_h(t)(n_{cc}-n_{ce}(t) - n_{ch}(t)) - \beta_{eh}n_{ce}(t)n_h(t) + s_{STH}n_{STH}(t)exp(\frac{-A_{STH}}{kT}) + s_h n_{ch}(t)exp(\frac{-A_h}{kT}) + s_{TH}n_{TH}(t)exp(\frac{-A_{TH}}{kT})$

(3) $\frac{dn_{STH}(t)}{dt} = \beta_{STH}n_h(t)(n_{hh}-n_{STH}(t))-s_{STH}n_{STH}(t)exp(\frac{-A_{STH}}{kT})-\beta_{STH}n_e(t)n_{STH}(t)$

(4) $\frac{dn_{TH}(t)}{dt} = \beta_{TH}n_h(t)(n_{hh} - n_{TH}(t)) - s_{TH}n_{TH}(t)exp(\frac{-A_{TH}}{kT}) - \beta_{STE}n_e(t)n_{TH}(t)$

(5) $\frac{dn_{ce}(t)}{dt} = \beta_{0e}n_e(t)(n_{cc} - n_{ce}(t) - n_{ch}(t)) - s_e n_{ce}(t)exp(\frac{-A_e}{kT}) - \beta_{eh}n_{ce}(t)n_h(t)$

(6) $\frac{dn_{ch}(t)}{dt} = \beta_{0h}n_h(t)(n_{cc} - n_{ce}(t) - n_{ch}(t)) - s_h n_{ch}(t)exp(\frac{-A_h}{kT}) - \beta_{he}n_{ch}(t)n_e(t)$

(7) $\frac{dn_{STE}(t)}{dt} = \beta_{STE}n_e(t)(n_{STH}(t) + n_{TH}(t)) - s_{STE}n_{STE}(t)exp(\frac{-A_{STE}}{kT}) - \frac{n_{STE}}{\tau_{STE}} + \alpha(t)r_{ex}$

(8) $\frac{dn^*(t)}{dt} = \beta_{he}n_e(t)n_{ch}(t) + \beta_{eh}n_h(t)n_{ce}(t) - \frac{n^*(t)}{\tau_A}$

(5.1)

Let us move to the description of the terms in the Rate Equations (eq. 5.1). In first equation term $\alpha(t)(1 - r_{ex})$ describes the electron-hole creation rate in the crystal under irradiation. Here coefficient $(1 - r_{ex})$ indicated that the part of the correlated electron-hole pairs giving direct creation of excitons is skipped. Term $-\beta_{0e}n_e(t)(n_{cc} - n_{ce}(t) - n_{ch}(t))$ describes electron capture by activator centers A^+. Minus sign indicated that such process leads to decrease of free electrons' concentration. Term $-\beta_{he}n_{ch}(t)n_e(t)$ is for electron capture by A^{++} centers. Bimolecular

capture coefficient in case of a changed center β_{he} is different from that in case of capture by a neutral center β_{0e}. Term $+s_e n_{ce}(t) exp(\frac{-A_e}{kT})$ describes thermal release of electrons from A^0. Expression $-\beta_{STE} n_e(t)(n_{STH}(t) + n_{TH}(t))$ characterizes electron capture by STH with creation of STE.

Second equation of the system describes time change of free holes. Term $\alpha(t)(1 - r_{ex})$ – is the electron-hole creation rate under irradiation. Expression $-\beta_{STE} n_h(t)(n_{hh} - n_{STH}(t))$ characterizes self-trapping of holes in regular CsI lattice (not too close to the A^0 centers), and term $-\beta_{TH} n_h(t)(n_{hh} - n_{TH}(t))$ - self trapping of holes in vicinity of A^0-centers. Member $-\beta_{0h} n_h(t)(n_{cc} - n_{ce}(t) - n_{ch}(t))$ describes capture of holes by neutral activator centers A^+, and term $-\beta_{eh} n_{ce}(t) n_h(t)$- by activator center with electrons A^0. Expressions $+s_{STH} n_{STH}(t) exp(\frac{-A_{STH}}{kT})$, $+s_h n_{ch}(t) exp(\frac{-A_h}{kT})$, and $+s_{TH} n_{TH}(t) exp(\frac{-A_{TH}}{kT})$ describe thermally activated delocalization of self-trapped holes, holes trapped by activators, and holes which are self-trapped in vicinity to A^0 centers, respectively.

Equations 3-6 of the system describe the balance of holes trapped in proximity of A^0 centers $\frac{dn_{TH}(t)}{dt}$, regular STH $\frac{dn_{STH}(t)}{dt}$, electrons trapped by activator ions $\frac{dn_{ce}(t)}{dt}$, and holes trapped by activator ions $\frac{dn_{ch}(t)}{dt}$. Terms in the corresponding equations are described above.

Equation number seven is for the balance of STE. First term in the right part $\beta_{STE} n_e(t)(n_{STH}(t) + n_{TH}(t))$ describes capture of electron by self-trapped holes with creation of STE. Term $-s_{STE} n_{STE}(t) exp(\frac{-A_{STE}}{kT})$ takes into account temperature quenching of STE emission. Term $-\frac{n_{STE}}{\tau_{STE}}$ describes radiative decay of STEs, and $+\alpha(t) r_{ex}$ - direct creation of excitons.

Eighth equation of the System, which characterizes the balance of excited activator centers, contains term describing electron capture by A^{++} centers $\beta_{he} n_e(t) n_{ch}(t)$, capture of holes by A^0 centers $+\beta_{eh} n_h(t) n_{ce}(t)$, and also a term describing radiative decay of excited activator centers $-\frac{n^*(t)}{\tau_A}$.

Such a system of differential equations does not have an analytical solution. However, a numerical solution can be found if initial conditions and parameter values are set. Many of the parameters can be eliminated from experiment, other can be at least estimated.

5.2.3 System parameters determination and numerical solution

I. Frequency factors and trap depths

Energies of thermal release of charge carriers from traps (trap depths) as well as the frequency factors of such delocalization can be derived from glow curve analysis [McKeever, 1985]. For CsI:Tl and CsI:In single crystals parameters of some traps are obtained using the initial rise method. Following X-ray irradiation with of 30mA 35kV during 10 minutes, partial cleaning of the glow curve was done by heating the sample up to the temperature of the peak maximum (Fig. 5.7) in order to separate the overlapping peaks and to see its initial rise profile. The peak at 60K (hopping diffusion of holes) does not disappear completely, because it corresponds to the same centers as 90K peak–self trapped holes. In radiative recombination with A^0-centers at 60K recombine only those STH which are spatially correlated with (i.e. in the vicinity of) A^0-centers.

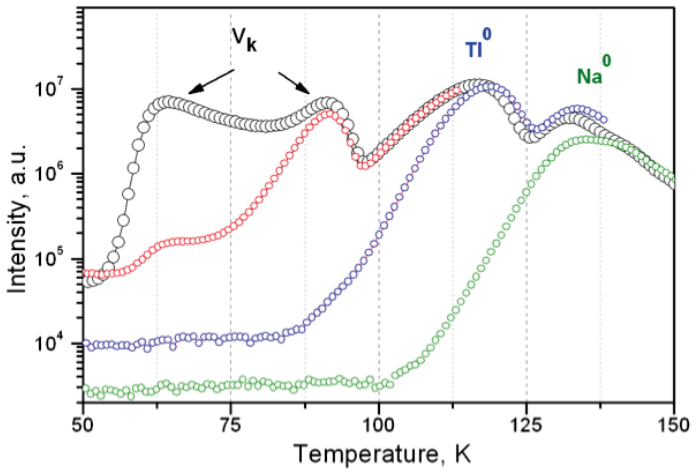

Figure 5.7: *TSL curves of CsI:Tl crystal measured at sequential destruction of peaks by means of the intermediate heating up to the temperature of the following peak maximum*

Glow peak around 240K in CsI:In cannot be treated in frame of the first order kinetics (when probability of recombination after detrapping is much higher than the probability of repetitive trapping of the carriers). Parameters of this peak were found by means of fitting the glow curve with the equation for general order kinetics TSL intensity (eq. 5.2). The best match was obtained with the parameters given in Table 5.1.

$$I(T) = n(0)s^{"}exp(\frac{-E_A}{kT})\left[1 + \left(\frac{(b-1)s^{"}}{T'}\right)\int_{T_0}^{T} exp(\frac{-E_A}{kT})dT\right]^{b(b-1)} \quad (5.2)$$

where b is kinetic order,

$n(0)$ – concentration of filled traps,

s – frequency factor,

E_A – trap depth,

k – Boltzmann constant,

T – temperature,

T' – heating rate.

Table 5.1: *Trapping parameters in CsI:Tl and CsI:In*

Crystal	Peak Temp., K	E_A, eV	s, sec^{-1}	kin. order	LifeTime at 300K, sec
CsI:Tl,CsI:In	60	0.23	4.8×10^{16}	1	
CsI:Tl,CsI:In	90	0.15	3.0×10^{6}	1	10^{-4}
CsI:Tl	115	0.28	3.3×10^{10}	1	1.4×10^{-6}
CsI:In	240	0.59	1.1×10^{11}	1.6	

Table 5.1 collects parameters of Tl, In and intrinsic traps in CsI, which were used in the System of rate equations. Apparently the tunneling diffusion of holes to the luminescence centers is the main reason of the abnormally high frequency factor and thermal energy of delocalization, obtained for the peak at 60K. Trap parameters from Table 5.1 were used for fitting of experimental TSL curves with expression (eq. 5.2).

Fitting of experimental TSL curves of CsI:Tl and CsI:In with eq. 5.2 is presented in Fig. 5.8 (a, b). The fit is in fair agreement with experiment, except for the 60K glow peak.

Mean time a charge carrier spends in the trap at given temperature is given as:

$$\tau = \frac{1}{s}exp(\frac{E_A}{kT}) \quad (5.3)$$

where s – frequency factor, E_A – trap depth.

It is important to note that above delocalization temperature point the lifetime in traps can be significant. In our case, using the trap parameters from Table 5.1,

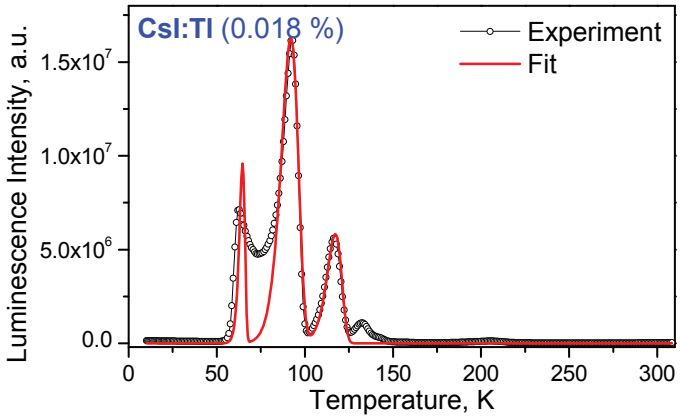

(a)

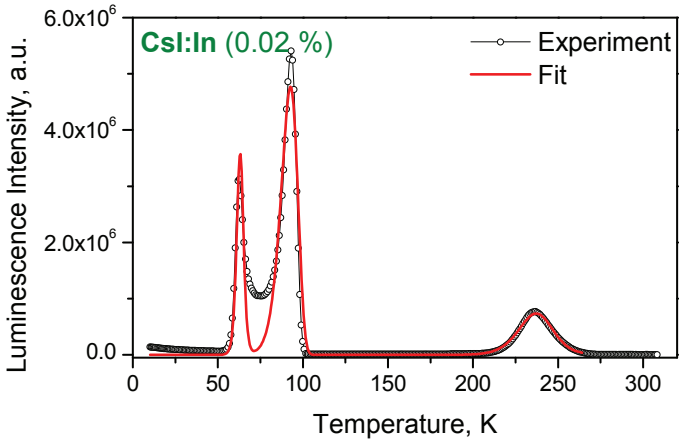

(b)

Figure 5.8: *Fitting of CsI:Tl (a) and CsI:In (b) glow curves with eq. 5.2 using trap parameters from Table 5.1*

one can get the mean lifetime of STHs at 300K is about 10^{-4} sec. For comparison, lifetime of Tl^0 centers (electors trapped in Tl) is 1.4×10^{-6} sec, which is two orders of magnitude smaller. This suggests that even at RT self-trapping of holes still occurs, and these STH can capture electrons with following radiative/non-radiative STE recombination.

Frequency factors and trap depths for holes captured by activator in CsI:A cannot be obtained from the glow curves, since there are no TSL peaks corresponding to hole release from A^{++}. Absence of those peaks can be explained as follows: all the A^0 centers are destroyed at lower temperature (115K for CsI:Tl and 240K for CsI:In). So that even if some holes are left trapped by the activator, their thermal release will not give creation of $(A^+)^*$ followed by the activator luminescence [Babin et al., 2002a, Gridin et al., 2014b]. However, as reported in [Spaeth et al., 1994], in CsI:Tl by

means of EPR methods holes were found to remain localized in Tl sites for a few minutes after heating the crystal up to RT. This result suggest that Tl-related hole trap in CsI should be stable enough at 300K. Finally, parameters of activator related hole traps were chosen to be: $A_h = 0.7eV$ and $s_h = 10^{11}\ sec^{-1}$ for CsI:Tl, and $A_h = 1.0eV$, $s_h = 10^{11}\ sec^{-1}$ for CsI:In. Variation of these parameters further showed no significant change in simulations of light yield temperature dependence and TSL of CsI:A in the region 10-300K.

II. Bimolecular capture coefficients β

Parameters β_{ij}, determine capture probability of charge carriers by corresponding centers. In the diffusion approximation, these coefficients can be expressed through diffusion coefficients and capture radii: $\beta_{ij} = 4\pi D_j R_{ij}$, Here D_j – are diffusion coefficients of corresponding charge carrier, and R_{ij} – capture radius of carrier j by center i. Diffusion coefficients for electrons and holes significantly depend on temperature. For the case of hopping diffusion (which is true for CsI at low temperatures), the diffusion coefficients for holes can be written as $D_h = a_h^2 \nu_h / 3$, where a_j – is the distance of a single hop, ν_j – frequency of hops. Value of a_j can be estimated as CsI lattice constant (0.47 nm),and ν_j - as frequency of LO phonons. Capture radius R_{0j} can be estimated as 2.5×10^{-7} cm [Gridin et al., 2014c]. This gives the estimation of capture coefficients by regular activator ions $\beta_{0e} = \beta_{0h} \sim 10^{-8} cm^3/sec$. In case of electron or hole capture by charged centers (i.e. by self-trapped holes or by activator centers which have already trapped a carrier of opposite sign) capture radius is the Onsager radius [Kirkin et al., 2012, Vasil'ev and Gektin, 2014] (for CsI at 80K $R_{Ons} = 4 \times 10^{-6} cm$). This estimate of capture by charged centers gives $\beta_{STE} = \beta_{he} = \beta_{eh} \sim 10^{-7} cm^3/sec$. Strictly speaking, approach to estimation of the diffusion coefficient done here is applicable only for holes in CsI a low temperatures, when hopping diffusion mechanism is active. Moreover, both diffusion coefficient and capture radius are dependent on temperature. However, in present work the estimation are used to simulate dynamics of relaxation channels' efficiency in CsI:A.

III. Other parameters

STE radiation time in CsI τ_{STE}, as well as activation energy of intrinsic temperature quenching of STE A_{STE} and its frequency factor s_{STE} were obtained previously. Radiation time parameter of excited In and Tl activator centers τ_A was chosen equal 10^{-6} sec, which is close to experimentally obtained values for CsI:Tl and CsI:In under intracenter photo excitation (see Chapter 3 and Chapter 4).

Parameter $\alpha(t)$ – elector-hole pair creation rate – was estimated as follows. X-ray photon flux falling onto the sample surface was 6.5×10^9 $photons/(cm^2 sec)$. Given the cathode-anode voltage of 35kV, attenuation length of such X-ray quanta is about 10 μm [Nis, 2014]. Energy efficiency of an electron-hole pair creation in CsI can be estimated as 1.6 E_g, which is about 10eV per e-h pair [Gridin et al., 2014c]. Then one X-ray photon with an average energy 21 keV (average energy of X-ray spectrum in our experiment) creates 2100 e-h pairs in the crystal. Finally, average electron excitations creation rate in 10 μm surface layer of CsI will be about 10^{16} $cm^{-3} sec^{-1}$.

Parameter r_{ex} (direct creation of excitons) is typically of the order of 0.1 in inorganic scintillators [Vasil'ev and Gektin, 2014]. In present simulation it was chosen to be 0.2.

5.2.4 Comparison of simulation and experiment

I. Temperature dependences

Comparison of experimental and simulated temperature dependences of STE (340nm) and activator (550nm) emission channels of CsI:Tl and CsI:In is presented in Fig. 5.9 and Fig. 5.10, respectively. Activator concentrations for the simulated curves (panels *b* and *d* in Fig. 5.9 and Fig. 5.10) were chosen close to the real activator concentrations in investigated crystals.

Fair agreement between the experimental results and simulated curves is evident for both CsI:Tl and CsI:In. Simulated STE emission intensity tends to decrease as temperature grows up. Overall STE emission yield also drops as activator concentration decreases (Fig. 5.9 a,b and Fig. 5.10 a,b). Activator emission channel drops at low temperature range. Activator energy losses in (10-60)K temperature region (Fig. 5.9 d and Fig. 5.10 d) are similar to those obtained in the experiment (Fig. 5.9 c and Fig. 5.10 c).

The simulated curves are modulated with similar valleys as the experimental dependences are. Those valleys correspond to the intense intrinsic and activator-related glow peaks in corresponding TSL curves, and are related to trapping of charge carriers. As temperature reaches 90K (point of hole self-trapping in CsI), an evident decrease of the activator channel yield is observed in the simulated curves, too.

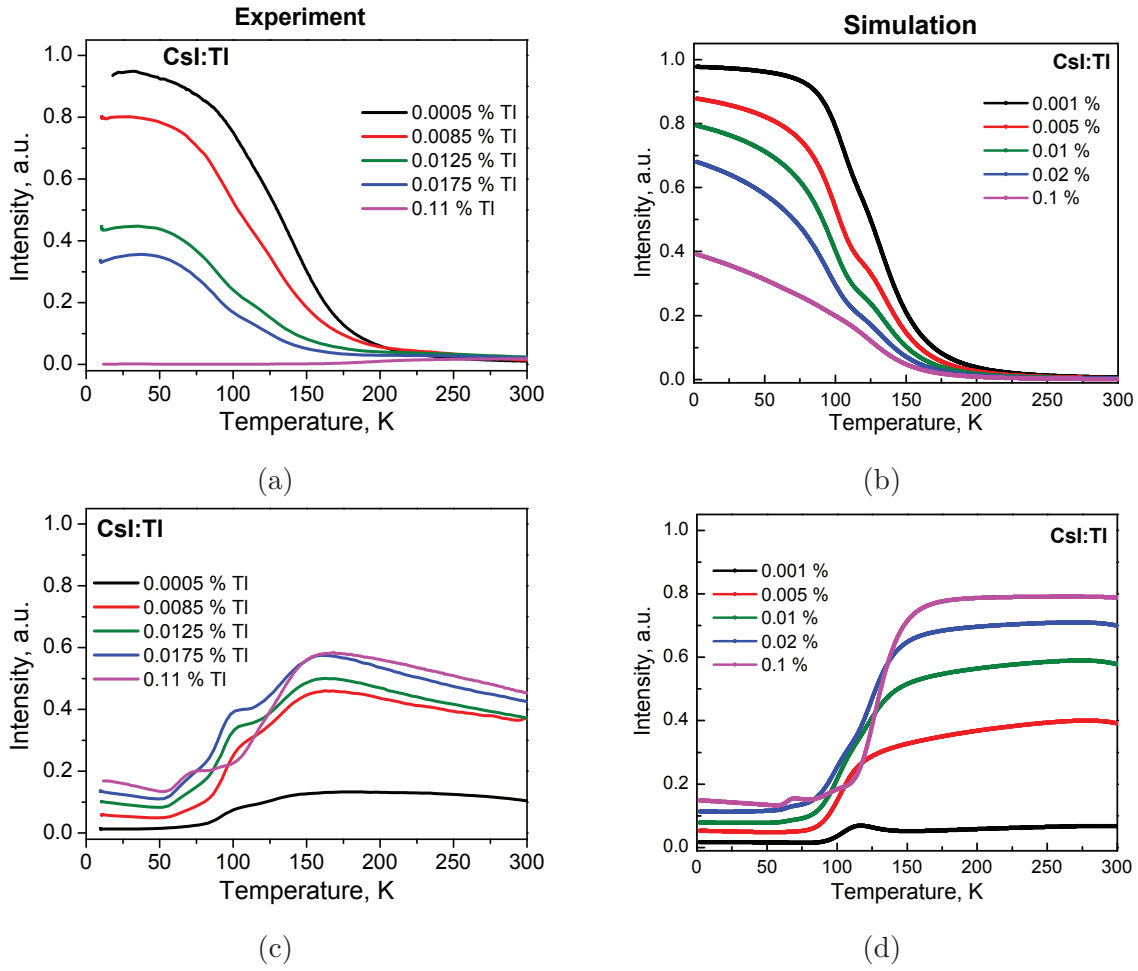

Figure 5.9: *Experimental temperature dependences of STE 340nm (a) and activator 550nm (c) emission channels in CsI:Tl for different activator concentrations in comparison with simulated curves for STE (b) and activator (d) yields*

Overall, temperature behavior and tendencies of scintillation yield obtained in the experiment are reflected in the simulation. This means that the model of energy relaxation presented in Fig. 5.6 takes into account the most important processes of energy localization and relaxation in CsI:A. It also confirms that the parameters used for numerical solution of the system of rate equations (eq. 5.1) were well evaluated.

Nevertheless, the simulations somewhat overestimates the STE recombination channel at relatively high activator concentrations. Besides, activator emission yield at around 300K makes about 80% of STE efficiency which is also somewhat overestimated. According to the experimental results, activator emission yield at 300K in CsI:A is about 50% of STE. Keeping in mind that some of the system parameters are roughly estimated, let us see how change of certain parameters affects the efficiency

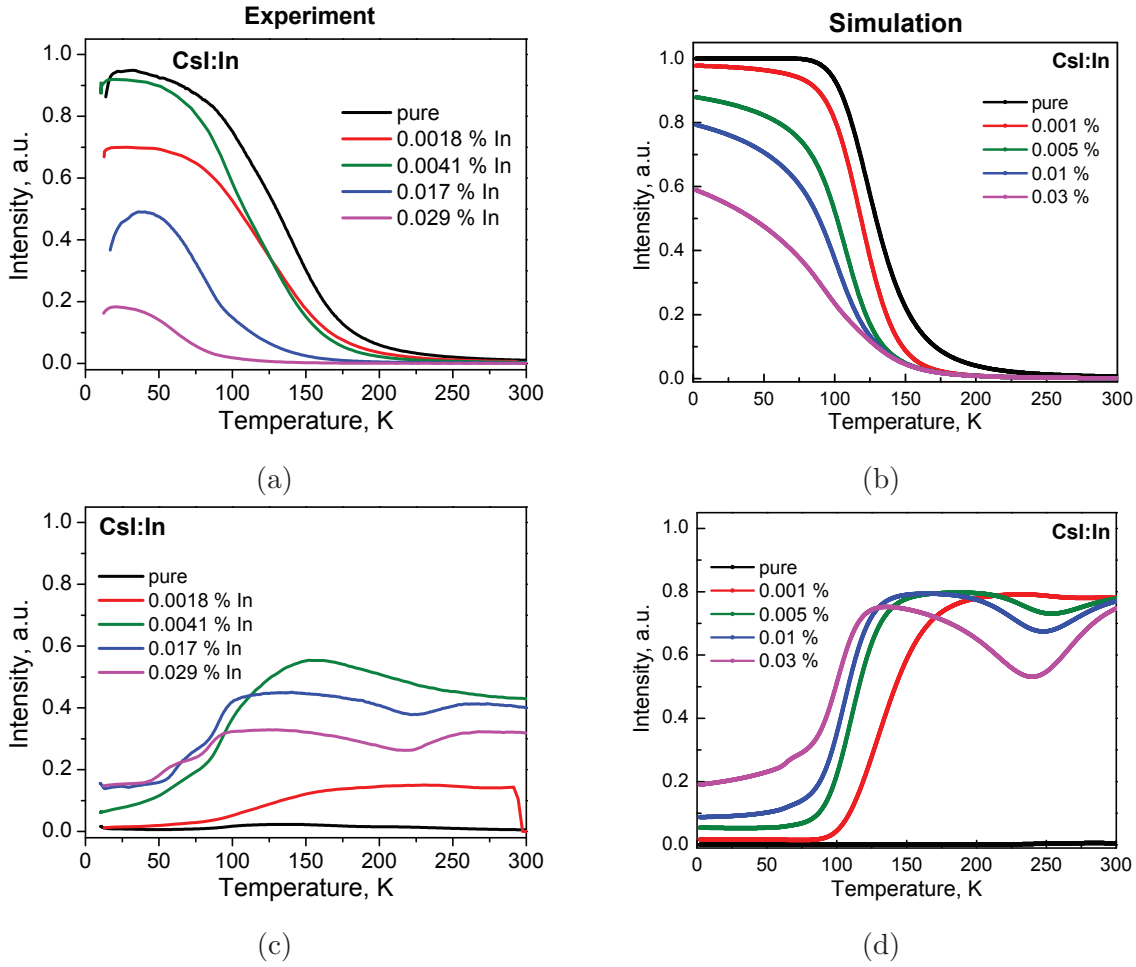

Figure 5.10: *Experimental temperature dependences of STE 340nm (a) and activator 550nm (c) emission channels in CsI:In for different activator concentrations in comparison with simulated curves for STE (b) and activator (d) yields*

of the intrinsic and activator relaxation channels in CsI:A.

Fraction of direct creation of excitons r_{ex} was estimated as 0.2 for CsI (see previous Section). More accurate evaluation of this parameter is difficult. Increase of r_{ex} value naturally leads to rise of STE emission channel (Fig. 5.11 a). On the other side, activator emission yield drops down as rex growths (Fig. 5.11 b). Fraction of the activator energy losses within (150-300)K temperature region basically corresponds to r_{ex} value. Setting it to 0.4-0.5 allows to reproduce activator emission yield around RT. It was noted earlier that valued of this parameter in CsI can be higher in view of the band structure of CsI [Vasil'ev and Gektin, 2014]. Auger decay of 5pCs core holes should result in creation of low energy electron-hole pairs which would the fraction of excitons created.

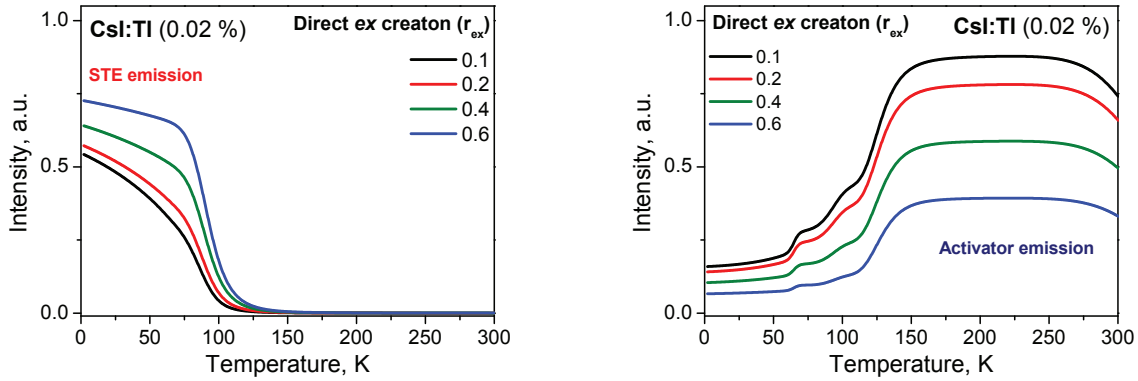

(a) (b)

Figure 5.11: *Temperature dependence of STE (a) and activator (b) luminescence yield in CsI:Tl as a function of direct exciton creation parameter r_{ex} (Simulation)*

Excitation creation rate $\alpha(t)$ strongly depends on the irradiation conditions. In you experiment it was estimated to be about 10^{15} – 10^{16} *pairs* $cm^{-3}sec^{-1}$ (X-ray 30mA 35kV excitation source). It was found that temperature dynamics of emission channels in CsI:A strongly depends on this parameter (Fig. 5.12).

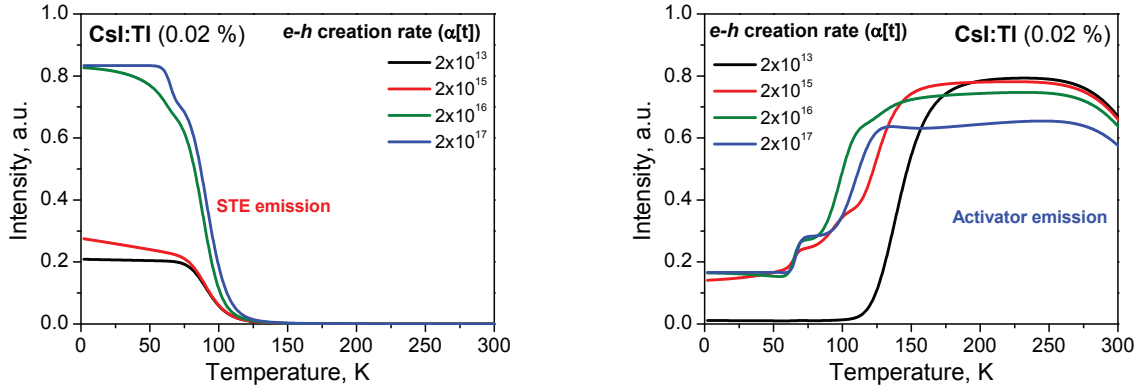

(a) (b)

Figure 5.12: *Temperature dependence of STE (a) and activator (b) luminescence yield in CsI:Tl as a function of excitation creation rate (Simulation)*

The simulation is done for CsI:Tl scintillator with 0.02% mol Tl. Excitaion creation rate is varied from 10^{13} to 10^{17} e-h *pairs* $cm^{-3}sec^{-1}$. At low excitation creation rates (about 10^{13}) STE recombination yield is limited by r_{ex} value (0.2% in the simulation), in accordance with Fig. 5.12 (a). Activator yield below 100K is practically none (Fig. 5.12 b). Since distribution of electron excitations is assumed homogeneous, electron and hole created most likely will find themselves spatially

separated from each other. Consequently, the hole will be self-trapped, whereas the electron will be capture by an activator ion. Energy losses due to trapping of charge carriers are the greatest in this case. Increase of the e-h creation rate reasonably leads to increase of STE recombination yield at temperatures below LNT (Fig. 5.12 a). However, activator yield around (150-300)K tends to decrease as soon as excitation density reaches activator concentration in the crystal (Fig. 5.12 b).

II. Concentration dependences

Now let us consider the processes which determine scintillation efficiency of the investigated scintillation system at RT and at LHeT. Experimental concentration dependences of the X-ray luminescence yield in comparison with simulation results are given in Fig. 5.13.

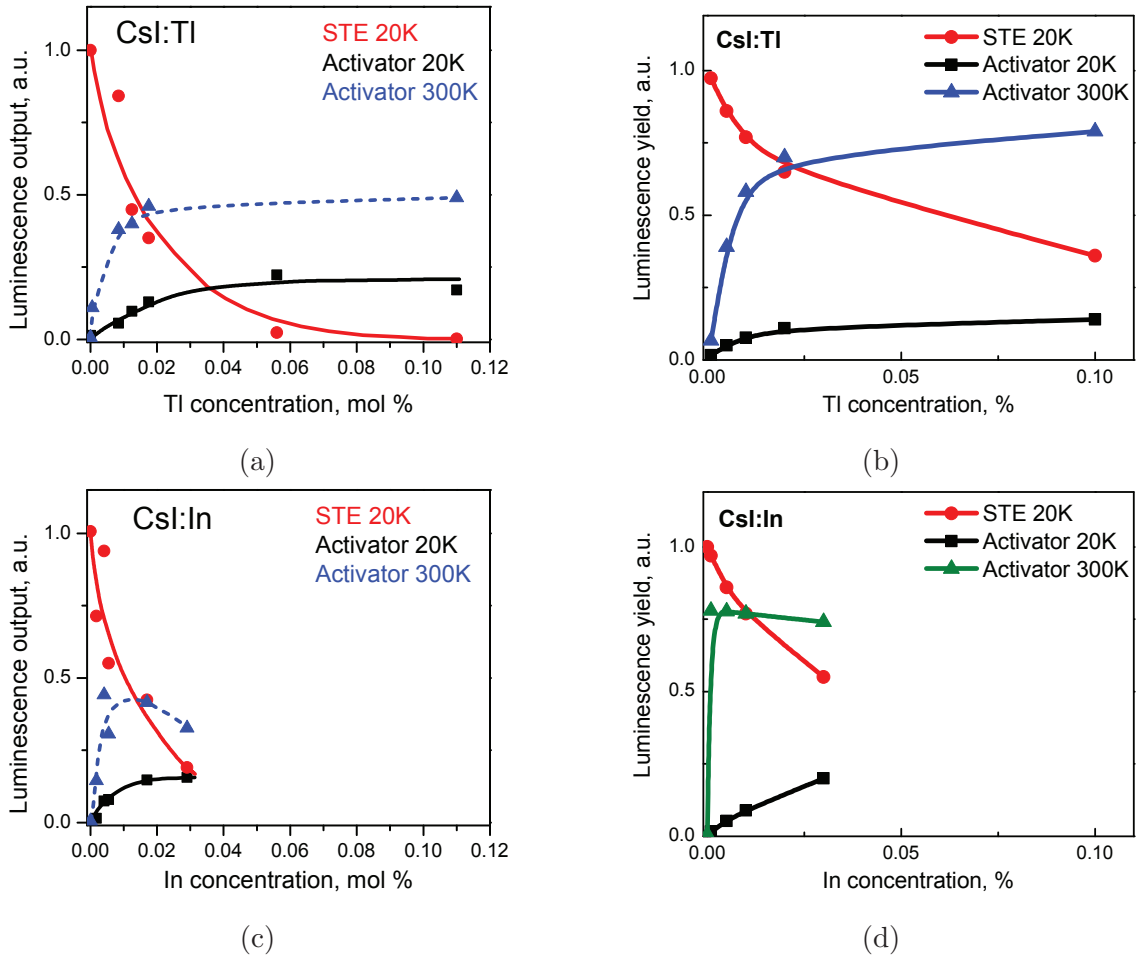

Figure 5.13: *Concentration dependences of the STE and activator emission yield of CsI:Tl (a-experiment, b-simulation) and CsI:In (c-experiment, d-simulation) at RT and LHeT*

At LHeT (20K) STE emission intensity drops down quickly with activator con-

centration increase in CsI:Tl and CsI:In (Fig. 5.13 a, c) according to the experiment. In case of CsI:Tl in particular, at activator concentration around 0.1% mol STE emission almost completely disappears. When it comes to simulated curves however, STE channel yield at this activator concentration is still about 0.25.

Simulated concentration dependences of the activator luminescence yield at RT are in good qualitative agreement with the experiment (Fig. 5.13). At high activator concentrations (0.02–0.1 % mol) the simulated activator luminescence yield is mostly stable and saturated, like the experimental curves show. At very low activator concentrations (below 0.01 % mol for CsI:Tl and below 0.005 % mol for CsI:In) simulated activator yield drops down, which quite closely follows the experimental data.

III. Account of energy transfer from STE to activator

This overestimation of the STE channel of relaxation might be due to presence of some additional channel of non-radiative STE relaxation related to activator, or else due to energy transfer from STE to activator, as suggested in [Gridin et al., 2014c]. Possible change of simulation results if such energy transfer is taken into account is shown in Fig. 5.14. Here dipole-dipole energy transfer between STE and Tl emission centers is assumed. Fraction of excitons which pass their energy to the activator:

$$F = \frac{2\pi^2}{3} n_A R_{d-d}^3 exp(\frac{4\pi^3}{9} n_A^2 R_{d-d}^6) \left(1 - Erf(\frac{2\pi^{3/2}}{3} n_A R_{d-d}^3)\right) \tag{5.4}$$

where R_{d-d} is the radius of dipole-dipole energy transfer, n_A is the activator concentration, and Erf is the error function. As one can see in Fig. 5.14, account of the energy transfer results to decrease of the STE intensity, with respective increase of the activator yield.

Decrease of the excitonic channel intensity with the increase of the activator content (experimental and simulated curves at 20K in Fig. 5.13) is accompanied with some increase of the activator emission yield. However, the total radiative recombination yield (excitonic and activator-related) is much lower than unity at high activator concentrations. This effect is also reflected in the simulation, and it originates from trapping of electrons by activator ions while holes become self-trapped in CsI lattice.

IV. Temperature quenching of FIL in CsI

As can be seen from a comparison of the experimental and simulated curves (see Fig. 5.9, Fig. 5.10) the activator luminescence yield of CsI:A is somewhat overesti-

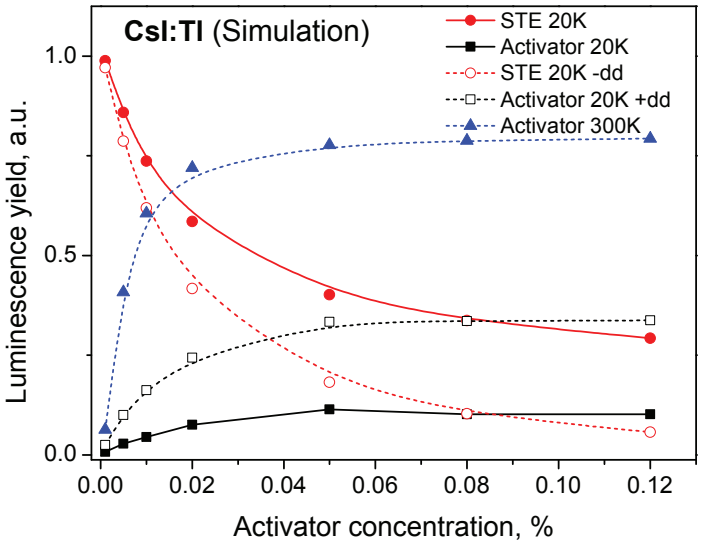

Figure 5.14: *Change in STE and activator yield concentration dependence produced by account of energy transfer between STE and Tl emission (Simulation)*

mated in the simulations. It concerns temperature range 150-300K. The additional channel of energy loss can be temperature quenching of the fast intrinsic luminescence (FIL) peaking at 300nm. X-ray excited luminescence yield temperature dependence of this band is shown in Fig. 5.15. At low temperatures (15-80K) in the overall yield of the intrinsic emission is mainly due to the STE (340nm) luminescence, whereas the intensity of the FIL band (300nm) is negligible. As can be seen from Fig. 5.15, STE luminescence temperature dependence under x-ray excitation is in good agreement with the curve in [Lamatsch et al., 1970] obtained under direct excitation of excitons. FIL emission intensity reaches its maximum yield at about 150K. At this temperature, the yield is about 20% of the maximum efficiency.

Further temperature increase results in continuous decrease of the FIL luminescence yield. At 300K it amounts about 2-5% of the maximum. As mentioned in Chapter 1, the nature of this emission is not completely clear [Belsky et al., 1994, Nishimura et al., 1995]. Nevertheless, the slope of the luminescence yield temperature dependence around 150-300K can be explained by the FIL temperature quenching. Scintillation decay curves for this emission measured under monochromatic x-ray excitation as a function of temperature are shown in Fig. 5.16.

According to Fig. 5.16, at 145K (when luminescence yield FIL is maximal) there is mostly one exponential component in the scintillation decay. As temperature goes up, the decay kinetics of this luminescence is greatly accelerated. In addition,

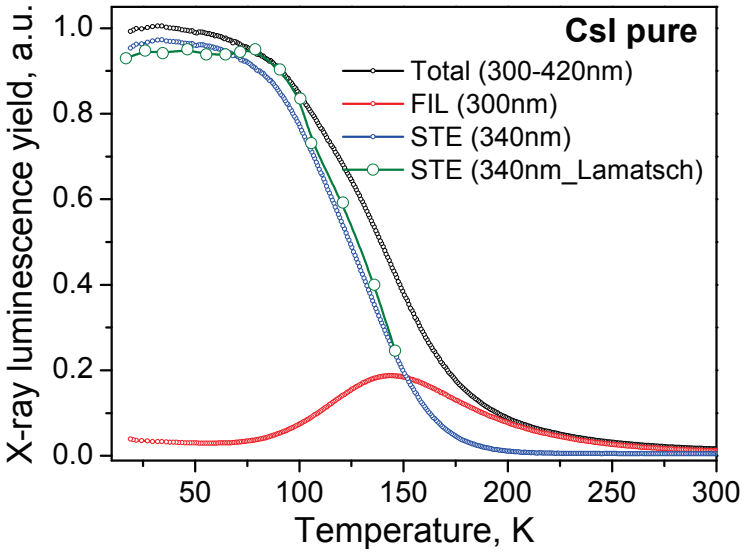

Figure 5.15: *Temperature dependences of the scintillation yield of STE (340nm) and FIL (300nm) emission in CsI pure. STE (340 nm) emission intensity under direct excitation form [Lamatsch et al., 1970]*

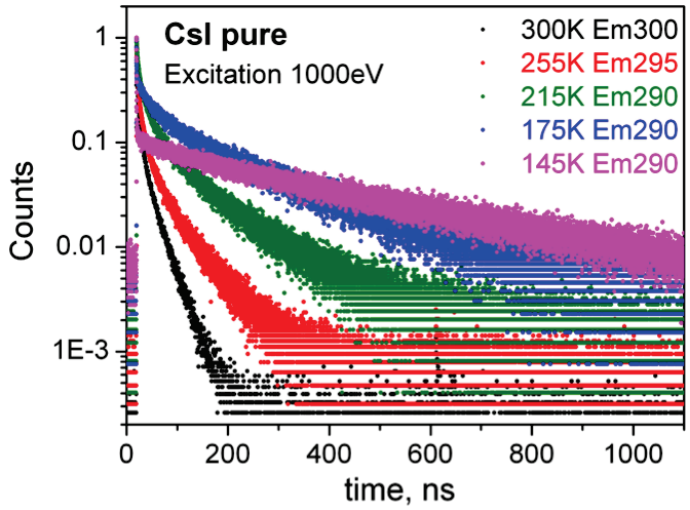

Figure 5.16: *Scintillation decay curves for FIL 300nm emission measured under 1000eV monochromatic X-ray excitation as a function of temperature*

the acceleration of the decay kinetics is accompanied by deviation from the exponential law. The acceleration observed for the FIL luminescence decay indicates non-radiative relaxation of the FIL excited state with temperature increase.

It should be noted that the 300nm FIL emission band overlaps the A absorption band in CsI:Tl and CsI:In. Thus, non-radiative energy transfer from FIL excited state to the activator centers is possible. The probability of such transfer will be strongly dependent on the activator concentration (eq. 5.4). In addition, a competi-

tion between activator centers and the FIL excited state in terms of charge carriers capture can be also the case. Nevertheless, the FIL non-radiative relaxation channel may cause up to 20% of energy loss at RT in CsI:A scintillators.

V. Simulation of the energy loss channels in CsI:A

Let us now try to explain the major features of CsI:A scintillation yield as a function of activator concentration and temperature through the prism of the suggested Model. We shall focus on two key aspects which follow from experimental curves in Fig. 5.13. First, activator yield of X-ray luminescence in CsI:A at 300K is about twice lower than the maximum STE emission yield in pure CsI. Second, total emission intensity in highly doped CsI:A crystals at LHeT is about 0.2-0.3, compared with STE maximum yield. These energy losses can be explained in frame of the suggested Model of energy relaxation in CsI:A, with no additional channel(s) of non-radiative relaxation.

The energy loss in CsI:A at 300K can be explained partially by STE quenching. Simulated radiative and non-radiative relaxation processes in CsI:Tl (0.1 % mol Tl) are shown in Fig. 5.17. STE quenching becomes significant above 100K, and about 0.2 of the whole electron excitations undergo non-radiative recombination in form of thermal quenching of STE. The dominating fraction of created STE here are those created by the direct recombination. Fraction of this directly created excitons created in CsI under X-ray may be quite significant. As discussed in [Vasil'ev and Gektin, 2014], high fraction of low energy electrons is generated in 5pCs band through Auger process in CsI. Although, it is likely some additional channel of non-radiative relaxation (some sort of lattice defects, perhaps) is in fact present in CsI:A, and it introduces some migration energy loss affection the separated electron-hole excitations.

The energy loss in CsI:A at low temperatures can be explained in the following way. Below the hole self-trapping point (90K in case of CsI), cross-trapping of charge carriers occurs. I.e. electrons are trapped by activator ions, but holes become instantly self-trapped. Simulation of this effect of energy storage in CsI:Tl is presented in Fig. 5.18. As temperature goes down and reaches the point of thermal release of electrons from Tl sites, number of electrons captured by the activator (Tl^0 centers) starts increasing. This goes with an equivalent increase of the number of activator captured holes (Tl^{++} centers). One temperature is low enough for efficient

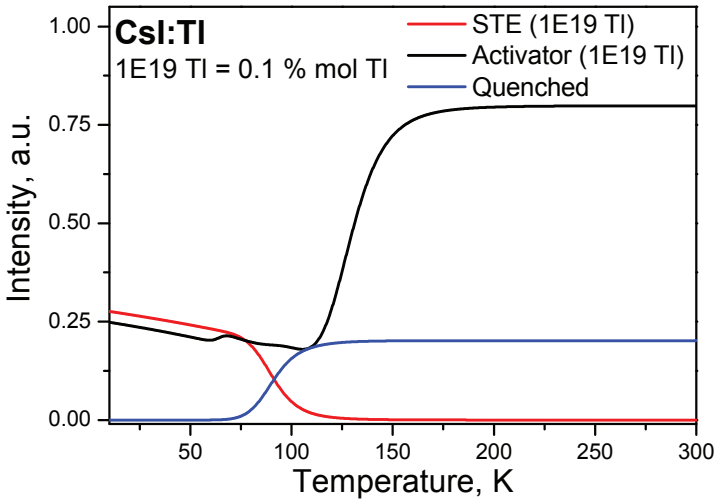

Figure 5.17: *Simulation of STE luminescence quenching as a function of temperature*

STH creation (around 90K in CsI), number of STHs starts increasing (black curve in Fig. 5.18). Along with that, growth of Tl^{++} centers concentration gets slower, and at some point their content starts decreasing, since self-trapping of holes becomes more efficient. Glow peaks' positions of the TSL simulation curve correspond to the peculiarities of X-ray luminescence temperature dependences (gray dashed in Fig. 5.18).

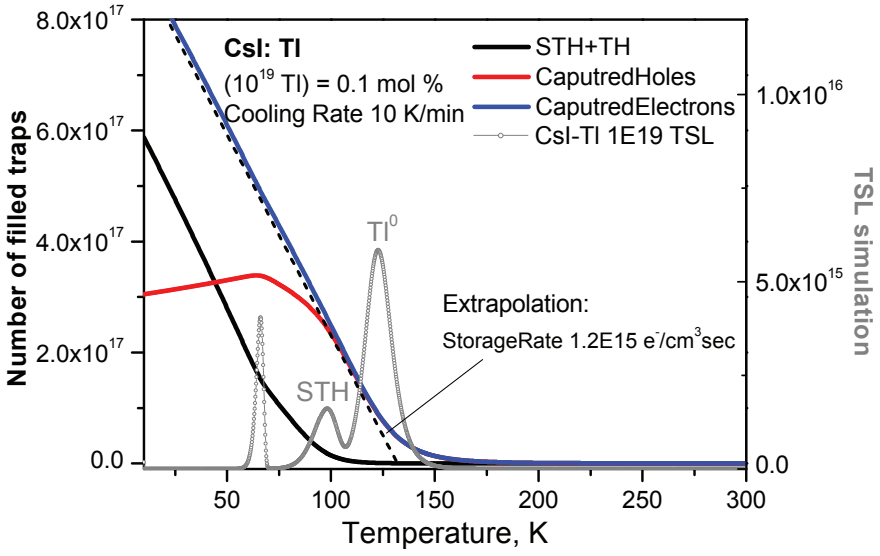

Figure 5.18: *Energy storage in CsI:A at low temperatures. Holes become self-trapped, and electrons are trapped by activator centers*

Extrapolation of the curve for capture electrons on the Temperature axis (see black dotted curve in Fig. 5.18) gives the electron trapping rate of 1.2×10^{15}

$electrons/cm^3sec$ under particular irradiation and cooling conditions. Given the e-h pair creation rate $\alpha(t) = 2 \times 10^{15} e - h/cm^3 sec$, the radiative relaxation channel loses more than half of electron excitations created. Indeed, as it follows from experimental and simulated temperature dependences of activator yield in CsI:Tl (Fig. 5.13 a,b), below 60K at 0.1% mol Tl STE and activator channels together give less that 50% of maximum emission efficiency.

5.3 Model of the luminescence rise and the afterglow with account of the activator traps

Let's try to apply the same model of energy relaxation in CsI:A to investigate the activator role in the luminescence kinetics. Based on the experiments in Section 4.4.2, we can assume that after first irradiation intrinsic traps in CsI:A are completely filled, and the role of the activator related capture is dominant in the emission rise profile. This assumption allows using the model of the electronic excitations in crystals of CsI:A (Fig. 5.6). Besides, given the measurements of emission rise and afterglow were done at 300K, we will neglect here the possibility of STE creation. In addition, the above mentioned experiment in Section 4.4.2 allows us to neglect the charge carriers' capture by the intrinsic traps in CsI. As a result, in order to describe the role of the activator in the luminescence rise and the afterglow, we are using a simplified set of electron excited states as shown in Fig. 5.19.

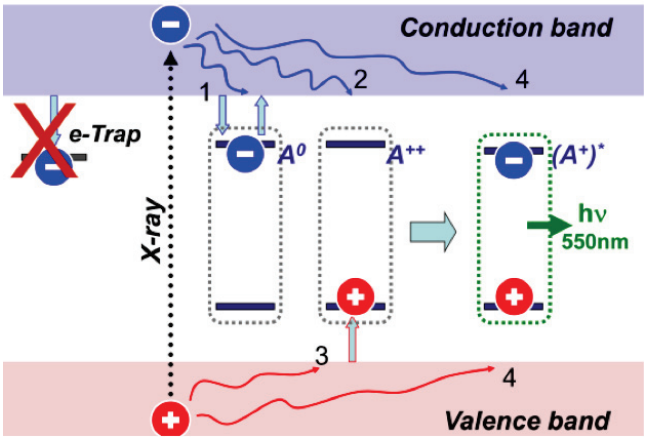

Figure 5.19: *Model of electron excitations in CsI:A to study the activator role in the luminescence rise and the afterglow*

This model takes into account the following processes. Process 1 involves the

ability of a effectively neutral A^+ center to capture free electrons with formation of A^0. Process 2 indicates free electrons capture by positively charged activator centers with formation of excited activator ions $A^{++} + e^- \rightarrow (A^+)^*$. Process 3 illustrates capture of holes by activator centers $A^+ + h^+ \rightarrow A^{++}$. We suppose that at room temperature the lifetime of the hole on the activator is much larger than that of electrons. Therefore, the probability of hole release form activator cites should be low. Process 4 is for activator capture of a correlated e-h pair (an exciton) $ex + A^+ \rightarrow (A^+)^*$ (direct excitation of the activator). Here we assume that a fraction of thermalized electron-hole pairs are spatially correlated with each other, and transfer their energy directly to the activator.

This model of energy relaxation in the CsI:A leads to simplified system of rate equations. In this case, the energy relaxation model has only 5 of the electronic states, the kinetic equations which make up the system (eq. 5.5):

System of rate equations

$$\frac{dn_e(t)}{dt} = \alpha(t)(1 - r_{ex}) - \beta_{0e} n_e(t)(n_{cc} - n_{ce}(t) - n_{ch}(t)) + s_{ce} n_{ce}(t) exp(\frac{-A_e}{kT}) - \beta_{he} n_{ch}(t) n_e(t)$$

$$\frac{dn_h(t)}{dt} = \alpha(t)(1 - r_{ex}) - \beta_{0h} n_h(t)(n_{cc} - n_{ce}(t) - n_{ch}(t)) + s_{ch} n_{ch}(t) exp(\frac{-A_h}{kT}) - \beta_{eh} n_{ce}(t) n_h(t)$$

$$\frac{dn_{ce}(t)}{dt} = \beta_{0e} n_e(t)(n_{cc} - n_{ce}(t) - n_{ch}(t)) - s_{ce} n_{ce}(t) exp(\frac{-A_e}{kT}) - \beta_{eh} n_{ce}(t) n_h(t)$$

$$\frac{dn_{ch}(t)}{dt} = \beta_{0h} n_h(t)(n_{cc} - n_{ce}(t) - n_{ch}(t)) - s_{ch} n_{ch}(t) exp(\frac{-A_h}{kT}) - \beta_{he} n_{ch}(t) n_e(t)$$

$$\frac{dn^*(t)}{dt} = \alpha(t) r_{ex} + \beta_{he} n_e(t) n_{ch}(t) + \beta_{eh} n_h(t) n_{ce}(t) - \frac{n^*(t)}{\tau_A}$$

(5.5)

All the parameters and the variables in system (eq. 5.5) have the same meaning as described in Section 5.2.2. Apart from the r_{ex} value, which here describes the fraction of the direct activator excitation. This parameter is assumed to be 0.6 based

on the fact that the luminescence rise profile of CsI:In samples (Fig. 4.11 a) starts with a pedestal of about that height. Numerical solution of (eq. 5.5) with respect to $\frac{dn^*(t)}{dt}$ allows simulating the activator yield as a function of time.

Comparison of the simulated CsI:A emission with the experimental curves is shown in Fig. 5.20. Here for the experimental curves the emission rise profiles form Irradiation 3 in Fig. 4.14, since in this experiment the intrinsic traps are mostly filled. This allows distinguish the role of activator centers in the energy storage. Fig. 5.20 shows a good qualitative agreement between the experimental and simulated emission rise curves for CsI:Tl, and for CsI:In.

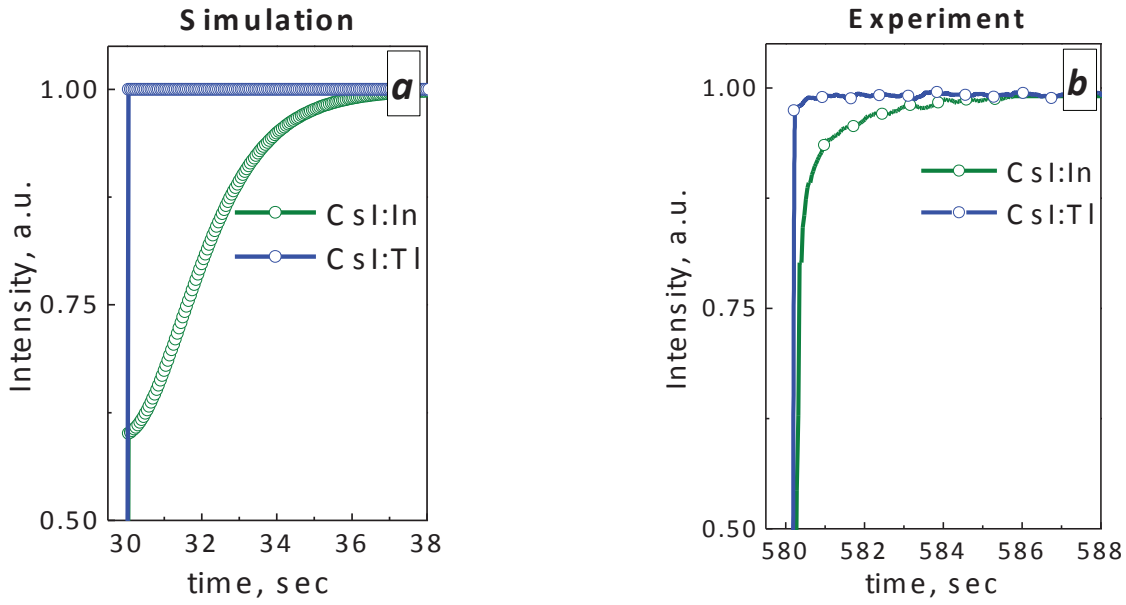

(a) (b)

Figure 5.20: *Simulated (a) and experimental curves (b) of luminescence rise in CsI:A crystals at 300K*

Simulation of the afterglow curves after X-ray irradiation for 180 seconds in comparison with the corresponding experimental curves presented in Fig. 5.21. Note that in the experimental afterglow curves (see Fig. 5.21 b) contain contribution of both the intrinsic traps (which are stable at RT, and responsible for the slow component), and the faster recombination component of charge carriers stored at the activator centers. In the presented time scale (Fig. 5.21) contribution of the activator traps crystal CsI:In quite large. Overall, the afterglow simulation (Fig. 5.21 a) qualitatively well reproduces the difference in the afterglow intensity between CsI:Tl and CsI:In.

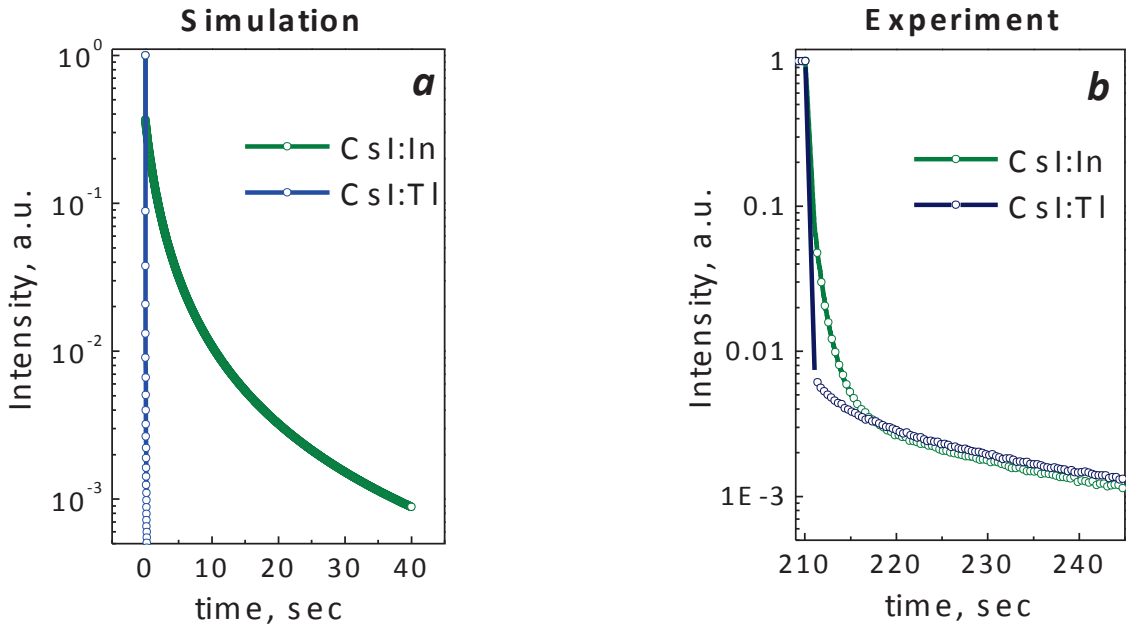

(a) (b)

Figure 5.21: *Simulated (a) and experimental curves (b) of the activator luminescence afterglow for CsI:A at 300K*

To illustrate the energy storage mechanism associated with electron trapping by the activator in CsI:A model shown in Fig. 5.22 can be used. After thermalization of the electron excitations certain amount of genetic electron-hole pairs are separated by ∼100nm distance. As follows from the electron mean free path distribution function at Fig. 1.7 in Chapter 1, this fraction of excitations can be quite significant in CsI, in view LO phonons have relatively low energy.

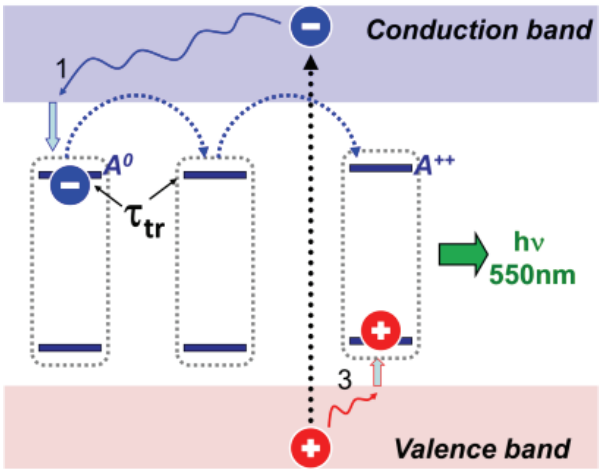

Figure 5.22: *Model of delayed activator recombination in CsI:A*

Let us consider spatially separated thermalized electron-hole pair (Fig. 5.22). The hole will be captured by the nearest activator center (process 3), and will stay trapped on it. The separated electron will be instantly captured by another activator center (process 1), to form an A^0 center which is unstable at RT. Thus, on the way to recombine with the positively charged activator center A^{++}, the electron will be captured several times by neutral activator centers. And hence, the migration time of this separated electron on the way to recombination will be substantially determined by the mean lifetime of the A^0 state.

The average lifetime of an electron trapped at an activator site can be evaluated the trap parameters: the trap depth E, and the frequency factor s. It can be estimated using eq. 5.3.

The average lifetime of electrons on thallium and indium centers is given in Table 5.2. The lifetime of electrons on thallium centers is $\sim 10^{-6}$ seconds. It value is close to the radiation time of the excited $(Tl^+)^*$ (see Chapter 3). Therefore, in the time scale of about 1 sec in the case of CsI:Tl there is no significant effect of the activator neither on the luminescence rise nor on the afterglow. In the case of CsI:In activator plays a role of a stable electron traps, the average lifetime of which is ~ 0.1 sec. As a consequence, its influence on the luminescence kinetics is much more important.

Table 5.2: *Average lifetime of electrons on the activator traps in CsI:A at 300K*

Activator	E_A, eV	s, sec^{-1}	τ_{tr} (300K), sec
Tl	0.28	3.3×10^{10}	1.5×10^{-6}
In	0.59	1.1×10^{11}	7.4×10^{-2}

In this approach we have neglected the intrinsic traps in CsI, which correspond to the TSL peaks above RT (Fig. 4.12). As shown in this section, CsI:In luminescence kinetics at RT is mostly determined by the activator electron trap. However, when it comes to CsI:Tl crystals the key role in the afterglow belongs to the intrinsic traps above RT. Investigation of the activator luminescence kinetics with account of the intrinsic traps in CsI:Tl is beyond the scope of the present work.

5.4 Conclusions

In this Chapter a model of energy relaxation in CsI:A is suggested based on the experimental study of the scintillation crystals. The model takes into account main electron excited states in CsI:A, giving rise to intrinsic (STE) and activator relaxation. Three charge states of activator (A^+, A^0, and A^{++}) are taken into account. The only channel of non-radiative relaxation is STE temperature quenching.

• A system of rate equations was set to describe the dynamics of energy relaxation processes in CsI:A. The model of energy relaxation processes in CsI:A allows satisfactory numerical simulation of intrinsic and activator scintillation efficiency as a function of temperature and activator concentration. Account of charge carriers capture parameters by luminescence centers for CsI:Tl and CsI:In crystals allowed adequately simulate many properties as a function of temperature and activator concentration. Those include X-ray emission temperature dependences, concentration dependences of the yield, emission rise profile, afterglow and some others. This confirms validity of the model.

• Efficiency of radiative relaxation channels and energy loss channels in CsI:A strongly depends on the system parameters. Depending on temperature and the activator content, the following energy relaxation mechanisms can be marked out in CsI:A:

a) In pure CsI crystals ($c = 0$) the mechanism of energy relaxation if creation of STEs. The only channel of energy loss is temperature quenching of STEs. At low temperatures ($T < 80K$) maximum scintillation efficiency is reached, since there is no other channels of energy losses (Fig. 5.23 a);

b) In activated CsI:A crystals ($c > 0$) there are two channels of relaxation: excitonic and activator-induced. At $T < 80K$ decrease of the scintillation yield occurs due to storage of non-correlated charge carriers on stable traps: self-trapping of holes, and electron capture by activator centers A^+ with creation of A^0. Release of charge carriers from those traps gives intense glow peaks in TSL curves. Energy storage is the reason of scintillation efficiency decrease in CsI:A at $T < 80K$ (Fig. 5.23 b);

c) At $T > 150K$ self-trapping of holes in CsI is not efficient. In activated crystals ($c > 0$) separated e-h pairs are mostly captured by the activator centers. However, excitons are also created, mainly for account of direct e-h recombination. Losses

in scintillation efficiency of CsI:A can be in part explained by non-radiative STE relaxation (Fig. 5.23 c)

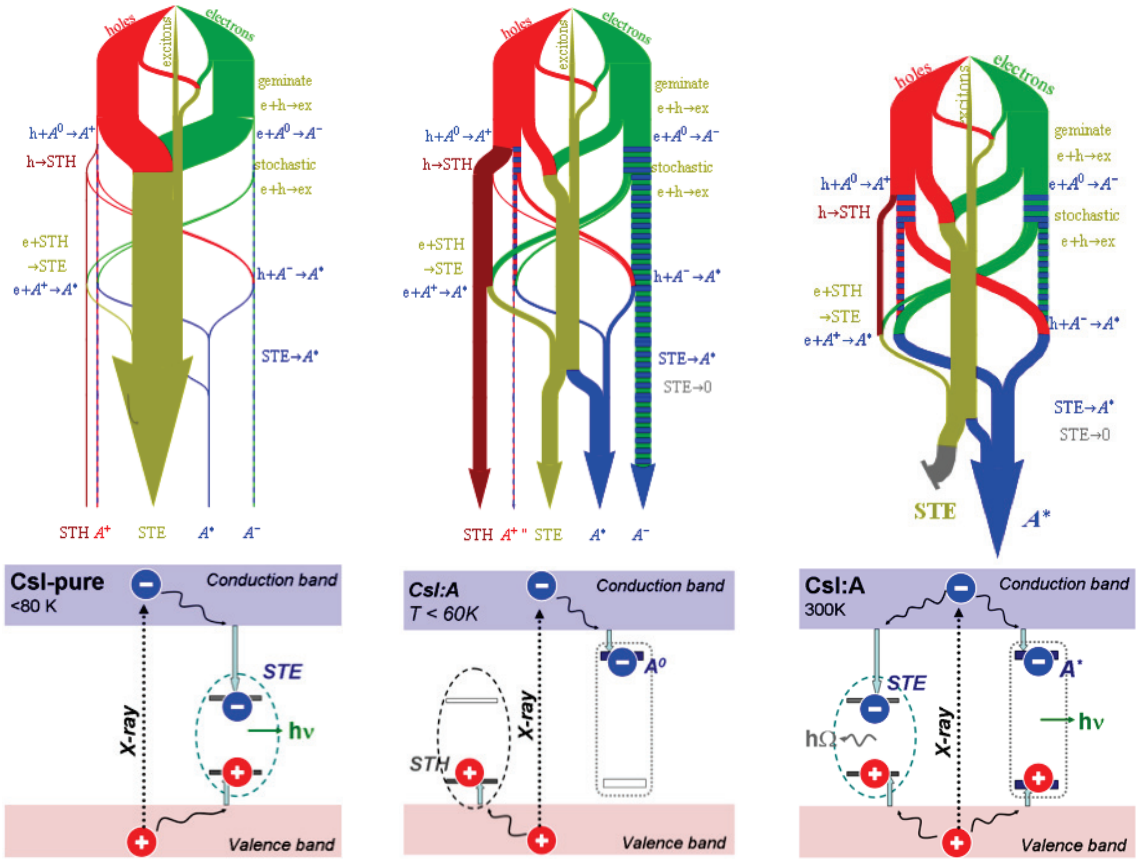

(a) (b) (c)

Figure 5.23: *Channels of energy loss and relaxation in CsI:A: a – pure crystal, b – activated crystal below 80K, c – activated crystal at RT*

The modeling approach applied is rather general and can be used for a large variety of scintillation materials. Appropriate modification of the rate equations will be needed, as well as some experimental data for the parameters estimation. It is shown that detailed and accurate evaluation/estimation of the parameter of the system allows reasonable simulations of many scintillation properties of CsI:A.

General conclusions and perspectives

General conclusions

Comparative study of luminescence properties of CsI:In and CsI:Tl concentration series allows making general conclusions about radiation-induced processes in this system.

1. Concentration series of CsI:In and CsI:Tl single crystals were synthesized. Set of CsI:In samples was grown by us using the Bridgman method in quartz vacuum sealed ampules. Series of CsI:Tl crystals was obtained using modified Czochralski method. Activator concentration in the crystals was determined using inductively coupled plasma emission spectroscopy. The crystals are transparent in visible region, and contain negligible amount of oxygen containing impurities, as was checked with IR spectroscopy.

2. Based on the fluorescence spectroscopy study at various temperatures form 10K to 300K a model of activator emission centers in CsI:A has been proposed. Difference in luminescence properties between the activators is caused by the positions of the activator levels relative to the forbidden band of the crystal. In CsI:In crystals excited $^3P_1$ and $^1P_1$ activator levels lay at the top of the forbidden band. This is why account of only electron transitions in the activator ion allows explaining spectroscopic properties of CsI:In. Those levels in thallium doped CsI are overlapping with the conduction band. Therefore, in CsI:Tl ionization of the activator occurs under excitation in the activator absorption region. Impurity bound exciton state $(Tl^{++} + e^-)$ is used to explain the origin of the visible emission in CsI:Tl.

3. Scintillation properties of new CsI:In scintillator were investigated. The activator is not toxic in contrast with Tl, and the crystals are easy to grow from melt using the Bridgman or the Czochralski method. Light yield of CsI:In crystals mea-

sured with chanting time around 10 μs was found to be 27 000 photons/MeV, which is twice lower than in CsI:Tl. Scintillation yield of indium doped crystals is limited by presence of slow component in the scintillation pulse. The delay in radiative recombination is caused by an activator electron trap, which is stable at RT. Thanking to high temperature stability of its scintillation yield, CsI:In is a good candidate for well-logging experiments.. Scintillation properties of CsI:In (light yield and energy resolution) could be improved if crystal growth technology is optimized.

4. A general model of energy relaxation processes in CsI:A is suggested. It includes the most important electron excited states in this type of scintillators. A system of rate equations is used to simulate the energy relaxation processes in CsI:A. Temperature and the activator concentration are the main parameters used to verify the model. Account of the interaction and transformation of electron excitations in CsI:A allows to simulate both radiative and non-radiative relaxation processes, as well as the energy storage.

5. Energy losses observed in CsI:A below LNT ($T < 80K$) have to do with energy storage. Tl-like activator ions can act both as electron trap and hole traps in CsI crystals. On the other side, below 90K self-trapping of holes gives stable V_k centers. As a result, separated electron hole pairs may be trapped in different states: holes become self-trapped in regular CsI lattice positions (STH), whereas electrons are stably trapped by the activator centers (creation of A^0 centers). In this way only spatially correlated electron-hole pairs give rise to emission either in STE of in activator channel. Given that the excitation creation rates is several orders of magnitude lower than the activator concentration (which is normally the case under X-ray or γ-ray excitation), the activator traps are never completely filled. This is why X-ray luminescence yield of CsI:A drops down to 20% of the maximum at 20K.

6. Energy losses at around 300 K in CsI:A crystals amount about 50% independently of the activator type. These losses can be explained by temperature quenching of the intrinsic emission (STE and FIL). These short living intrinsic excitations are created in all CsI crystals regardless the activator type. Energy transfer from them to activator centers is limited, so non-radiative recombination of the excitons in CsI limits the efficiency of the activator relaxation channel. The intrinsic origin of these losses suggests that the activator yield is limited by 50% of the maximum in CsI:A.

Perspectives

• Temperature stability of CsI:In scintillation yield makes it a good candidate for well logging applications. Scintillation properties of CsI:In crystals have some potential to improvement. First, presence of slow component in scintillation decay if CsI:In limits its light yield to 50% of CsI:Tl. If this trap is related to the activator, its impact cannot be avoided. However, stability of the In-related activator trap is supposed to decrease with increase of temperature. This could allow using conventional integration times to collect most of the emitted scintillation light form CsI:In. Second, energy resolution of CsI:In crystals obtained ranges from 8.5% to 11%, which is significantly poorer than typical values of CsI:Tl ($\sim 6-7\%$). However, the series of experimental CsI:In crystals was grown by the Bridgman method, which does not guarantee homogeneous activator distribution. Use of the Czochralski method of synthesis and optimization of crystals growth technology might improve energy resolution of CsI:In.

• Numerical modeling of energy relaxation processes in CsI:A has some limitations and simplifications. We assume that the density of electron excitations is average in the crystal, as well as the activator concentration. This is not the case in real scintillation process. Distribution of electrons and holes created is assumed to be homogeneous in the mathematical simulation applied in Chapter 5. However, ionization track is strongly non-homogeneous. It contains high excitation density regions with distance between excitation under 3nm, where energy losses occur due to concentration quenching. Fraction of such high excitation density regions depend on the energy of the incident irradiation. Further development of this modeling method is possible with account of spatial distribution of electron excitation in the excited region of scintillators. This could broaden applicability of the mathematical method of analysis used in the work.

• Energy losses in CsI:A limiting scintillation yield at RT can be related to non-radiative relaxation of STE. In CsI:A crystals overlap between the activator absorption bands and the STE emission band is rather small. Besides, activator concentration about 1% is impossible to reach due to low segregation coefficient of the activator impurity. This is why energy transfer to activator centers is mostly from consecutive capture of separated charge carriers. Spatially correlated electron-hole pairs form excitons and non-radiatively recombine at RT. Whereas in alkali-earth halides Eu^{2+} related absorption band overlap better with the intrinsic emission

band. This could lead to efficient STE to activator energy transfer in this class of scintillators. Non-radiative energy transfer between STE and activator emission centers could be one of the reasons of extremely high efficiency of Eu-doped alkali-earth halide scintillators. Investigation of the non-radiative energy transfer efficiency from intrinsic to activator luminescence centers in alkali-earth halides in comparison with the classical alkali halides can be an interesting direction for the further study.

Bibliography

[Sci, 2014] (2014). Scintillation Properties. `http://scintillator.lbl.gov/`. Accessed: 13/10/14.

[xRa, 2014] (2014). X-Ray Attenuation Length. `http://henke.lbl.gov/optical\_constants/atten2.html`. Accessed: 28/05/14.

[Nis, 2014] (2014). X-Ray Mass Attenuation Coefficients - Cesium Iodide. `http://physics.nist.gov/PhysRefData/XrayMassCoef/ComTab/cesium.html`. Accessed: 28/05/14.

[Agranovich and Galanin, 1982] Agranovich, V. and Galanin, M. (1982). *Electronic excitation energy transfer in condensed matter*.

[Antonov-Romanovskiy, 1966] Antonov-Romanovskiy, V. V. (1966). *Photoluminescence kinetics of crystal phosphors [in Russian]*.

[Babin et al., 2002a] Babin, V., Kalder, K., Krasnikov, A., and Zazubovich, S. (2002a). Luminescence and defects creation under photoexcitation of CsI : Tl crystals in Tl + -related absorption bands. *Journal of Luminescence*, 96:75–85.

[Babin et al., 2002b] Babin, V., Krasnikov, a., Wieczorek, H., and Zazubovich, S. (2002b). Luminescence of complicated thallium centres in CsI:Tl. *Nuclear Instruments and Methods in Physics Research Section A: Accelerators, Spectrometers, Detectors and Associated Equipment*, 486(1-2):486–489.

[Barland et al., 1981] Barland, M., Duval, E., and Nouailhat, A. (1981). Migration of V k centres in CsI crystal. *Journal of Physics C: Solid State Physics*, 14(29):4237–4245.

[Bartram et al., 2008] Bartram, R. H., Kappers, L. A., Hamilton, D., Lempicki, A., Brecher, C., Gaysinskiy, V., Ovechkina, E. E., and Nagarkar, V. V. (2008).

Afterglow Suppression and Non-Radiative Charge-Transfer in CsI:Tl,Sm. *IEEE Transactions on Nuclear Science*, 55(3):1232–1236.

[Belsky et al., 1997] Belsky, A., Cortes, R., Gektin, A., Martin, P., Mikhailin, V., and Pédrini, C. (1997). Excitation mechanisms of CsI fast intrinsic luminescence. *Journal of Luminescence*, 72-74:93–95.

[Belsky et al., 1998] Belsky, A., Garnier, N., Dujardin, C., Pedrini, C., Varrel, B., Chevallier, P., and Firsov, A. (1998). THE EFFECT OF THALLIUM DISTRIBUTION ON LUMINESCENCE OF CsI:Tl. *Proceeding of the Seventh international Symposium on « Physics and Chemistry of Luminescence materials », Electrochemical Society Proceeding*, 98-24:195–200.

[Belsky et al., 2013] Belsky, A., Ivanovskikh, K., Vasil'ev, A., Joubert, M.-F., and Dujardin, C. (2013). Estimation of the Electron Thermalization Length in Ionic Materials. *The Journal of Physical Chemistry Letters*, 4(20):3534–3538.

[Belsky et al., 1994] Belsky, A., Vasil'ev, A., Mikhailin, V., Gektin, A., Martin, P., Pedrini, C., and Bouttet, D. (1994). Experimental study of the excitation threshold of fast intrinsic luminescence of CsI. *Physical Review B*, 49(18):13197–13200.

[Belsky et al., 1992] Belsky, A., Vasil'ev, A., Mikhailin, V., Gektin, A., Shiran, N., Rogalev, A. L., and Zinin, E. I. (1992). Time-resolved XEOL spectroscopy of new scintillators based on CsI. *Review of Scientific Instruments*, 63(1):806.

[Bizarri et al., 2011] Bizarri, G., Bourret-Courchesne, E., Yan, Z., and Derenzo, S. (2011). Scintillation and Optical Properties of BaBrI:Eu and CsBa2I5:Eu. *IEEE Transactions on Nuclear Science*, 58(6):3403–3410.

[Bizarri et al., 2009] Bizarri, G., Moses, W. W., Singh, J., Vasil'ev, A., and Williams, R. T. (2009). An analytical model of nonproportional scintillator light yield in terms of recombination rates. *Journal of Applied Physics*, 105(4):044507.

[Blasse and Grabmaier, 1994] Blasse, G. and Grabmaier, B. C. (1994). *Luminescent Materials*. Springer Berlin Heidelberg, Berlin, Heidelberg.

[Boatner et al., 2013] Boatner, L. a., Neal, J. S., Kolopus, J. a., Ramey, J. O., and Akkurt, H. (2013). The characterization of scintillator performance at tempera-

tures up to 400 degrees centigrade. *Nuclear Instruments and Methods in Physics Research Section A: Accelerators, Spectrometers, Detectors and Associated Equipment*, 709:95–107.

[Brecher et al., 2006] Brecher, C., Lempicki, A., Miller, S., Glodo, J., Ovechkina, E., Gaysinskiy, V., Nagarkar, V. V., and Bartram, R. (2006). Suppression of afterglow in CsI:Tl by codoping with Eu2+—I: Experimental. *Nuclear Instruments and Methods in Physics Research Section A: Accelerators, Spectrometers, Detectors and Associated Equipment*, 558(2):450–457.

[Cherepy et al., 2008] Cherepy, N. J., Hull, G., Drobshoff, A. D., Payne, S. A., van Loef, E., Wilson, C. M., Shah, K. S., Roy, U. N., Burger, A., Boatner, L. a., Choong, W.-S., and Moses, W. W. (2008). Strontium and barium iodide high light yield scintillators. *Applied Physics Letters*, 92(8):083508.

[Chowdhury et al., 1999] Chowdhury, M., Watts, S., Imrie, D., McKemey, A., and Holmes-Siedle, A. (1999). Studies of radiation tolerance and optical absorption bands of CsI(Tl) crystals. *Nuclear Instruments and Methods in Physics Research Section A: Accelerators, Spectrometers, Detectors and Associated Equipment*, 432(1):147–156.

[de Haas and Dorenbos, 2008] de Haas, J. and Dorenbos, P. (2008). Advances in Yield Calibration of Scintillators. *IEEE Transactions on Nuclear Science*, 55(3):1086–1092.

[Dorenbos, 2012] Dorenbos, P. (2012). Modeling the chemical shift of lanthanide 4f electron binding energies. *Physical Review B*, 85(16):165107.

[Elango, 1991] Elango, M. A. (1991). *Elementary Inelastic Radiation-Induced Processes*.

[Evans, 1955] Evans, R. (1955). *The Atomic Nucleus*.

[Fok, 1964] Fok, M. V. (1964). *Introduction to luminescence kinetics of crystal phosphors [in Russian]*.

[Förster, 1948] Förster, T. (1948). Zwischenmolekulare Energiewanderung und Fluoreszenz. *Annalen der Physik*, 437(1-2):55–75.

[Glukhov and Vasil'ev, 1995] Glukhov, R. A. and Vasil'ev, A. (1995). Monte-Carlo simulation of the creation of excited regions in insulators by a photon. *Radiation Effects and Defects in Solids*, 135(1-4):315–319.

[Grabmaier, 1984] Grabmaier, B. C. (1984). Crystal Scintillators. *IEEE Transactions on Nuclear Science*, 31(1):372–376.

[Gridin et al., 2014a] Gridin, S., Belsky, A., Moszynski, M., Syntfeld-Kazuch, A., Shiran, N., and Gektin, A. (2014a). Scintillation properties of CsI:In single crystals. *Nuclear Instruments and Methods in Physics Research Section A: Accelerators, Spectrometers, Detectors and Associated Equipment*, 761:13–18.

[Gridin et al., 2014b] Gridin, S., Belsky, A., Shiran, N., and Gektin, A. (2014b). Channels of Energy Losses and Relaxation in CsI:A Scintillators (A=Tl,In). *IEEE Transactions on Nuclear Science*, 61(1):246–251.

[Gridin et al., 2014c] Gridin, S., Vasil'ev, A., Belsky, A., Shiran, N., and Gektin, A. (2014c). Excitonic and activator recombination channels in binary halide scintillation crystals. *physica status solidi (b)*, 251(5):942–949.

[Gwin and Murray, 1963] Gwin, R. and Murray, R. (1963). Scintillation Process in CsI(Tl). I. Comparison with Activator Saturation Model. *Physical Review*, 131(2):501–508.

[Hamada et al., 2001] Hamada, M., Costa, F., Pereira, M., and Kubota, S. (2001). Dependence of scintillation characteristics in the CsI(Tl) crystal on Tl/sup +/ concentrations under electron and alpha particles excitations. *IEEE Transactions on Nuclear Science*, 48(4):1148–1153.

[Hofstadter, 1948] Hofstadter, R. (1948). Alkali Halide Scintillation Counters. *Physical Review*, 74(1):100–101.

[Hofstadter, 1949] Hofstadter, R. (1949). The Detection of Gamma-Rays with Thallium-Activated Sodium Iodide Crystals. *Physical Review*, 75(5):796–810.

[Holl et al., 1988] Holl, I., Lorenz, E., and Mageras, G. (1988). A measuremets of the light yield of common inorganic scintillators. *IEEE Transactions on Nuclear Science*, 35(1):105–109.

[Kerisit et al., 2008] Kerisit, S., Rosso, K. M., and Cannon, B. D. (2008). Kinetic Monte Carlo Model of Scintillation Mechanisms in CsI and CsI(Tl). *IEEE Transactions on Nuclear Science*, 55(3):1251–1258.

[Kerisit et al., 2009] Kerisit, S., Rosso, K. M., Cannon, B. D., Gao, F., and Xie, Y. (2009). Computer simulation of the light yield nonlinearity of inorganic scintillators. *Journal of Applied Physics*, 105(11):114915.

[Kerisit et al., 2014] Kerisit, S., Wang, Z., Williams, R. T., Grim, J. Q., and Gao, F. (2014). Kinetic Monte Carlo Simulations of Scintillation Processes in NaI(Tl). *IEEE Transactions on Nuclear Science*, 61(2):860–869.

[Kirkin et al., 2012] Kirkin, R., Mikhailin, V., and Vasil'ev, A. (2012). Recombination of Correlated Electron–Hole Pairs With Account of Hot Capture With Emission of Optical Phonons. *IEEE Transactions on Nuclear Science*, 59(5):2057–2064.

[Kirm et al., 2009] Kirm, M., Nagirnyi, V., Feldbach, E., De Grazia, M., Carré, B., Merdji, H., Guizard, S., Geoffroy, G., Gaudin, J., Fedorov, N., Martin, P., Vasil'ev, A., and Belsky, A. (2009). Exciton-exciton interactions in CdWO4 irradiated by intense femtosecond vacuum ultraviolet pulses. *Physical Review B*, 79(23):233103.

[Kolotilin and Shtanko, 1984] Kolotilin, V. and Shtanko, V. (1984). Intrinsic hole color centers in irradiated CsI single crystals. *Solid State Physics*, 26(1):236–238.

[Kudin et al., 2009] Kudin, A., Shkoropatenko, A., Ovcharenko, N., Alekseev, V., Trefilova, L., and Shpilinskaya, A. (2009). Suppression mechanism of millisecond afterglow in CsI:Tl crystals by Eu2+ impurity. *Functional Materials*, 16:275–278.

[Kudin et al., 2005] Kudin, A., Sysoeva, E. P., Sysoeva, E. V., Trefilova, L., and Zosim, D. (2005). Factors which define the α/γ ratio in CsI:Tl crystals. *Nuclear Instruments and Methods in Physics Research Section A: Accelerators, Spectrometers, Detectors and Associated Equipment*, 537(1-2):105–112.

[Lamatsch et al., 1970] Lamatsch, H., Rossel, J., and Saurer, E. (1970). Localized and Self-Trapped Excitons in CsI. *Physica Status Solidi (B)*, 41:605–614.

[Lamatsch et al., 1971] Lamatsch, H., Rossel, J., and Saurer, E. (1971). Kinetics of Self -Trapped Exciton Recombination in CsI. *Physica Status Solidi (B)*, 48:311–318.

[Lecoq et al., 2006] Lecoq, P., Annenkov, A., Gektin, A., Korzhik, M., and Pedrini, C. (2006). *Inorganic Scintillators for Detector Systems*. Particle Acceleration and Detection. Springer-Verlag, Berlin/Heidelberg.

[Luschick and Luschick, 1989] Luschick, C. and Luschick, A. (1989). *Deconvolution of electorn excitations with defect creatoin in solids [in Russian]*.

[Martinez et al., 1964] Martinez, P., Senftle, F., and Page, M. (1964). Trapping Levels and Thermoluminescence of CsI Doped with Various Activators. *Phys. Rev. Letters*, 12(13):12–15.

[Masunaga et al., 1966] Masunaga, S., Morita, I., and Ishiguro, M. (1966). Optical Properties of CsI : Tl and CsBr : Tl. *Journal of the Physical Society of Japan*, 21(4):638–644.

[McKeever, 1985] McKeever, S. W. S. (1985). *Thermoluminescence of Solids*. Cambridge University Press, Cambridge.

[Mengesha et al., 1998] Mengesha, W., Taulbee, T., Rooney, B., and Valentine, J. (1998). Light yield nonproportionality of CsI(Tl), CsI(Na), and YAP. *IEEE Transactions on Nuclear Science*, 45(3):456–461.

[Michal'chenko et al., 1966] Michal'chenko, G. A., Kondrat'ko, M. Y., and Vinogradova, T. P. (1966). STABLE COLOR CENTERS IN CESIUM HALIDES. *Zhumal Prikladnoi Spektroskopii*, 4(3):278–279.

[Mikhailin, 1987] Mikhailin, V. (1987). Excitation of secondary processes in the vacuum ultraviolet range. *Nuclear Instruments and Methods in Physics Research Section A: Accelerators, Spectrometers, Detectors and Associated Equipment*, 261(1-2):107–114.

[Mikhailin, 1995] Mikhailin, V. (1995). Luminescence of solids excited by synchrotron radiation. *Nuclear Instruments and Methods in Physics Research Section B: Beam Interactions with Materials and Atoms*, 97(1-4):530–535.

[Moretti et al., 2014] Moretti, F., Patton, G., Belsky, A., Fasoli, M., Vedda, A., Trevisani, M., Bettinelli, M., and Dujardin, C. (2014). Radioluminescence Sensitization in Scintillators and Phosphors: Trap Engineering and Modeling. *The Journal of Physical Chemistry C*, 118(18):9670–9676.

[Moszynski et al., 2005] Moszynski, M., Balcerzyk, M., Czarnacki, W., Kapusta, M., Klamra, W., Schotanus, P., Syntfeld, A., Szawlowski, M., and Kozlov, V. (2005). Energy resolution and non-proportionality of the light yield of pure CsI at liquid nitrogen temperatures. *Nuclear Instruments and Methods in Physics Research Section A: Accelerators, Spectrometers, Detectors and Associated Equipment*, 537(1-2):357–362.

[Moszynski et al., 2003] Moszynski, M., Czarnacki, W., Klamra, W., Szawlowski, M., Schotanus, P., and Kapusta, M. (2003). Application of large area avalanche photodiodes to study scintillators at liquid nitrogen temperatures. *Nuclear Instruments and Methods in Physics Research Section A: Accelerators, Spectrometers, Detectors and Associated Equipment*, 504(1-3):307–312.

[Moszynski et al., 1997] Moszynski, M., Kapusta, M., Mayhugh, M., Wolski, D., and Flyckt, S. (1997). Absolute light output of scintillators. *IEEE Transactions on Nuclear Science*, 44(3):1052–1061.

[Nagirnyi et al., 1995] Nagirnyi, V., Stolovich, A., Zazubovich, S., Zepelin, V., Mihokova, E., Nikl, E., Pazzi, G. P., and Salvini, L. (1995). Peculiarities of the triplet relaxed excited-state structure and luminescence of a CsI:Tl crystal. *Journal of Physics: Condensed Matter*, 7(18):3637–3653.

[Nagirnyi et al., 1994] Nagirnyi, V., Zazubovich, S., Zepelin, V., Nikl, M., and Pazzi, G. P. (1994). A new model for the visible emission of the CsI: Tl crystal. *Chemical Physics Letters*, 227(4-5):533–538.

[Nikl et al., 1993] Nikl, M., Hlinka, J., Mihokova, E., Polak, K., and Fabeni, P. (1993). Decay kinetics of CsI : Tl luminescence excited in the A absorption band. *PHILOSOPHICAL MAGAZINE B*, 67(5):627–649.

[Nishimura et al., 1995] Nishimura, H., Sakata, M., Tsujimoto, T., and Nakayama, M. (1995). Origin of the 4.1 eV luminescence in pure CsI scintillator. *Physical Review B*, 51(4):2167–2172.

[Onsager, 1938] Onsager, L. (1938). Initial Recombination of Ions. *Physical Review*, 54(8):554–557.

[Pedrini et al., 1993] Pedrini, C., Moine, B., Bouttet, D., Belsky, A., Mikhailin, V., Vasil'ev, A., and Zinin, E. I. (1993). Time-resolved luminescence of CeF3 crystals excited by X-ray synchrotron radiation. *Chemical Physics Letters*, 206(5-6):470–474.

[Ranfagni et al., 1983] Ranfagni, A., Mugnai, D., Bacci, M., Viliani, G., and Fontana, M. (1983). The optical properties of thallium-like impurities in alkali-halide crystals. *Advances in Physics*, 32(6):823–905.

[Ritchie et al., 1975] Ritchie, R. H., Tung, C. J., Anderson, V. E., and Ashley, J. C. (1975). Electron Slowing-Down Spectra in Solids. *Radiation Research*, 64(1):181.

[Robbins, 1980] Robbins, D. J. (1980). On Predicting the Maximum Efficiency of Phosphor Systems Excited by Ionizing Radiation. *Journal of The Electrochemical Society*, 127(12):2694.

[Rozenberg et al., 1974] Rozenberg, G., Ptitsyn, G., Chajkovskij, E., Stroilova, D., and Protsenko, V. (1974). Distribution of NaI impurity in CsI crystals [in Russian]. *Fizika Tverdogo Tela*, 16(11):3336–3339.

[Savon et al., 2012] Savon, A. E., Spassky, D., Vasil'ev, A., and Mikhailin, V. (2012). Numerical simulation of energy relaxation processes in a ZnMoO4 single crystal. *Optics and Spectroscopy*, 112(1):72–78.

[Simkin et al., 1984] Simkin, D. J., Belliveau, T. F., Sivasankar, V. S., Schmitt, K., and Jacobs, P. W. M. (1984). LUMINESCENCE OF In+ AND Tl+ IN ALKALI HALIDES WITH THE CAESIUM CHLORIDE STRUCTURE. *Journal of Lununescence*, 31&32:320–322.

[Sivasankar and Jacobs, 1985] Sivasankar, V. S. and Jacobs, P. W. M. (1985). Luminescence spectroscopy of CsI: Tl +. *Philosophical Magazine Part B*, 51(5):479–488.

[Sivasankar et al., 1985] Sivasankar, V. S., Schmitt, K., and Jacobs, P. W. M. (1985). LUMINESCENCE AND DECAY TIMES OF CsI: In. *Journal of Luminescence*, 33:409–426.

[Song and Williams, 1993] Song, K. S. and Williams, R. T. (1993). *Self-Trapped Excitons*, volume 105 of *Springer Series in Solid-State Sciences*. Springer Berlin Heidelberg, Berlin, Heidelberg.

[Spaeth et al., 1994] Spaeth, J. M., Meise, W., and Song, K. S. (1994). The nature of the X-ray-induced luminescence and the hole centres in CsI:Tl studied by optically detected electron paramagnetic resonance. *Journal of Physics: Condensed Matter*, 6(21):3999–4008.

[Stoneham, 2001] Stoneham, A. M. (2001). *Theory of Defects in Solids: Electronic Structure of Defects in Insulators and Semiconductors*.

[Trefilova et al., 2003] Trefilova, L., Charkina, T., Kudin, A., Kosinov, N., Kovaleva, L., and Mitichkin, A. (2003). Radiation defects creation in CsI(Tl) crystals and their luminescence properties. *Journal of Luminescence*, 102-103:543–550.

[Trefilova et al., 2002] Trefilova, L., Kudin, A., Kovaleva, L., Zaslavsky, B., Zosim, D., and Bondarenko, S. (2002). Concentration dependence of the light yield and energy resolution of NaI:Tl and CsI:Tl crystals excited by gamma, soft X-rays and alpha particles. *Nuclear Instruments and Methods in Physics Research Section A: Accelerators, Spectrometers, Detectors and Associated Equipment*, 486(1-2):474–481.

[Vasil'ev, 1999] Vasil'ev, A. (1999). Relaxation of hot electronic excitations in scintillators : account for scattering , track effects , complicated electronic structure. In *Proceedings of the 5th International Conference on Inorganic Scintillators and Their Applications (SCINT99)*, number 1, pages 43–52.

[Vasil'ev, 2008] Vasil'ev, A. (2008). From Luminescence Non-Linearity to Scintillation Non-Proportionality. *IEEE Transactions on Nuclear Science*, 55(3):1054–1061.

[Vasil'ev and Gektin, 2014] Vasil'ev, A. and Gektin, A. (2014). Multiscale Approach to Estimation of Scintillation Characteristics. *IEEE Transactions on Nuclear Science*, 61(1):235–245.

[Vasil'ev and Michailin, 1986] Vasil'ev, A. and Michailin, V. V. (1986). Role of phonon relaxation in cascade multiplication process of electron excitations created by an X-ray. *Bulletin of the AS of USSR*, 50(3):537–541.

[Vasil'ev et al., 1985] Vasil'ev, A., Michailin, V. V., and Ovchinnikova, I. V. (1985). Effect of hot separaton of electron-hole pairs on the quantum yield of crystallophosphor with traps [in Russian]. *Bulletin of the AS of USSR*, 49(10):2044–2048.

[Vasil'ev and Mikhailin, 2008] Vasil'ev, A. and Mikhailin, V. (2008). *Principles of Insulator Spectroscopy*. Moscow.

[Wang et al., 2013] Wang, Z., Williams, R. T., Grim, J. Q., Gao, F., and Kerisit, S. (2013). Kinetic Monte Carlo simulations of excitation density dependent scintillation in CsI and CsI(Tl). *physica status solidi (b)*, 250(8):1532–1540.

[Wang et al., 2012] Wang, Z., Xie, Y., Campbell, L. W., Gao, F., and Kerisit, S. (2012). Monte Carlo simulations of electron thermalization in alkali iodide and alkaline-earth fluoride scintillators. *Journal of Applied Physics*, 112(1):014906.

[Wang et al., 2011] Wang, Z., Xie, Y., Cannon, B. D., Campbell, L. W., Gao, F., and Kerisit, S. (2011). Computer simulation of electron thermalization in CsI and CsI(Tl). *Journal of Applied Physics*, 110(6):064903.

[Weber, 2002] Weber, M. (2002). Inorganic scintillators: today and tomorrow. *Journal of Luminescence*, 100(1-4):35–45.

[Williams et al., 2011] Williams, R. T., Grim, J. Q., Li, Q., Ucer, K. B., and Moses, W. W. (2011). Excitation density, diffusion-drift, and proportionality in scintillators. *physica status solidi (b)*, 248(2):426–438.

[Yan et al., 2013] Yan, Z., Bizarri, G., and Bourret-Courchesne, E. (2013). Scintillation properties of improved 5% Eu2+-doped BaCl2 single crystal for X-ray and γ-ray detection. *Nuclear Instruments and Methods in Physics Research Section A: Accelerators, Spectrometers, Detectors and Associated Equipment*, 698:7–10.

[Zaslavsky, 1999] Zaslavsky, B. (1999). Automated pulling of large-diameter alkali halide scintillation single crystals from the melt. *Journal of Crystal Growth*, 200(3-4):476–482.

[Zimmerer, 2007] Zimmerer, G. (2007). SUPERLUMI: A unique setup for luminescence spectroscopy with synchrotron radiation. *Radiation Measurements*, 42(4-5):859–864.

Acknowledgements

First of all I am indebted to my supervisors Dr. Alex Gektin and Dr. Andrei Belsky for their guiding, support, and scientific advice during the whole period of my PhD study program. I admire their patience and enthusiasm when proofreading my reports, paper drafts, and this manuscript. Without them this work would be impossible.

Then I would like to acknowledge the discussions of my work and the criticism I received from Dr. Andrey Vasil'ev and Dr. Nataly Shiran. Their deep professional knowledge and experience have helped me improve (hopefully) my scientific skills. Speaking of criticism, I would like to express my appreciation to Dr. Irina Kamenskikh and Dr. Dmitry Spassky for their stimulating analytical judgment of some of my paper drafts.

I am grateful for the support I received from the team "Luminescence" in Institut Lumière Matière, Université Claude Bernard Lyon 1. In particular I would like to thank Prof. Christophe Dujardin for his advice on the research, Dr. Frederico Moretti for his guiding with the glow curve analysis, Gael Patton for his assistance with X-ray luminescence rise and afterglow measurements.

I want to thank my colleagues from Institute for Scintillation Materials in Kharkov, Ukraine. It is a pleasure to acknowledge helpful interaction with Yanina Boyarintseva, PhD and Svetlana Neicheva, PhD as well as their advice with experimental data analysis at the first steps of my PhD study. My specials gratitude goes to Sergey Vasyukov and Evgeniy Galenin for their assistance with crystal growth.

I appreciate the experimental results on the scintillation properties obtained by Prof. Moszynski and his team from the National Centre for Nuclear Research in Otwock-Swierk, Poland.